DOE ARM contract # DE-FG02-90ER61066



# DEVELOPMENT OF AN UPPER-LEVEL CLOUD PARMETERIZATION FOR LARGE SCALE MODELS

by Sharon E. Nebuda

William R. Cotton, P.I.

Colorado State University

DEPARTMENT OF ATMOSPHERIC SCIENCE

PAPER NO. 582

# DEVELOPMENT OF AN UPPER-LEVEL CLOUD PARAMETERIZATION FOR LARGE SCALE MODELS


by

**Sharon E. Nebuda**

Department of Atmospheric Science

Colorado State University

Fort Collins, CO 80523



Research Supported by

**Department of Energy**

**Atmospheric Radiation Measurement program**

under Contract # DE-FG02-90ER61066

August 3, 1995

Atmospheric Science Paper No. 582

## ABSTRACT


### DEVELOPMENT OF AN UPPER-LEVEL CLOUD PARAMETERIZATION FOR LARGE SCALE MODELS

The interaction of clouds with the general circulation is generally agreed upon to be the most important physical process requiring improvement in today's climate models. Due to the limited spatial and temperal resolution of most large-scale models, representing the detailed physical properties of clouds has been difficult. To overcome this limitation, a one-dimensional, upper-level cloud model has been developed which can be nested in time and space in a localized area with limited frequency. The adaptive cloud model will provide microphysical and radiative information for the large-scale model.

The cloud parameterization was developed using the existing physics in the Regional Atmospheric Modeling Systems (RAMS) developed at Colorado State University (CSU). The microphysical routine requires the large-scale model to maintain the variables of liquid and ice water as well as total ice number concentration. The cloud model includes six water species of total water, water vapor, rain, small ice (pristine ice), large ice (snow), and aggregates. Cloud water is computed as a residual of the other water categories. A subgrid turbulence scheme which predicts the vertical velocity variance provides the mixing created by radiative destabilization. The radiation routine distinguishes between liquid and ice water and computes heating rates which can significantly influence the large-scale circulation.

To evaluate the upper-level cloud model several initializations were used by both a psuedo-1D format of RAMS and a psuedo-GCM format of RAMS in conjunction with the cloud model to simulate cirrus. The results from the cirrus cases created by the pseudo-1D format of RAMS provides an understanding of the response of RAMS physics to the 1D

dynamics. These simulations also provide a control run for judging the cloud model when called by the psuedo-GCM RAMS. The cirrus initializations range in altitude from 125 mb to 450 mb at both tropical and middle latitudes. The cloud was initiated by either elevated relative humidity (large-scale weather disturbance) or addition of cloud water (detrainment from convection). The results indicate the upper-level cloud model is successful at reproducing the same features of the cloud as modeled by the psuedo-1D version of RAMS. Among the features of the cirrus is the deepening of the cloud layer through gravitational settling of larger ice particles which can significantly alter the radiative heating rates in the cloud layer. Clouds created by large-scale weather disturbances warmer than $-50°C$ or initiated by convection with significant amounts of ice (0.5 g/kg) are more likely to generate radiative forcing that would noticably impact the large-scale circulation. The performance of the upper-level cloud model was highly dependent on the quality of initialization by the large-scale model. Preliminary results suggest the cost of the upper-level cloud model can be reduced by limiting its frequency and diagnosing the precipitation of large ice crystals from the cloud layer similiar to the technique of Ghan and Easter (1992).

Sharon E. Nebuda
Department of Atmospheric Science
Colorado State University
Fort Collins, Colorado 80523
Summer 1995

## ACKNOWLEDGEMENTS

I would like to thank my advisor, William R. Cotton, for the opportunity to conduct this research as well as the advice and direction he has provided during the course of this work. I am also grateful for the time and consideration given by my committee members, David Randall and David Dandy, in reviewing this research. The assistance by Robert Walko with RAMS was invaluable and much appreciated. Help from Jerry Harrington in understanding and modifying the microphysical package of RAMS is also greatly appreciated. I would also like to thank Brenda Thompson and Abby Hodges for their generous support as well as Donna Chester for much needed computer support. Assistance and suggestions from past and present officemates, Greg Thompson, Brian Beitler, Jerry Harrington, and Brian Gaudet, not only made life bearable but were invaluable in accomplishing this research. Finally, I want to thank Andrew Heidinger, my family, and the friends I've made at Colorado State University for their support and patience during the preparation of this thesis.

This research was supported by the Department of Energy (DOE) Atmospheric Radiation Measurement program (ARM) under contract # DE-FG02-90ER61066.

TABLE OF CONTENTS

LIST OF FIGURES

## LIST OF TABLES

# Chapter 1

# INTRODUCTION

Clouds and climate are closely related through processes of radiation and transport of water, latent heat, and momentum. The interaction of clouds and the atmosphere is highly dependent on cloud composition, location, coverage, and duration. One such interaction, cumulus convection in the tropics, is the dominant transport of latent heat into the upper troposphere through condensation, nucleation, and evaporation. This transport allows energy to be advected away from the tropics to regions receiving less incoming solar energy (Rhiel and Malkus, 1958). The more complicated feedback of clouds may be that of radiation. Clouds have two physical properties which will significantly dictate how the cloud will modify the radiation balance, optical depth and temperature. The optical depth of the cloud will determine the transparency to solar radiation whereas the cloud top temperature dictates the longwave emission to space. A cold, optically thin cirrus will behave differently than a cold, optically thick cumulonimbus which in turn is unlike a warm, optically thick low-level stratus deck. The two sometimes counteracting effects of longwave and shortwave heating makes this cloud feedback critical to understand in order to determine the correct influence of clouds on the general circulation and climate.

To study climate, scientists have developed general circulation models (GCMs) as numerical laboratories. The GCM allows the researcher to examine features of the atmosphere which can not be directly measured or observed. The atmosphere can also be perturbed to simulate the effects of natural or anthropogenic changes. The quality of this research tool is only as good as the physics represented in the model. Early GCMs dealt only with a crude representation of the water cycle and clouds. Through the years, significant errors were found, a majority being attributed to the inaccurate or lack of representation of clouds

(Cess *et al.*, 1990). Cloud physics must be included in some manner to obtain accurate results from GCMs about climate change.

Since the first climate model was developed, researchers have been improving representation of clouds concurrently with other advances in the model physics. Continuing this evolution of GCMs, this research will develop a cloud parameterization to represent the formation of upper-level clouds from both large-scale forcing as well as detrainment from convection. This parameterization will be created by modifying the physics in a regional model to develop a one-dimensional (1D) nested cloud model. The initial performance of the parameterization will be examined to determine if this application of a cloud parameterization is a feasible solution to modeling upper-level clouds in a GCM.

Most cloud parameterizations deal with two individual cloud regimes: convective clouds and layer clouds formed by large-scale weather disturbances. Traditionally, layer cloud models are based on large-scale variables such as temperature, vertical velocity, and relative humidity. For cirrus formed by convective outflow into dry, stable conditions, the available methods of parameterizations for layer clouds will most likely not work. The need for a model which includes the creation of upper-level clouds through convection was pointed out by Randall (1989) in which he suggestes this deficiency in GCMs is responsible for the largest inaccuracy in modeling cloud feedback. Ramaswamy and Ramanathan (1989) also believe the radiative and water budget impact from cirrus created by convective outflow may account for a large portion of the discrepancies in GCMs and observations. The potential for improving GCMs justifies designing an upper-level cloud model which will not only model clouds created by large-scale forcing but clouds originating from convection as well. This research will assess the feasibility of using such a cloud parameterization to adequately model upper-level clouds without hampering the speed and memory requirements of the GCM.

### 1.1 Previous Research

Many researchers have suggested various means of modeling clouds in GCMs. The earliest GCMs dealt with the hydrological cycle only in the simplest terms. Manabe *et al.* (1965) simulated the water cycle with only water vapor as a predicted variable. Water that became saturated in an unstable, convective column was removed instantly as precipitation. The column was then adjusted back to a stable lapse rate. The radiation budget was based on climatological values of water vapor and neglected any cloud feedback. Further work was completed on improving convective transport of latent and sensible heat by Kuo (1965, 1974), Arakawa and Schubert (1973), Emanuel (1991) among others. Attention was next given to improving the calculation of cloudiness to allow a feedback between clouds and radiation. Most cloudiness parameterizations were diagnosed from grid volume averaged variables of temperature, vertical velocity, mass flux, and relative humidity (Sasamori, 1975; Geleyn, 1981; Slingo, 1987). Many studies were made of the accuaracy using relative humidity to determine cloudiness (Hense and Heise, 1984; Xu and Krueger, 1991) and concluded relative humidity was the optimal variable for tropical stratiform clouds but not necessarily for all cloud types.

The next phase of cloud parameterization developments included the explicit prediction of cloud water (Sundqvist, 1978; Smith, 1990) to improve the radiative feedback of clouds. Assumptions about the size distributions of cloud water and omission of ice were necessary. Ghan and Easter (1992) were among the first to include both ice and liquid water in their stratiform cloud parameterization to account for the inherent differences of terminal velocities and optical properties of water and ice. As seen from the above discussion, the research of cloud parameterizations is heading towards more explicit modeling of cloud physics.

The current state of cloud physics in GCMs was presented by Cess *et al.* (1990) in which 19 climate models simulated a perpetual July atmosphere with a perturbed sea surface temperature to investigate the model response to climate change. When clouds were included in the simulations, some climate models with similar responses achieved their results through very different, counteracting cloud feedbacks. The models' clear sky cases produced similar changes in global-mean surface temperature for a given change in sea surface temperature. But when clouds were included in the simulations, the difference in the global-mean surface temperature between some models was threefold. The consensus from this model comparison was that improvement in cloud feedback is the highest priority in the development of the next generation of GCMs.

Randall (1989) attributed the worst cloud feedback error to the lack of upper-level clouds created by detrainment of convection. The error can be seen in the NCAR Community Climate Model cold bias in the upper troposphere at the equator (Fig. 1.1). Ramaswamy and Ramanathan (1989) propose the error is caused by the lack of cirrus radiatively warming the upper tropopsphere through longwave absorption. The work by Ose (1993) and Smith and Randall (1992) addressed this problem by including explicit microphysics and linking it to the existing convective parameterization in each GCM.

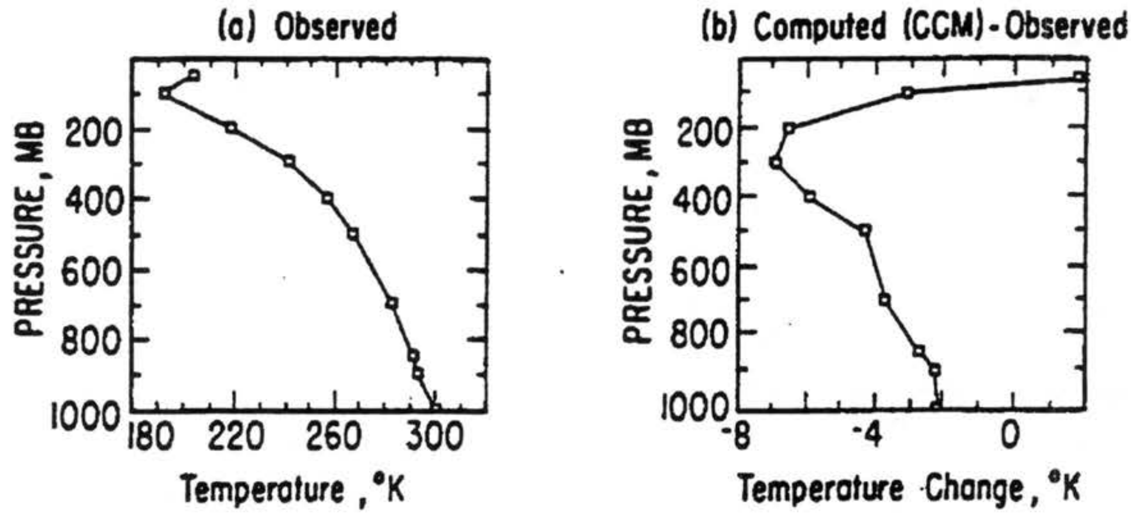


Figure 1.1: Vertical distributions of (a) observed zonal mean temperature and (b) differences between the GCM computed zonal mean temperature and observed zonal mean temperatures at the equator for January. (Ramaswamy and Ramanathan, 1989)

The characteristics of the convectively created cirrus relative to other upper-level clouds differ enough that existing layer models or large-scale condensation would not create the correct type of cirrus clouds. Cumulonimbus anvils were found by Heymsfield and Knollenberg (1972) to have higher ice particle concentrations (140,000 $m^3$ vs. 50,000 $m^3$), different ice crystal shapes (spherical vs. bullet), higher ice densities (1 $g/m^3$ vs. 0.4 $g/m^3$) and less dynamic motion. Anvils are created in dry, cold temperatures where other parameterizations would yield low ice densities (Ackerman et al., 1988). Convectively-generated cirrus would therefore be radiatively thicker (Liou 1986), have different scattering properties, have long lifetimes of around 6 hours (Leary and Houze, 1979), and advect far from the source of their generation (Webster and Stephens, 1980). As described by Heymsfield and Knollenberg (1972), "Most cirrus is not a cloud in the usual sense. Rather, it is a mass of growing precipitation elements (ice crystals)." But the cumulonimbus anvil does not fit this description, anvils are formed by direct deposit of ice through convection into the upper troposphere. Therefore, it is unlikely that a cloud parameterization developed for layer clouds based on entirely different physics would also work for cumulonimbus anvils.

The work by Ose (1993) and Smith and Randall (1992) is the most relevant work to this research. They took the approach of developing an upper-level cloud parameterization by linking the explicit microphysics to the existing convective parameterization in each GCM. The GCM was run to examine the climatic changes by the addition of cumulonimbus anvil. No subgrid parameterization for turbulence, radiation, or microphysics was used for specifically modeling the clouds. The actual composition of the upper-level clouds were not studied in detail. Instead emphasis was placed on the models response to explicitly resolved microphysics provided by the convective output.

For Fowler and Randall (1992), the convective parameterization based on Arakawa and Schubert (1974) was modified to provide a total water transport to a microphysical package which explicitly modeled the hydrometeor species of cloud water, cloud ice, snow, and rain. A 17 layer version of the Colorado State University (CSU) GCM was run with one minute timesteps for the microphysics to explicitly model settling and precipitation of the hydrometeor species. Two different configurations were used, a 3 hour simulation using a standard, 3D version of the GCM to examine the instantaneous distributions of cloud water and ice (Smith and Randall, 1992) and a 15 day simulation using a modified 1D version of the GCM to examine the temperal interaction of the cumulus parameterization and microphysics (Fowler and Randall, 1992). The results indicate a good global distribution of cloud water and ice for the 3D case. The longer, 15 day simulation suggest the model will capture the cycle of layer clouds generated by convective detrainment. These initial studies do not link the radiation scheme to the detailed information of the cloud microphysics or cloud fraction.

Ose (1993) also added explicit microphysics to the 9 level, 4° X 5° University of California, Los Angeles (UCLA) GCM for examining the cloud feedback of convective detrainment.

Like Fowler and Randall (1992), the Arakawa and Schubert (1974) convective parameterization was modified to provide explicit cloud water and ice to the microphysical scheme. Between the temperatures of −10°C and −40°C both cloud ice and water coexist as a linear function of temperature. Rain and snow species are diagnosed. Unlike Fowler and Randall (1992), Ose (1993) chose to keep the standard timestep of one hour for the UCLA GCM simulations. Precipitation (rain and snow) are assumed to reach the ground after appropriate evaporation within the hour timestep. Shortwave properties are prescribed as a function of cloud top temperature while longwave emissivity is proportional to the liquid and ice water paths. This radiative interaction improves the simulation of cloud feedback compared the work of Fowler and Randall (1992). Ose (1993) has compromised by using a simplier microphysics to gain better radiative feedback and the ability to compute longer simulations.

The results from the six 28 day perpetual July simulations confirm that cumulus detrainment is just as important (northern hemisphere, midlatitudes) or even more important (tropics) than the large-scale lifting as a source of condensate. Ose (1993) also demonstrated the failing of predicting ice water content (IWC) as a function of temperature for regions of large cumulus detrainment. Two cloud regimes of the midlatitude southern hemisphere and tropics can be seen in Fig. 1.2. The good correlation between IWC predicted by temperature in the midlatitudes and the observed ice content is contributed to by large-scale condensation. However, the scatter in the midlatitude results and the lack of correlation in the tropics is attributed to the upper-level clouds created by detrainment from convection.

The difficulty of achieving desirable cloud lifetimes of up to 6 hours is discussed by Ose (1993). Among suggestions for capturing this feature is to include sub-grid turbulence and radiative heating profiles. Higher vertical resolution and better microphysics are also presented as means of resolving the long-lived nature of this cirrus. Randall (1989) also suggested a 500 m vertical resolution may be necessary to parameterize upper-level clouds properly in a GCM.

This research will approach the same problem from a different angle. A detailed cloud model will be developed using a limited regional model as a host model framework where the parameterized clouds will be examined for accuracy. Only after the model proves feasible

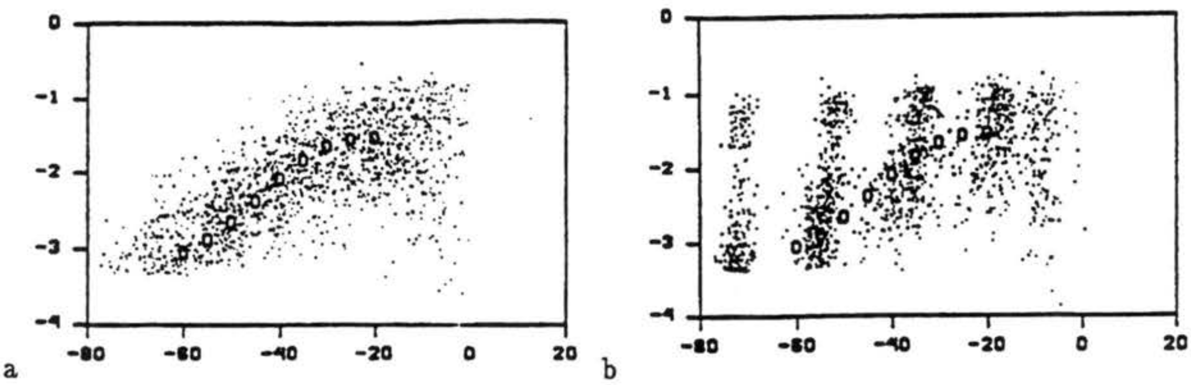


Figure 1.2: Dots represent the relationship between the simulated cloud ice content and temperature (°C). Cloud ice content is represented by $\log_{10}(g/m^3)$. 'O's are observations for (a) the midlatitude Southern Hemisphere and (b) the tropics. (Ose, 1993)

will the next stage of development be attempted. This parameterization will address the needs of GCMs to improve the climate feedback of upper-level clouds.

## 1.2 Purpose

This research will develop a preliminary upper-level cloud model. The physical parameterizations for turbulence, radiation, and microphysics will be borrowed from the CSU Regional Atmospheric Modeling System (RAMS). The design requirements for this upper-level cloud model include the following:

- Accurate computation of upper-level cloud features such as water and heat budgets which are important to the large-scale circulation and climate response.
- Limited memory and computational requirements.
- Adaptability to handle all types of upper-level clouds.
- Potential for upgrading model physics as improvements become available.
- Flexibilty of application in various large-scale models.

The purpose of this research is outlined below:

- Assess the feasibility of creating a model which meets the design requirements.
- Develop the core components of the cloud model.

- Test the performance of the cloud model against an explicit 1D simulation.
- Begin a preliminary optimization of the application of the cloud model in large-scale model.
- Discuss the implications of the results on the future development of the cloud model.
- Suggest areas for future research.

As mentioned above, the cloud model is designed to encompass all upper-level layer clouds which includes cirroform as well as stratiform clouds. To limit the scope of this research the development of the cloud model will be initially focused at cirroform clouds. Therefore, a short discussion of cirrus is provided in Chapter 2. The model description of both the cloud model and RAMS can be found in Chapter 3. A psuedo-1D format of RAMS was used with a fine vertical resolution to simulate several cirrus cloud cases. The sensitivity tests in Chapter 4 provide both an understanding of the RAMS physics response to various initializations as well as a control simulation for evaluating the cloud model results. A few selected cirrus cases from Chapter 4 are repeated using the nested cloud model in Chapter 5. A preliminary investigation is provided in Chapter 6 about the optimization of the cloud model implementation in a large-scale model. Summary and conclusions are presented in Chapter 7.

# Chapter 2

# CIRRUS

To limit the scope of this research, the development of the upper-level cloud model for application in a GCM will focus on modeling cirroform clouds. On average, cirrus cover 20% of the globe (Liou, 1986) but have only recently begun to be recognized as a critical component of the general circulation and climate. The difficulty in measuring cirrus properties have also hindered our understanding of the role of cirrus in our atmosphere. Several field projects in recent years have been directed towards improving the knowledge of cirrus. A review of the current understanding of cirrus characteristics follows.

## 2.1 Composition and structure of cirrus

Many categories of cirriform clouds exist such as cirrus, cirrostratus, cirrocumulus, cirrus, cirrus uncinus, cirrus spissatus, and cumulonimbus anvil. Liou (1986) described these clouds as sharing the common characteristics of crystalline habit of predominantly bullets, columns, and plates. The longer axis of the ice crystals are usually oriented horizontally. Ice crystal size distributions do vary from cloud to cloud being strongly dependent on temperature. Heymsfield (1975a) presented a typical ice crystal size spectra for both a cirrus uncinus and cirrostratus cloud (Fig. 2.1). The cirrus uncinus has a bimodal distribution with a secondary maximum around the 500 $\mu m$ size. Both clouds have the largest number of crystals at the smallest sizes. Arnott *et al.* (1993) also reported a minimum around 120 $\mu m$ to 140 $\mu m$ in the size spectra of ice measured in cirrus near Coffeyville, Kansas. Ice water content was also found by Heymsfield and Platt (1984) to be a strong function of temperature (Fig. 2.2).

Measurements taken at the First ISCCP (International Satellite Cloud Climatology Project) Regional Experiment (FIRE) on 28 October 1986 near Madison, Wisconsin were

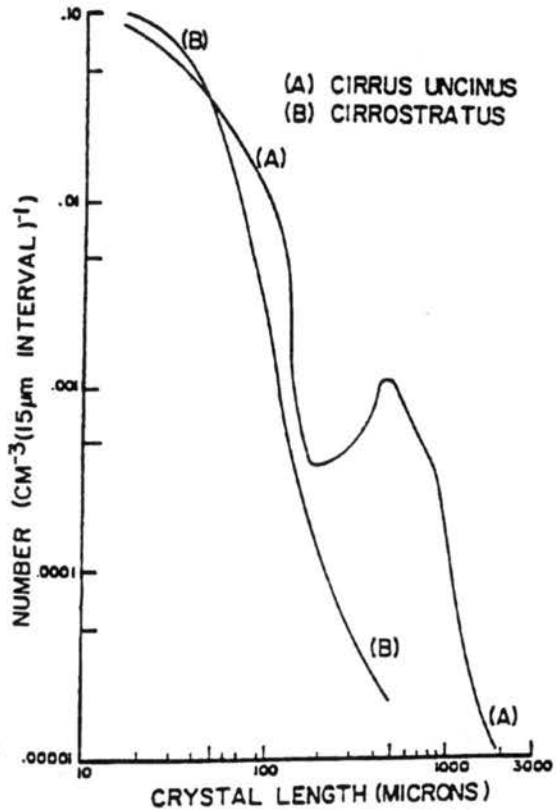


Figure 2.1: Ice crystal size distributions for cirrus clouds. (Liou, 1986)

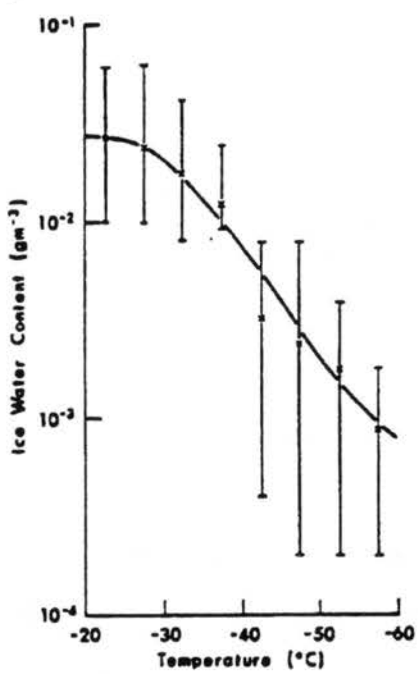


Figure 2.2: Ice water content as a function of temperature. Data from Heymsfield and Platt (1984). The solid curve represents the best fit to the data points. (Liou, 1986)

examined by Heymsfield *et al.*, (1990). For this particular cirrus, aggregation of small ice particles at temperatures as low as $-56°C$ were believed responsible for the creation of large ice particles (500-800 $\mu m$) not diffusional growth. The mass distribution spectrum broadened with decreasing height in the cloud to such an extent that approximately 30% of the ice mass was composed of aggregates. Aggregation provides a means for lowering the cloud base through gravitational settling of the large ice particles.

Cirrus macrophysical properties generally are cloud base temperatures colder than $-20°C$ at a wide range of altitudes from 4 to 15 km. A climatic value of cloud depth for cirrus appears to vary around 2 km (Liou, 1986 and Platt *et al.*, 1986). The turbulent nature of cirrus is generally two dimensional with the surrounding stable layers restraining the buoyant turbulent production of turbulent kinetic energy within the cirrus layer (Flatau *et al.*, 1990). Liou (1986) concluded that cirrus and cirrostratus were associated with upper level troughs and high pressure systems while cirrus uncinus were caused by mesoscale or synoptic disturbances. A summary of cirrus characteristics is shown in Table 2.1 (Liou, 1986).

## 2.2 Radiative properties of cirrus

Cirrus radiative properties are a function of cloud temperature, water content, ice crystal habit and ice crystal number distributions. The scattering properties of ice crystals are complicated by their nonspherical shapes and wide range of sizes (10 $\mu m$ – 1000 $\mu m$). Ackerman *et al.* (1988) concluded the single most important parameter for radiative properties in cumulonimbus anvil is the average ice water content (IWC). However, the vertical distribution of ice and the depth of the cloud will also strongly dictate the heating rates in the cloud (Fig. 2.3). Fig. 2.4 and Fig. 2.5 show infrared and solar heating rates as a function of ice water content for a cumulonimbus anvil (Ackerman *et al.*, 1988). The magnitude of the heating rate is strongly dependent on ice water content especially for values greater than 0.02 $g/m^3$.

Stackhouse and Stephens (1991) demonstrated that heating in a cirrus cloud is also dependent on location. Fig. 2.6 show heating rates for tropical and subartic winter atmospheres containing cirrus of the same ice water content. The difference in infrared radiative

Table 2.1: Aircraft observations of the composition and structure of cirrus clouds (Liou, 1986).

| Investigator | Cloud type | Synoptic condition | Composition |
|---|---|---|---|
| Weickmann (1945, 1947) | cirrostratus, cirrocumulus | – | column, bundle of columns<br>$L \sim 100 - 300\ \mu m$<br>$IWC \sim 0.01\ g/m^3$ |
| Heymsfield and Knollenberg (1972) | cirrus uncinus, cirrostratus, anvil | – | bullet rosette, column (75%), plate (25%)<br>$L \sim 600 - 1000\ \mu m$<br>$IWC \sim 0.15 - 0.25\ g/m^3$ |
| Hobbs *et al.* (1975) | cirrus, cirrostratus ($\sim 6 - 7\ km$) | upper level trough, frontal system | bullet, column, plate<br>$L \sim 100 - 700\ \mu m$<br>$IWC \sim 0.01 - 0.1\ g/m^3$ |
| Heymsfield (1975) | cirrus unicnus | Temp.$\sim$ -19 to $-58$°C, strong wind shear | bullet, rosette, column, plate<br>$L \sim 20 - 2000\ \mu m$<br>$IWC \sim 0.01 - 0.1\ g/m^3$ |
| | cirrostratus | | $L \sim 20 - 500\ \mu m$<br>$IWC \sim 0.01 - 0.15\ g/m^3$ |
| Heymsfield (1977) | stratiform ice clouds | Temp.$\sim$ $-10$ to $-60$°C frontal system jet stream | bullet rosette, column, thick plate<br>$L \sim 300 - 600\ \mu m$<br>$IWC \sim 0.001 - 1\ g/m^3$ |
| Varley *et al.* (1978-1980) | thin cirrus, cirrostratus ($\sim 8 - 9\ km$) | upper level trough high pressure system | bullet rosette, column, plate, $L \sim 20 - 2000\ \mu m$<br>$IWC \sim 0.001 - 0.05\ g/m^3$ |

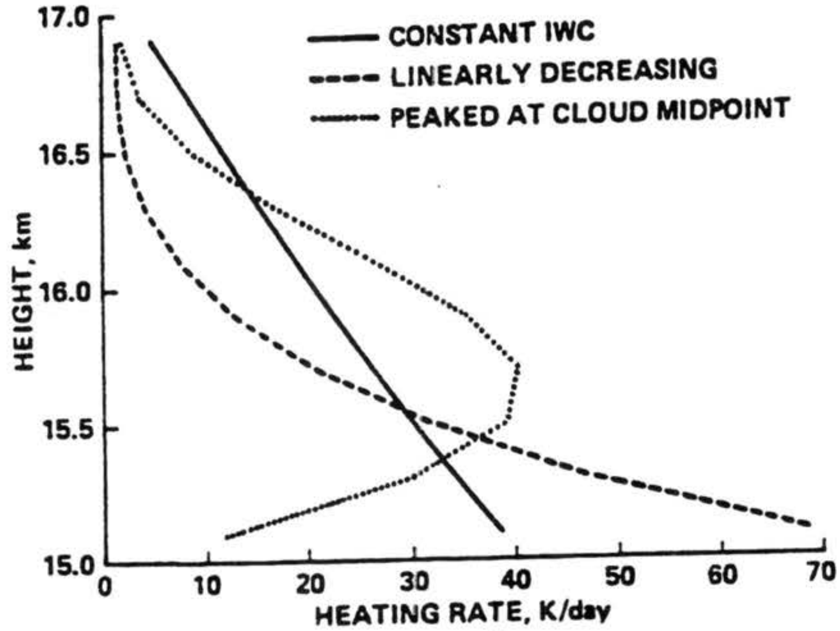


Figure 2.3: In-cloud heating rates as a function of height for three IWC profiles all with the same optical depth: constant with altitude (solid curve) linearly decreasing with altitude (dashed), and peaked at cloud midpoint (dotted). (Ackerman *et al.*, 1988)

heating rates was as large as 150 K/day while the solar heating rates varied as wide as 30 K/day.

Starr and Cox (1985a) developed a numerical cloud model to explictly model the physical processes in a weakly forced, thin cirrus. Among the conclusions made by Starr and Cox (1985b) was a significant difference between day and nightime cirrus simulations. In general the daytime cirrus case exhibited a more cellular but less dense structure. Infrared cooling at night which enhances ice production also limits the activity in the updraft regions of the cloud decreasing the the strength of the cloud-scale circulations.

The radiative heating rates calculated for a given cirrus cloud will be highly dependant on the sophistication of the radiation parameterization. A minimum requirement for capturing the interaction of the cloud and radiation would be a parameterization which includes a vertically-varying ice water content. For the solar wavelengths, a dependance on ice crytal habit and number concentration would also be desirable but is not available at this time for a GCM parameterization.

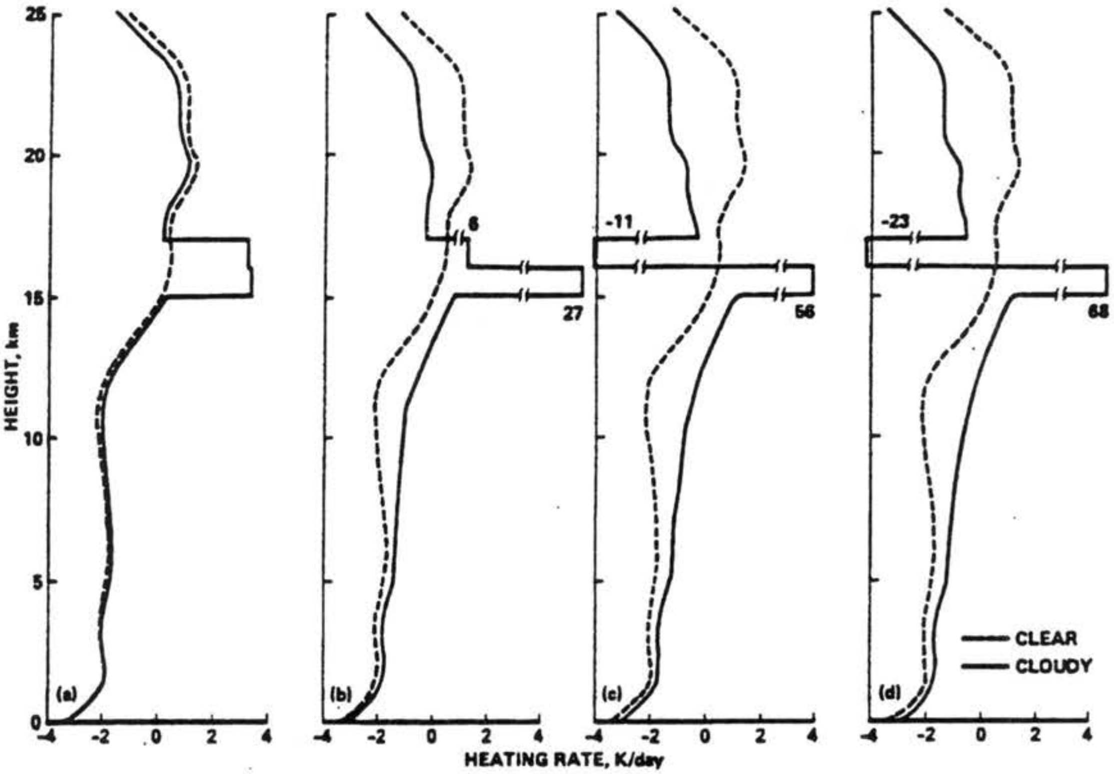


Figure 2.4: Infrared heating rate profiles for a clear atmosphere (dashed curves) and for atmospheres containing cirrus anvils (solid curves). Curves are shown for anvils with IWCs of (a) 0.002, (b) 0.02, (c) 0.06, and (d) 0.1 g/m$^3$. Note that the heating rates in the anvil itself in cases (b)-(d) are not plotted to scale. The numbers indicate the average heating rates in the top and bottom anvil layers. (Ackerman *et al.*, 1988)

## 2.3 Cirrus and the general circulation

Due to wide coverage, a variety of characteristics and location, cirrus continue to be an elusive element of the climate process. Cirrus play a critical role in the energy balance of the atmosphere such as in the tropics. Ramanathan (1989) believed the solar absorption by cumulonimbus anvil was responsible for warming and stabilizing the upper tropical troposphere. Differential heating from large cirrus shields also increase the zonal variance of temperature and generate eddy potential energy (Peixoto and Oort, 1992). The optically thin, nonblack cirrus also complicate the undestanding of the atmospheric response to climate change. The consensus among researchers appears to be that in order to truely understand the general circulation and the problem of climate change, an accurate representation of cirrus must exist in large-scale models.

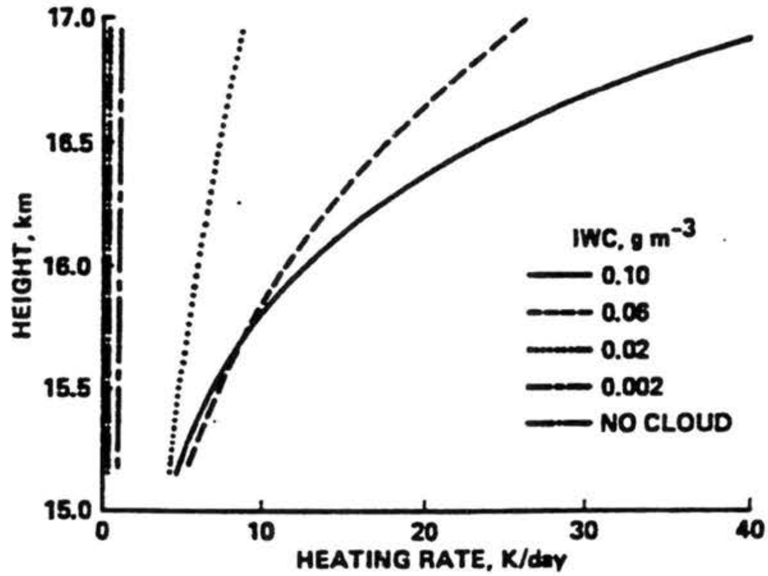


Figure 2.5: Solar heating rates as a function of height for IWCs of 0.002, 0.02, 0.06, and 0.1 g/m$^3$. The solar zenith angle is 53°. (Ackerman *et al.*, 1988)

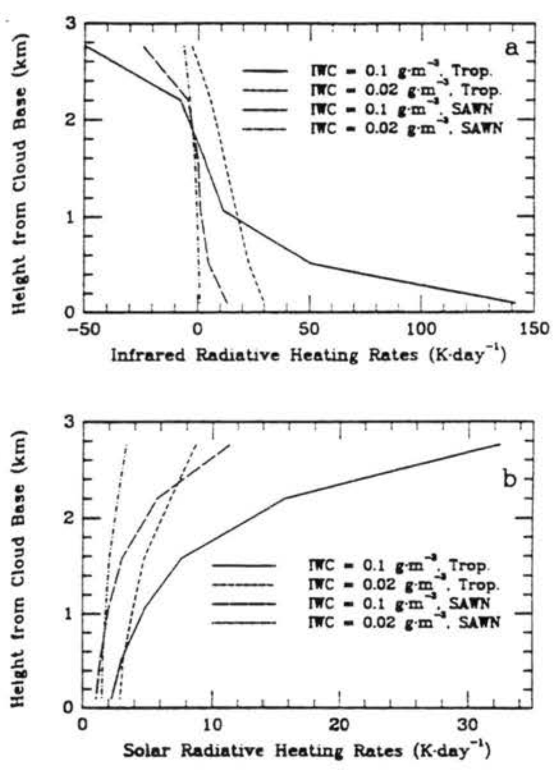


Figure 2.6: Radiative heating rates for a 3 km thick, uniform cirrus cloud with ice water contents of 0.02 and 0.1 g/m$^3$ imbedded in the tropical and subartic winter atmospheres as labeled in the (a) infrared and (b) solar wavelengths where the solar zenith angle is 61.3° and the surface albedo is 0.072. (Stackhouse and Stephens, 1991)

# Chapter 3

# MODEL DESCRIPTION

This chapter will outline the one-dimensional cloud model. A description of both the nested cloud model grid and components are provided. RAMS and it's function as a large-scale host model will also be presented. Changes necessary to use RAMS in a large-scale format are highlighted.

## 3.1 One dimensional cloud model

As in developing any computer model, the compromises between cost, speed, and accuracy must be kept in mind. The first priority for this cloud model is a design which adequately models the cirrus feedback to the large-scale flow. For this particular application, the cloud scale details are important only if they significantly impact the general circulation. Radiation and water transport are the first order feedbacks essential to capturing the physics of cloud interactions with the general circulation. Modeling precipitation is of secondary importance which may improve the accuracy of regional climatology in the GCM but will affect the large-scale circulation only indirectly through surface hydrology. For this research, which focuses primarily on cirrus, precipitation is usually virga made of small ice particles which moistens and cools the air below the cloud. This type of precipitation can have a significant impact on the radiative budget in the region of the cloud. These priorities must be considered in effectively designing the cloud model.

The framework for developing this cloud model starts with determining the physics that is essential to simulate the cloud. The physics of water vapor conversion to cloud species and precipitation will yield information for the radiative balance in the cloud. The complexity of the microphysics scheme will be chosen to optimize the accuracy while minimizing the computational cost of the model. The microphysics scheme in RAMS described by Walko *et* *al.* (1993) will be used for this model. The microphysics package includes eight species of water: total water, cloud water, small ice crystals (pristine ice), large-ice crystals (snow), aggregates, graupel, hail, and rain. Which of the 7 hydrometeor species to be included will be determined to minimize memory and computational costs.

The host model using this parameterization would be required to predict cloud water and ice or at least include the extra water variables in memory for treatment as tracers by advection and diffusional mixing. If the host model did not include any parameterization for microphysics, the cloud model could be triggered based on a cloud fraction scheme. The cloud model would then be responsible for initiating any cloud species. The nested cloud grid would diagnose any other species when spawned. Precipitation which may evaporate or reach the ground will be placed back onto the host grid accordingly. For these simulations, the nested grid extends to contain precipitation which falls from the main cloud layer. Any microphysical details besides mixing ratio such as particle number concentration, particle spectra, effective diameter, or particle shape could be retained for the radiation scheme. The complexity of this cloud parameterization is designed to match the sophistication of microphysics and radiation schemes expected in future GCMs.

A broadband radiation scheme based on the work by Chen and Cotton (1983) is called within the nested cloud model to model the interaction of cloud species and radiation. Radiation can either enhance or hinder ice production depending on the net heating rate. Destablization by cloud top cooling and cloud base warming will increase mixing and affect the longevity and liquid water contents of the cloud. To model buoyant mixing, a subgrid turbulence model will also be included which predicts the vertical velocity variance ($\overline{w'w'}$). ($\overline{w'w'}$) is treated as a scalar which could be transported from other parameterizations. The turbulence, microphysics, and radiation schemes were chosen as essential components in this 1D cloud model.

For this particular parameterization, the dynamics of cirrus suggest a 1D format may be adequate. The 1D model will minimize the number of calculations needed to simulate the dynamics of the problem. Fig. 3.1 demonstrates the speed of the cloud model to be strongly dependent on how often the radiative tendencies of potential temperature are computed. By limiting the frequency of updating radiative tendencies and the number of vertical levels, the cost of the cloud model can be reduced. The drawback of the 1D format, however, is the loss of explicitly-resolved cloud scale circulations. Hopefully, this limitation will not be critical; the main purpose of the parameterization is to capture the effects of the cloud which in turn affect the large-scale flow.

### 3.1.1 One dimensional nested grid

When, where, and how to spawn the nested cloud model are questions which must be answered for implementation of this parameterization. Nesting in the vertical direction and in time will allow the resolution necessary to model the important cloud processes. But once the cloud model has been triggered, the number of host timesteps to call the parameterization must be determined. If the cloud model is called every host timestep for the entire lifetime of the cloud, the model may prove to be too expensive to be useful. Possible solutions may be either to only call the model initially or less frequently than every timestep. Testing the cloud parameterization for optimal application will allow some design decisions to be made before implementation in a GCM.

Vertically nesting will provide the resolution necessary to model upper-level clouds, (less than 500 m, Randall, 1989) with minimal expense. Typical GCM vertical spacing is around 100 mb or on the order of 3000 m at the 200 mb level. The nest ratio of the cloud model can be set to obtain a vertical spacing on the order of 100 m. The grid is designed to nest vertically around the levels where cloud water and ice exist or could be triggered from a cloud fraction scheme. We will examine if a flexible nested cloud model is a viable solution to modeling upper-level clouds in a large-scale model.

Temporal nesting will provide the high resolution needed for fast processes of microphysics like collection, sedimentation and melting which cannot be modeled well in typical GCM timesteps (1 hour). Like the vertical nest ratio, the temporal nest ratio will be set to maintain a nested model timestep of 90 seconds. Sensitivity tests for both vertical and temporal resolution of the cirrus simulation will justify the choices sited here.

Calling the parameterization less frequently than every host timestep or only once for each new cloud will reduce the cost of this parameterization. Applying tendencies to potential temperature ($\theta$) and water variables for a determined lifetime of the cloud may prove

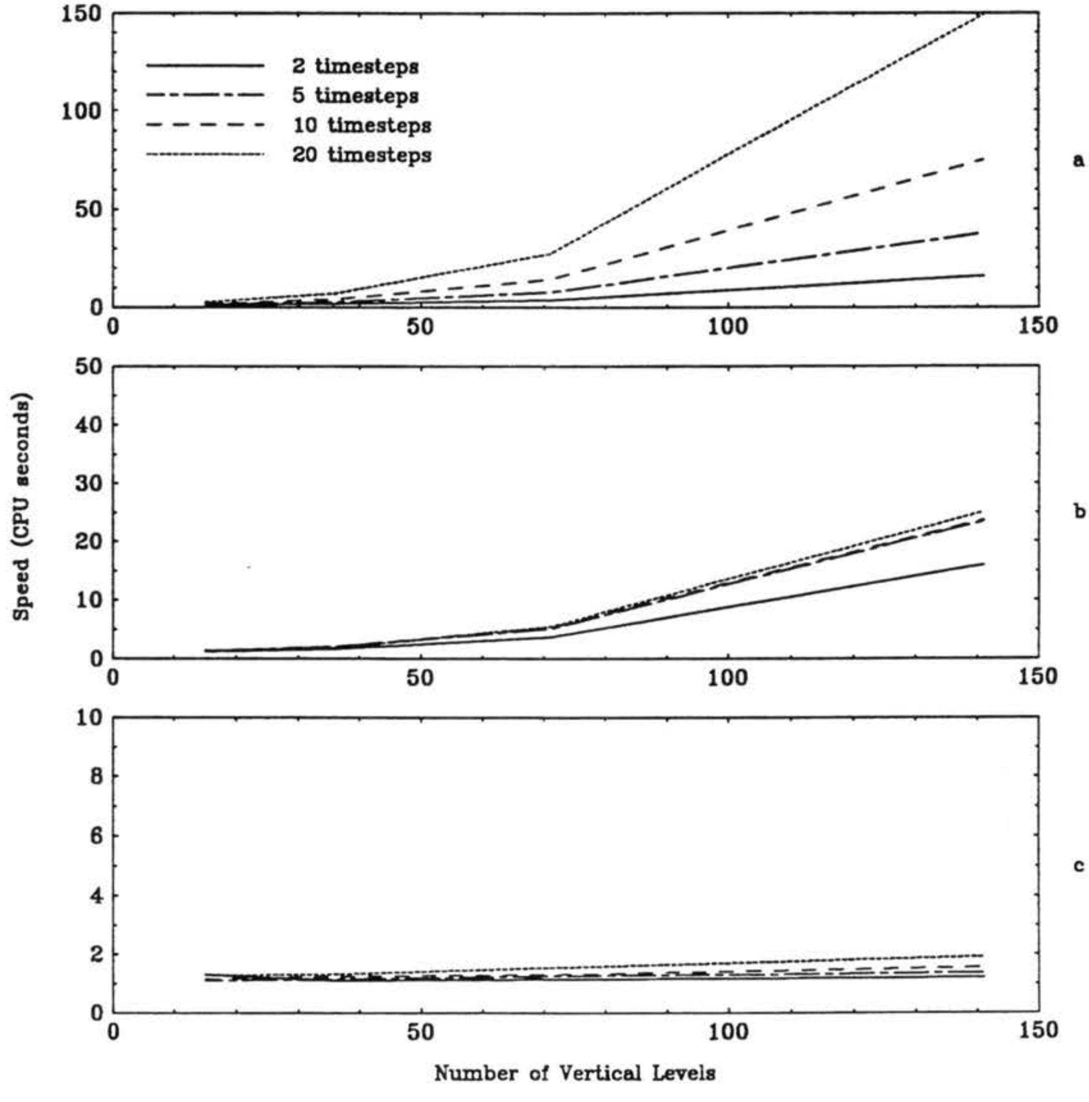


Figure 3.1: Computational speed of the cloud model for one host model timestep as a function of number of vertical levels for a range of nested cloud model timesteps when (a) the radiative tendencies are updated every nested cloud model timestep, (b) the radiative tendencies are updated at the beginning, middle, and end of the host model timestep, and (c) the radiative tendencies are not updated. The speed is based on calculations by an IBM RISC System 6000 model 370.

to be the best application of this parameterization. For testing this parameterization, the cloud model is spawned at the beginning of the host model simulation and called every host timestep. The results of a less frequently called model application will also be investigated.

The communication between the host model and the nested cloud model must be accomplished in such a manner as to avoid introducing errors. The host grid variables are linearly interpolated onto a nested grid. Tendencies computed by the cloud parameterization are averaged and returned to the host grid. Variables that are needed and returned by the nested grid are shown in Table 3.1. An example of the averaging on the nested variables is shown in Fig. 3.2. The discrepancy in the number of hydrometeor species between the cloud and host model is handled by summing the individual liquid and ice species together and returning the total tendency to the host model. Precipitation species are either summed as well or could be used in a precipitation parameterization. The detailed microphysical information can be retained for more sophisticated radiation schemes. Currently, for most GCMs, the only information needed by the radiation package is hydrometeor mass and cloud fraction. Tendencies for the vertical wind are also returned but may not significantly impact the larger circulations in the GCM.

Table 3.1: Variables passed to and returned by the nested cloud model

| Passed | Returned |
|---|---|
| Velocity: U, V, W | W tendency |
| Total water, cloud ice | Tendency of total water, cloud ice<br>Water and ice mixing ratio for radiation model |
| Exner function, density, potential temperature | Tendency of potential temperature |

The upper-level cloud model will be designed to have the flexibility to meet the changing needs of GCMs. The 1D, nested format allows a minimal requirement for grid points but will still provide the essential features of the upper-level clouds for the GCM. A range of microphysical information is available for different radiation scheme requirements. The optimal configuration of this cirrus parameterization will be determined to the highest extent possible at this design stage.

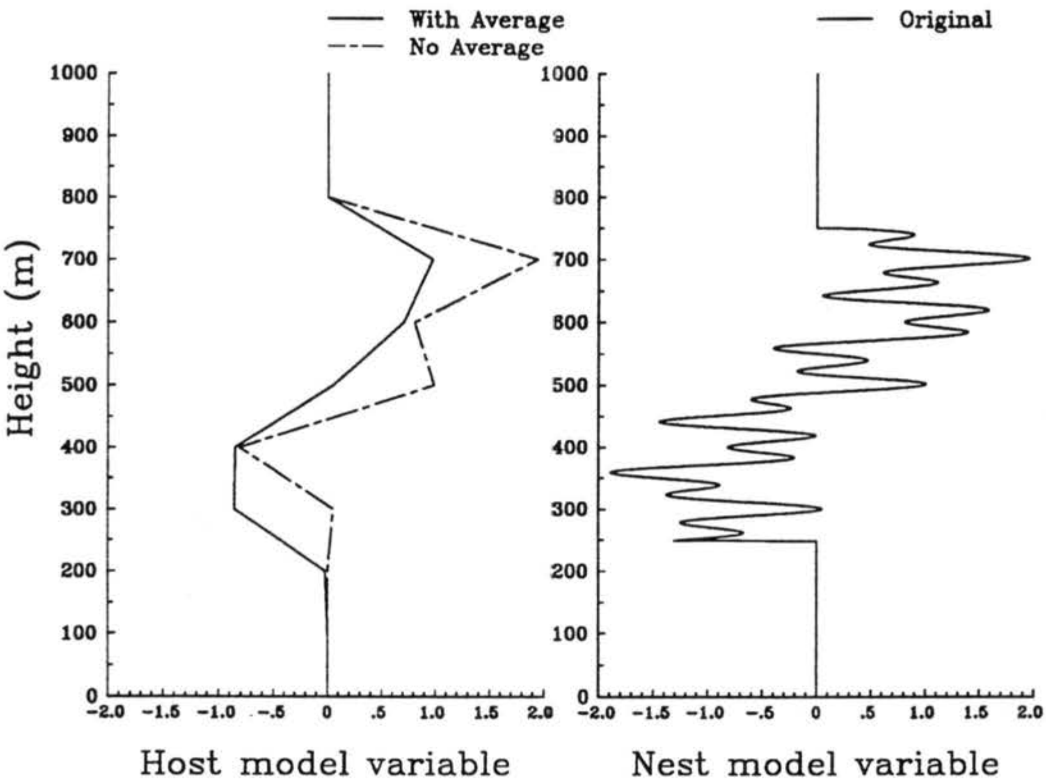


Figure 3.2: Example of averaging and not averaging nested model variables before interpolation back to the host model grid.

### 3.1.2 Turbulence parameterization

The subgrid turbulence model is adapted from the work by Weissbluth and Cotton (1993) and is converted to a 1D format. The closure is a level 2.5w as categorized by Mellor and Yamada (1974) and shown in Table 3.2. This model predicts a portion of the turbulent kinetic energy (TKE), vertical velocity variance ($\overline{w'w'}$) and includes terms for modeling buoyancy-driven mixed layers. Therefore, this sub-grid turbulence model is a good choice to predict the evolution of mixing forced by convective destabilization of radiation.

Because a 1D model was chosen over a 3D, cloud eddy resolving model, sub-grid diffusion will have to replace the mixing from cloud-scale circulations. Mesoscale variability created by convection or large-scale events seem to be associated with the presence of cirrus (Flatau *et al.*, 1990, Heckman and Cotton, 1993). If the host model included the prediction of $\overline{w'w'}$ in its diffusion or convection model, the triggering of the cloud parameterization

Table 3.2: Hiearchy of turbulence closures

| Level of closure | Predicted quantities includes |
|---|---|
| 2.5w | Vertical variance |
| 2.5 | Turbulent kinetic energy |
| 3 | Turbulent kinetic energy and potential temperature variance |
| 4 | All variances and covariances |

could be dependent on $\overline{w'w'}$. Research by Flatau *et al.* (1990) indicates cirrus clouds often exhibit 2D turbulence with horizontal velocity variance typically one order of magnitude larger than the vertical velocity variance. The dominant turbulent length scale in the vertical direction was on the order of 1 km. The cirrus tended to have a multilayer structure caused by the decoupling of layers in the stably stratified air. The individual layers in the cloud deck had thickness around 100 m to 400 m. A 1D cloud model would be able to resolve this layer structure if a high resolution initialization was available. Unfortunately, a GCM will not be able to provide this detailed information. So the primary goal for this parameterization is to model the general effect of cirrus on the large-scale circulations. To accomplish this goal, the application of this diffusion model will be adequate.

Dividing the variables as $W = \overline{W} + w'$ where the $\overline{W}$ is the grid-volume-average and $w'$ is the sub-grid scale deviation from the average, the 1D prognostic equation for the $\overline{w'w'}$ is given by

$$
\begin{aligned}
\frac{\partial}{\partial t}\overline{w'w'} &= \underbrace{-\overline{W}\frac{\partial}{\partial z}\overline{w'w'}}_{\text{ADV}} \underbrace{- 2\overline{w'w'}\frac{\partial \overline{W}}{\partial z}}_{\text{SHRPRD}} + \underbrace{2\beta_n \overline{w'\theta'_n}}_{\text{BUOPRD}} \\
&\quad \underbrace{-\frac{\partial}{\partial z}\overline{w'w'w'}}_{\text{EDYTRN}} \underbrace{- \frac{2}{\rho_o}\overline{w'\frac{\partial p'}{\partial z}}}_{\text{PRS}} \underbrace{- \frac{2}{3}\overline{\epsilon}}_{\text{DIS}} \,.
\end{aligned}
\tag{3.1}
$$

ADV, SHRPRD, EDYTRN are the mean advection, shear production, and eddy transport of $\overline{w'w'}$, respectively. PRS is the sub-grid scale pressure forces and DIS represents the dissipative force. BUOPRD is the production of $\overline{w'w'}$ by buoyancy which is defined by

$$\beta_n \overline{w'\theta'_n} = \begin{bmatrix} \frac{g}{\theta_n} \\ g(\frac{R_v}{R_a} - 1) \\ g(\frac{L_{lv\theta_0}}{C_pT} - R_vR_a \\ g(\frac{L_{iv\theta_0}}{C_pT} - R_vR_a \end{bmatrix} \begin{bmatrix} \overline{w'\theta'_{il}} \\ \overline{w'r'_t} \\ \overline{w'r'_l} \\ \overline{w'r'_i} \end{bmatrix}. \tag{3.2}$$

The dissipiation term is closed by assuming

$$\epsilon = \frac{1}{\sqrt{8}} \frac{q^3}{l} \tag{3.3}$$

where $q^2$ is the TKE and $l$ is the master length scale. To develop the relationship for the velocity variances and covariances as well as the diagnostic equations, a steady-state was assumed as well as neglecting the effects of advection, eddy transport, and precipitation. These assumptions required a restriction of the mixing coefficients when the turbulence changed rapidly. This limitation results in down-gradient transport of diagnosed quantities and restricting the turbulence to values that can be realized by the model.

The performance of this parameterization will be examined to determine the response of diffusion to destabilization from radiation. Production by buoyancy will most likely be the largest contributer to the $\overline{w'w'}$ tendency. The mixing created by this turbulence parameterization will affect the development of the cirrus by transport of water vapor and hydrometeors throughout the mixed layer.

### 3.1.3 Microphysics parameterization

The bulk microphysical parameterization from RAMS was used for this cloud parameterization to model the complicated interactions of several water species present in cirrus. The RAMS microphysical scheme will provide a detailed prognosis of water species behavior at a level of complexity appropriate for a GCM. The version of the RAMS microphysics used for this research predicts only one moment (mixing ratio) of the given size distribution except for the small ice category in which a second moment (total number concentration) is also predicted. The single moment scheme is less complex and more appropriate for this application than the more recent RAMS double moment microphysical scheme (Meyers, 1995). The single moment microphysical scheme is described in detail by Walko *et al.* (1993) but is summerized in this section.

A maximum of 8 water categories can be specified: total water, water vapor, small ice crystals (pristine ice), large ice crystals (snow), aggregates, graupel, hail, and rain. Graupel and hail were included in initial simulations of cirrus but were never present in significant numbers. Therefore, for all model simulations shown in this research, graupel and hail were not included. However, their description will still be included in this section. The two ice crystal categories, pristine ice and snow, represent a bimodal distribution of cloud ice (Harrington, 1994). Pristine ice diameter is assumed to be smaller than some arbitrary size currently set at 125 $\mu m$, while snow diameter is larger than 125 $\mu m$. Hail is a high density hydrometeor, graupel of intermediate density, and all other ice species of low density. Categorizing hydrometeor species in this manner allows a more accurate prediction of the hydrometeor's fall speed and rates of ventilation and collision. Cloud water is diagnosed as the residual of total water and all other categories. By including 8 categories of water, the bulk microphysical parameterization is capable of modeling the complex physics of clouds and precipitation.

The sources and sinks of the various hydrometeors include the processes of nucleation, vapor deposition/evaporation, collision, coalescence, and sedimentation. Cloud water and pristine ice are the only categories which nucleate from water vapor. Because cloud water is computed as a residual, the cloud water nucleation is approximated by assuming a user-specified, constant cloud droplet concentration. Pristine ice nucleation has several parameterizations to compute number of nucleated ice crystals created by the physical mechanisms of deposition, condensation-freezing, contact freezing, and homogeneous freezing of cloud and haze particles. Snow is created when pristine ice grows by vapor deposition beyond the bounding diameter between the two categories. Aggregates are formed by collection of pristine ice and snow. When snow or aggregates collect enough water through riming or by melting, the particle is recategorized as graupel. Likewise, when the percentage of liquid water of the graupel becomes large, the particle is redefined as hail. Rain is generated through an autoconversion parameterization of cloud water. Other processes of collection, melting, freezing, evaporation, and sedimentation modify the mass and total number concentration of each species. The complex growth and interaction of each hydrometeor are summerized in Table 3.3.

Table 3.3: Source and sinks of each hydrometeor

| Hydrometeor | Microphysical Process |
|---|---|
| Cloud Drops | • condense/evaporate instantaneously to maintain zero supersaturation |
| Pristine Ice | • deposition, condensation-freezing, contact freezing, and homogeneous nucleation from vapor |
| | • rime splintering of other ice categories |
| | • growth by vapor deposition to snow |
| | • loss by sublimation to vapor |
| | • loss by melt to rain |
| | • collection by other species |
| Snow | • pristine ice grown beyond 125 $\mu m$ by vapor deposition |
| | • growth by vapor deposition and riming |
| | • loss by sublimation to pristine ice and vapor |
| | • loss by melt to graupel or rain |
| | • collection by other species |
| Aggregates | • collection of pristine ice, snow and aggregate to aggregate |
| | • growth by vapor deposition and riming |
| | • loss by sublimation to vapor |
| | • melt to graupel |
| Graupel | • moderate to heavy riming and melt of pristine ice, snow, and aggregates |
| | • growth by vapor deposition and riming |
| | • loss by sublimation to vapor |
| | • collection by other species |
| | • melt to hail |
| Hail | • freezing of rain drops |
| | • melting of graupel |
| | • growth by vapor deposition |
| | • collection by other species |
| | • shedding excess liquid to rain |
| Rain | • collection of cloud drops |
| | • melting or shedding of hail to rain |
| | • growth by vapor deposition |
| | • loss by evaporation |

The mixing ratio of each water category is prognosed assuming the number concentration follows a generalized gamma distribution. The total number concentration ($N_t$) of pristine ice is also prognosed. Every other hydrometeor (except cloud water) has a user-specified mean diameter which is used to diagnose $N_t$. The generalized gamma distribution used as the basis function for each hydrometeor has a shape parameter ($\nu$) which can be set to unity to obtain the exponential or Marshall-Palmer (1948) distribution. The distribution function as described by Flatau *et al.* (1989) and Verlinde *et al.* (1990) is given by

$$f_{mg}(D) = \frac{1}{\Gamma(\nu)}\left(\frac{D}{D_n}\right)^{\nu-1}\frac{1}{D_n}\exp\left(-\frac{D}{D_n}\right) \tag{3.4}$$

where $D$ is the hydrometeor diameter and can range from zero to infinity, $\Gamma(\nu)$ normalizes the integral of $f_{mg}$ to unity over the range of zero to infinity, and $D_n$, the characteristic diameter, is used to nondimensionalize the function. Using the total concentration of the category, $N_t$, the number density distribution is defined by

$$n(D) = N_t f_{mg}(D). \tag{3.5}$$

The mean diameter, $D_{mean}$, of the distribution can be computed using

$$D_{mean} \equiv \int_0^\infty D f_{mg}(D)dD = D_n\frac{\Gamma(\nu+1)}{\Gamma(\nu)}. \tag{3.6}$$

Average mass ($\overline{m}$), and terminal velocity ($\overline{v_t}$) for the distribution when represented as power laws of the diameter are:

$$m = \alpha_m D^{\beta_m} \quad\rightarrow\quad \overline{m} = \alpha_m D_n^{\beta_m}\frac{\Gamma(\nu+\beta_m)}{\Gamma(\nu)} \tag{3.7}$$

$$v_t = \alpha_{vt} D^{\beta_{vt}} \quad\rightarrow\quad \overline{v_t} = \alpha_{vt} D_n^{\beta_{vt}}\frac{\Gamma(\nu+\beta_{vt})}{\Gamma(\nu)}. \tag{3.8}$$

All species except cloud drops fall. The shape of the particle in each category is defined by choosing the power law parameters, $\alpha$ and $\beta$.

The mixing ratio of the hydrometeor can be expressed by

$$r = \frac{N_t}{\rho_{air}}\alpha_m D_n^{\beta_m}\frac{\Gamma(\nu+\beta_m)}{\Gamma(\nu)} \tag{3.9}$$

where $\rho_{air}$ is the dry air density. Using this relationship, $N_t$ can be diagnosed when given $D_{mean}$, or $D_n$ will be diagnosed when $N_t$ is predicted (such as for pristine ice). The choices for the microphysical parameters are shown in Table 3.4. The power law parameters $\alpha_m$ and $\alpha_{vt}$ have dimensions of $kg[m^{\beta_m}]^{-1}$ and $m/s[m^{\beta_{vt}}]^{-1}$ respectively.

Table 3.4: Microphysical Parameters

| | |
|---|---|
| Cloud droplet concentration | 1E8 $number/m^3$ |
| Mean diameter | 400 $\mu m$, snow<br>400 $\mu m$, aggregates<br>1000 $\mu m$, graupel<br>1000 $\mu m$, hail<br>5000 $\mu m$, rain |
| $\alpha_m, \beta_m$ | 3.77E-3, 3, pristine ice<br>0.333, 2.4, snow<br>0.496, 2.4, aggregates<br>157, 3, graupel<br>471, 3, hail<br>524, 3, rain |
| $\alpha_{vt}, \beta_{vt}$ | 316., 1.01, pristine ice<br>4.836, 0.25, snow<br>3.084, 0.20, aggregates<br>93.3, 0.5, graupel<br>161, 0.5, hail<br>149, 0.5, rain |
| Minimum ice crystal mass | 1E-12 $kg$ |
| $\nu$ for the gamma distribution | 1, cloud water<br>1, pristine ice<br>4, snow<br>4, aggregates<br>1, graupel<br>1, hail<br>1, rain |

To demonstrate the behavior of the ice nucleation schemes (Meyers *et al.*, 1992 and DeMott *et al.*, 1993), a hypothetical sounding with 50% ice supersaturation ($SS_i$), between 600 mb and 100 mb was used to initialize the microphysical parameterization. The relative humidities before and after one model timestep of 90 seconds is shown in Fig. 3.3. Note that the sounding is saturated with respect to liquid from 600 mb to about 250 mb. Any water vapor above liquid saturation is instantly removed and placed into the residual cloud water category. The region between 300 mb and 200 mb shows the largest removal of water vapor with a sharp decrease of mass removal above this layer.

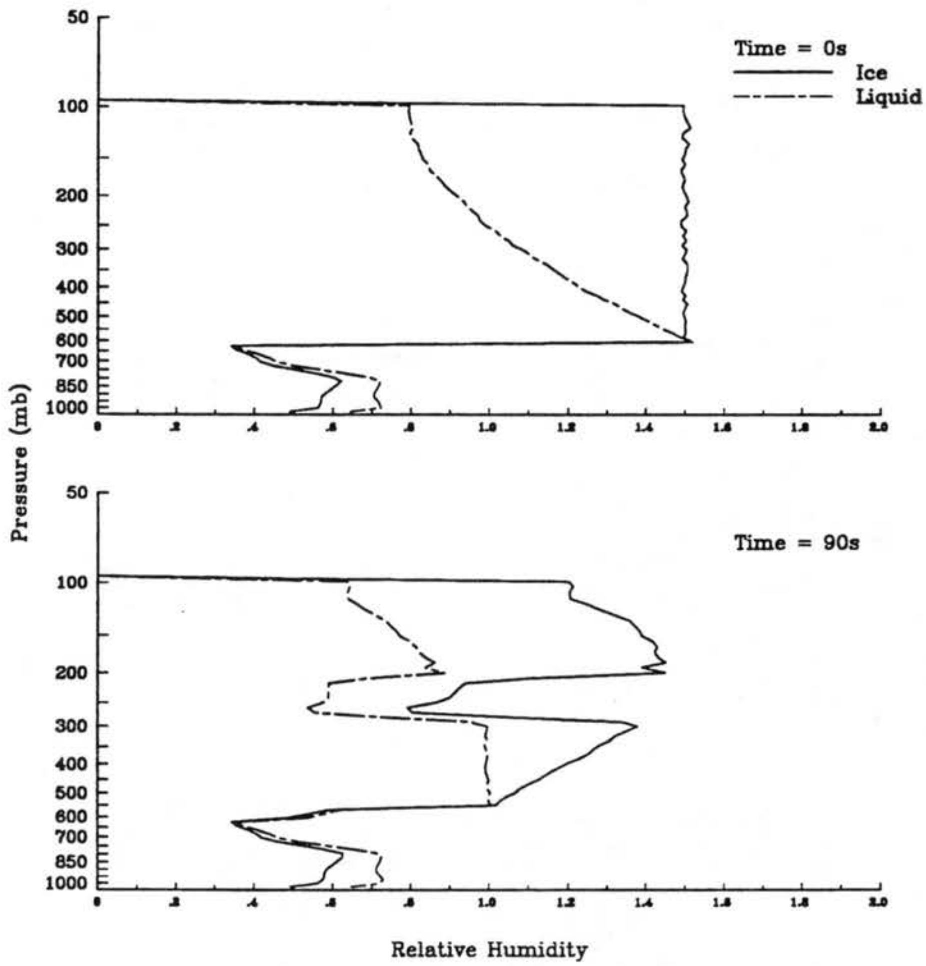


Figure 3.3: Relative humidities before and after nucleation.

The water mass nucleated into the pristine ice category in the 90 second timestep can be seen in Fig. 3.4. The microphysics scheme limits the vapor mass nucleated in one timestep to half of the available water vapor. Therefore, the displayed nucleation by haze, depositional/condensational-freezing, and contact freezing are numerically limited to the curve labeled "actual". The largest contribution to the nucleation is the homogeneous nucleation of haze in the area between 300 mb and 200 mb. For haze nucleation to occur the temperature must be colder than $-35°C$ and relative humidity with respect to liquid ($RH_l$), must be greater than 82%. The homogeneous nucleation of cloud drops also contributes to the nucleated mass in the region from 300 mb to 250 mb where temperature is colder than −30°C and cloud water is present. The nucleation of cloud water is an order of magnitude smaller than the contribution from the actual haze nucleation. Above 200 mb, where the $RH_I$ drops below 82%, the main contributer to the nucleated mass is the mechanism of deposition. No pristine ice mass is created by contact freezing.

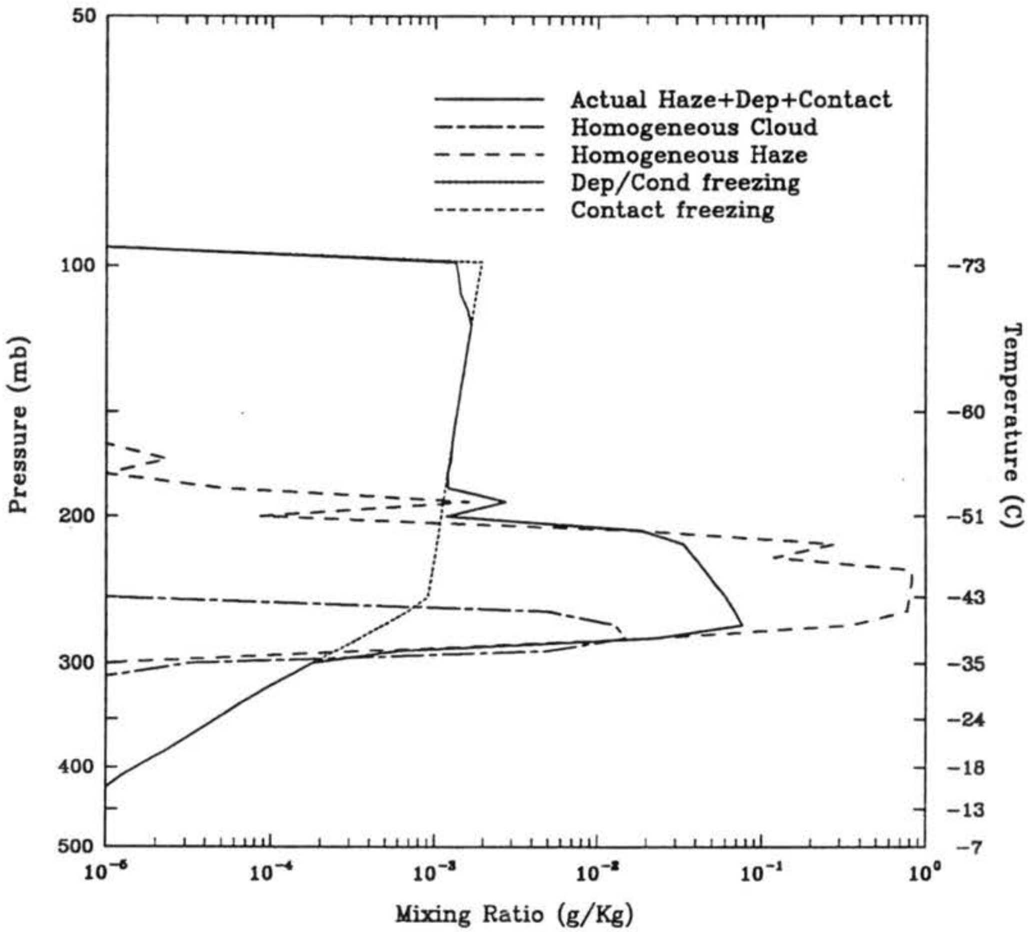


Figure 3.4: Mixing ratio of pristine ice nucleated in a 90 second timestep.

When significant amounts of hydrometeors fall from the main cloud layer, either the nested grid must extend to include the precipitation or the mass could be returned to the host layer below the nested grid. The latter option would allow the host model to explicitly handle precipitation. The precipitation trails from cirrus have been suggested to be likely sources of seeding ice crystals and preactivated ice nuclei for lower clouds (Braham and

Spyers-Duran, 1967). Further research would be needed to determine if this feature could be captured in GCM simulations. More likely to be modeled is the moistening and cooling from the evaporating virga in the subsaturated subcloud layer. A parameterization for ice precipatation may be necessary in the future to restrict the cost of the cloud model.

This microphysics scheme has the flexibility to examine up to 7 hydrometeors with several different physical mechanisms which cannot be explicitly represented in a GCM. Applying this microphysics in the nested cloud model will improve the GCM representation of upper-level clouds.

### 3.1.4 Radiation parameterization

To determine the cloud feedback, the RAMS broadband, flux emissivity radiation model developed by Chen and Cotton (1983), hereafter as CC, was modified to include the effects of cloud ice. The radiation routine is called every 450 seconds or every 5 nested timesteps to update the radiative tendency of potential temperature. Currently, the information of the whole vertical column is passed to the radiation routine. In the future, the radiation scheme could be modified to compute the flux divergence only within the cloud layer making the assumption that the fluxes near cloud top and bottom remain unchanged during the host timestep if necessary to limit the number of calculations. The basic format of the radiation model remains unchanged. The modifications to include the effects of ice was based on work by Starr and Cox (1985a) and Liou (1992). The original heating rates computed from these parameterizations using Stephens (1978) original model for water clouds is significantly changed when modeled as ice.

The broadband, flux emissivity model was originally developed by CC for simulating stratocumulus clouds and has been used in RAMS since that research. The scheme is based on the model presented by Stephens (1978) for water clouds with the added feature of cloud fraction. However, cloud ice was treated as liquid water in the model.

To investigate the ability of this cloud parameterization to create significant radiative feedbacks, the radiation model should include the distinction between ice and liquid water species. Emissivity and optical depths of ice based on the parameterizations of Starr and Cox (1985a) and Liou (1992) are shown in Figs. 3.5 and 3.6 as compared to the water parameterizations by Stephens (1978). For the same mass, the water parameterization yields an optical depth about one order of magnitude larger; therefore, treating ice as water would overestimate shortwave heating. Likewise, for water path, the emissivity is an order of magnitude smaller for ice than for liquid. This difference results in an overestimation of longwave cloud base heating and cloud top cooling if the ice were treated as water. This example supports the need to incorporate ice into the radiation model.

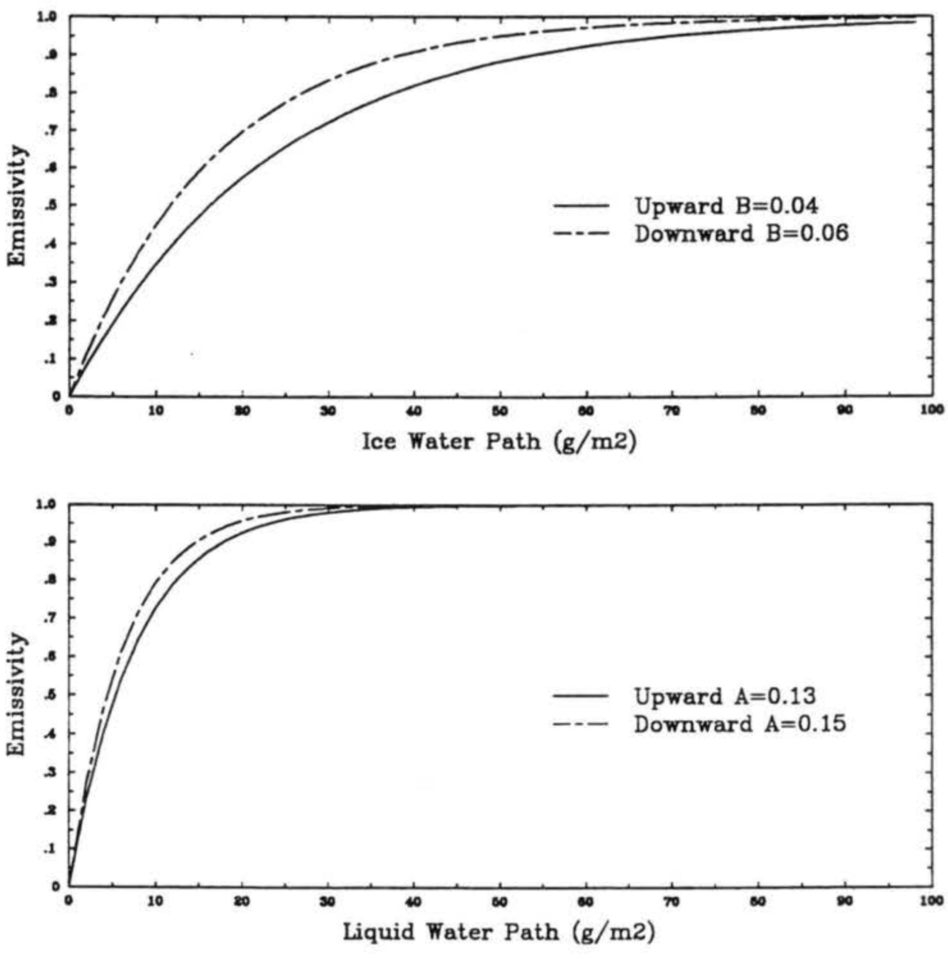


Figure 3.5: Ice and water emissivities as a function of water path.

The radiation model is described below with the addition of ice effects highlighted. Improvements in the radiation code by Drs. Greg Tripoli and Takmeng Wong (personal communication) have also been included. The longwave, broadband, flux emissivity model was developed by Stephens (1978) to imperically include the absorption by water vapor and

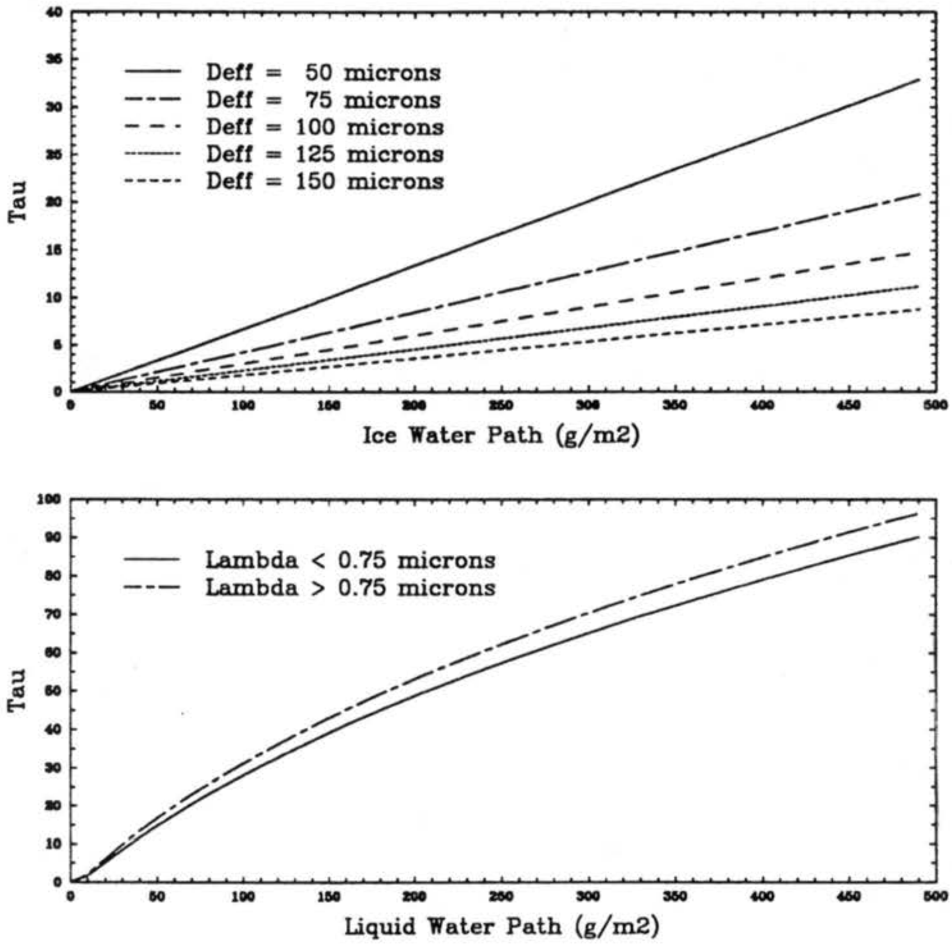


Figure 3.6: Ice and water optical depths as a function of water path where Deff is the effective diameter of the ice particle and Lambda is the wavelength.

carbon dioxide. When cloud water or ice is present, the layer emissivity is replaced by a mixed emissivity originally defined by Herman and Goody (1976) and expanded to include ice to be

$$(1-\epsilon_m) = (1-\epsilon_c)(1-H\epsilon_l)(1-H\epsilon_i) \tag{3.10}$$

where $\epsilon_m$, is the mixed emissivity. $\epsilon_c$, $\epsilon_l$, $\epsilon_i$, are the clear, liquid cloud, and ice cloud emissivities respectfully. $H$ is the cloud fraction which is either zero or unity for these simulations. Note that this formulation of mixed emissivity encompasses the definition for a layer with no cloud, liquid cloud, ice cloud, or mixed phased cloud. The emissivity for liquid cloud is given by

$$\epsilon_l \uparrow\downarrow = 1 - \exp(-a \uparrow\downarrow W) \tag{3.11}$$

with the coefficients $a \uparrow = 0.13$ and $a \downarrow = 0.158$. $W$ is the liquid water path $(g/m^2)$ defined by

$$W = \int \rho_o r_l dz \tag{3.12}$$

where $\rho_o$ is the density of dry air and $r_l$ is the mixing ratio of liquid water. The emissivity for an ice cloud is likewise given by (Starr and Cox, 1985a)

$$\epsilon_i \uparrow\downarrow = 1 - \exp(-b \uparrow\downarrow I) \tag{3.13}$$

with the coefficients $b \uparrow = 0.04$ and $b \downarrow = 0.06$. $I$ is the ice water path $(g/m^2)$ defined by

$$I = \int \rho_o r_i dz \tag{3.14}$$

where $r_i$ is the mixing ratio of ice water.

The shortwave model for a cloudy layer was parameterized as a function of solar zenith angle and liquid or ice water path by considering two spectral regions, an absorbing and nonabsorbing region. For the nonabsorbing region of liquid water ($\lambda < 0.75\mu m$) where the single scatter albedo ($\omega_o$) is 1, the reflectance, transmission, and absorption are computed based on the backscatter fraction ($\beta$), the cosine of the zenith angle ($\mu_o$), and the cloud optical thickness ($\tau_N$) using

$$\begin{aligned} Re_1(\mu_o) &= \frac{\beta_1(\mu_o)\tau_N/\mu_o}{1+\beta_1(\mu_o)\tau_N/\mu_o} \\ Tr_1(\mu_o) &= 1 - Re_1(\mu_o) \\ A_1(\mu_o) &= 0. \end{aligned} \tag{3.15}$$

For the absorbing spectrum ($\lambda > 0.75\ \mu m$), these relationships are used

$$
\begin{aligned}
Re_2(\mu_\circ) &= (u^2-1)[\exp(\tau_{eff})-\exp(-\tau_{eff})]/R \\
Tr_2(\mu_\circ) &= 4u/R \\
A_2(\mu_\circ) &= 1-Re_2(\mu_\circ)-Tr_2(\mu_\circ)
\end{aligned}
\tag{3.16}
$$

where

$$
\begin{aligned}
u^2 &= [1-\omega_\circ+2\beta_2\omega_\circ]/(1-\omega_\circ) \\
\tau_{eff} &= [(1-\omega_\circ)(1-\omega_\circ+2\beta_2\omega_\circ)]^{1/2}\tau_N/\mu_\circ \\
R &= (u+1)^2\exp(\tau_{eff})-(u-1)^2\exp(-\tau_{eff}).
\end{aligned}
\tag{3.17}
$$

The optical depth for the nonabsorbing region of the cloud layer ($\lambda < 0.75\ \mu m$) for a given liquid water path is

$$\log_{10}(\tau_N) = 0.2633 + 1.7095\log_e[\log_{10}(W)]. \tag{3.18}$$

Likewise, for the optical depth in the absorbing region of the cloud layer ($\lambda < 0.75\ \mu m$)

$$\log_{10}(\tau_N) = 0.3492 + 1.6518\log_e[\log_{10}(W)]. \tag{3.19}$$

For ice in both spectral regions (Liou, 1992)

$$\tau_N = I(-6.656E-3+3.686/D_{eff}) \tag{3.20}$$

where $D_{eff}$ ($\mu m$) is the effective diameter of ice taken to be $100\mu m$. The integrated reflectance, transmission, and absorption for a cloudy layer is

$$
\begin{aligned}
Re &= 0.517Re_1+0.483Re_2 \\
Tr &= 0.517Tr_1+0.483Tr_2 \\
A &= 0.483A_2.
\end{aligned}
\tag{3.21}
$$

The parameters, $\beta_1$ and $\beta_2$ are backscatter fractions of monodirectional incident radiation for a given zenith angle for liquid water. The backscatter fractions and single scatter albedo ($\omega_o$) are parameterized as functions of liquid water optical depth ($\tau_l$) and cosine of the solar zenith angle ($\mu_o$). These parameters have been tuned by Stephens (1978) to fit a set of data representing various types of liquid water clouds.

To apply these relationships to ice, the backscatter fraction and single scatter albedo have been set to representative values, $\beta = 0.17$ and $\omega_o = 0.98$, and are no longer a function of $\mu_o$ and $\tau$. This application is likely to prevent the same level of accuracy achieved for water clouds to be reached for ice clouds. For that accuracy to be possible, another extensive set of ice cloud data would be needed to perform a regression analysis to derive new functions of $\mu_o$ and $\tau$ for $\beta$ and $\omega_o$. So when only liquid water is present the standard radiation model is used. When only ice water is present, the Liou (1992) relationship is used to find optical depth, and $\beta$ and $\omega_o$ are set to constant values. For the case when both liquid and ice water exist, the optical depths for liquid and ice are added and used to find $\beta$ and $\omega_o$ as if all the water mass were liquid.

Improvements suggested by Drs. Greg Tripoli and Takmeng Wong (personal communication) were implemented to improve the shortwave model. The changes are highlighted below. The transmittance of the clear atmosphere is defined by the summation of an exponential function which originally had three terms. Dr. Takmeng Wong (personal communication) improved this exponential fit by increasing the number of terms to eight. Following the original derivation presented by Stephens (1977),

$$\begin{aligned} Tr(m) &= \sum_{n=1}^{8} W_n \exp(-K_n m) \\ &= \sum_{n=1}^{8} W_n Tr_n(m) \end{aligned} \tag{3.22}$$

where $m$ is the optical path length of water vapor ($g/m^2$). $W_n$ is the weighting function, and $K_n$ is the equivalent extinction coefficient shown in Table 3.5.

Table 3.5: Coefficients for the transmittance of a clear atmosphere

| $n$ | 1 | 2 | 3 | 4 | 5 | 6 | 7 | 8 |
|---|---|---|---|---|---|---|---|---|
| $W_n$ | 0.647 | 0.0698 | 0.1443 | 0.0584 | 0.0335 | 0.0225 | 0.0158 | 0.0087 |
| $K_n$ | 0.00004 | 0.002 | 0.035 | 0.377 | 1.95 | 9.40 | 44.6 | 190.0 |

CC used the division of the spectrum to define the layer transmission, reflectance, and absorption for a clear sky given by

$$\begin{aligned} Tr_{n/l} &= \exp[-K_n(m_{l+1} - m_l)] \\ A_{n/l} &= A_n(m_{l+1}) - A_n(m_l) \\ &= Tr_n(m_l)(1 - Tr_{n/l}) \\ Re_{n/l} &= 1 - Tr_{n/l} - A_{n/l} \end{aligned} \tag{3.23}$$

where $m_l$ ($g/cm^2$) is the total optical length of water vapor above the $l$th layer, and $Tr_n(m_l)$ is the transmittance of the atmosphere above the $l$th layer and is defined by

$$Tr_n(m_l) = \exp(-K_n m_l). \tag{3.24}$$

To model a clear-cloud mixed atmosphere, CC generalizes the definition of $Tr_n(m_l)$ to

$$Tr_n(m_l) = \prod_{i=1}^{l-1} Tr_{n/i}. \tag{3.25}$$

Using cloud fraction ($H$), the transmission, absorption, and reflectance are weighted linearly by $H$ to obtain an approximation of the clear-cloud radiative parameters. The final set of equations are written as

$$\begin{aligned} Tr_{n/l} &= H(0.517Tr_1 + 0.483Tr_2) + (1 - H)\exp[-K_n(m_{l+1} - m_l)] \\ A_{n/l} &= 0.483HA_2 + A_{ozn/l} + (1 - H)Tr_n(m_l)(1 - Tr_{n/l}) \\ Re_{n/l} &= H(0.517Re_1 + 0.483Re_2) \\ Tr_{n/l} &= 1 - A_{n/l} - Re_{n/l} \\ Tr_n(m_{l+1}) &= \prod_{i=1}^{l} Tr_{n/i} \end{aligned} \tag{3.26}$$

where $A_{ozn/l}$ is the ozone absorption which only has a significant value at the top boundary.

Note for this version, a $(1-H)Re_{clear}$ term representing Rayleigh scatter has been replaced by an effective Rayleigh surface albedo (Greg Tripoli, personal communication). The effective Rayleigh albedo ($\alpha_{ra}$), is calculated by

$$\begin{aligned}
\overline{Ra} &= \frac{P \times 0.219E-6}{1+0.816\mu_o} \\
\overline{\overline{Ra}} &= 1.44E-7 \times P \\
\alpha_{ra} &= \overline{Ra} + \frac{\alpha(1-\overline{Ra})(1-\overline{\overline{Ra}})}{(1-\alpha\overline{\overline{Ra}})}
\end{aligned} \tag{3.27}$$

where $\alpha$ is the original surface albedo and $P$ is the surface pressure (Pa).

With the addition of ice to this shortwave model, a correction was necessary in the original equations for a clear-cloud mixed atmosphere. In the original calculation, the backscatter fraction and single scatter albedo were computed as functions of the solar zenith angle and optical depth by Stephens (1978) based on a data set of liquid water clouds ranging in optical depth of 1 to 500. The two-stream radiation model for a cloudy layer was parameterized by using the observationally fit backscatter fraction and single scatter albedo. This cloudy layer parameterization would inherently include water vapor ($H_2O_g$) and carbon dioxide ($CO_2$) absorption and reflectance. But when the cloud consists of only ice, the parameters $\beta$ and $\omega_o$ were arbitrarly set to prescribed values independent of the optical depth and solar zenith angle. When the optical depth falls within the range of the original data set (1-500), the ice cloud will not inherently include $H_2O_g$ and $CO_2$ effects. The two-stream cloud calculation will only represent the cloud particles in the region of the cloud. As mentioned earlier, the optical depth of ice for a given amount of mass is approximately an order of magnitude smaller than liquid. This fact combined with the vertical resolution of the model and small mass amounts found in typical cirrus clouds results in model layers with ice optical depths smaller than unity. As the optical depth approaches zero, the transmittance goes to unity while absorption and reflection go to zero. But because the volume of the layer occupied by cloud, $H$, does not explicitly include clear sky absorption and reflection, that part of the grid box is erroneously treated as transparent. To avoid this error, a different set of equations are used when the absorption of the ice particles is less than the absorption by the clear sky.

When only ice is present and the absorption of the ice particles is less than the clear sky, the following set of equations replace Eqn. 3.26:

$$\begin{aligned}
Tr_{n/l} &= \exp[-K_n(m_{l+1} - m_l)]\{(1-H) + H(0.517Tr_1 + 0.483Tr_2)\} \\
A_{n/l} &= 0.483HA_2 + [A_{ozn/l} + Tr_n(m_l)(1 - Tr_{n/l})] \times \\
&\quad [(1-H) + H(0.517Tr_1 + 0.483Tr_2)] \\
Re_{n/l} &= H(0.517Re_1 + 0.483Re_2) \\
Tr_{n/l} &= 1 - A_{n/l} - Re_{n/l} \\
Tr_n(m_{l+1}) &= \prod_{i=1}^{l} Tr_{n/i}. \qquad (3.28)
\end{aligned}$$

These equations have been derived by assuming that in the cloudy portion of the grid box, the transmittion of $H_2O_g$, $CO_2$, and ice crystals multiply and that the reflectance by the $H_2O_g$ and $CO_2$ is zero. This assumtion was possible by the application of an effective Rayleigh albedo.

The radiation package of RAMS has been modified to include ice effects without inhibiting the model's original computational speed. The new radiation model will hopefully yield a more realistic measurement of feedback of the ice clouds to assist in the testing of this upper-level cloud parameterization scheme.

## 3.2 RAMS (Regional Atmospheric Modeling System)

The Regional Atmospheric Modeling System (RAMS) is a mesoscale model developed at Colorado State University (CSU). To test this parameterization, RAMS was set up in a large-scale format to act as a GCM. RAMS was the natural choice for the first design phase for two reasons. First, developing a parameterization on a full three dimensional GCM would be costly where as RAMS set up in a large-scale but limited area can be run cheaply, quickly, and effectively. Secondly, the physics used in the cloud model was adapted from already existing RAMS code; therefore, the turbulence, radiation, and microphysics routines were in a compatible format. A description of RAMS and any modifications are given below.

RAMS was created by combining a non-hydrostatic cloud model (Tripoli and Cotton, 1982) with a hydrostatic, mesoscale model (Mahrer and Pielke, 1977) in 1986. The variables predicted include the components of velocity, ice-liquid water potential temperature, perturbation Exner function, total water, and any specified hydrometeor mixing ratio on an energy conserving Arakawa-C grid (Arakawa and Lamb, 1981). Other quantities such as pressure, potential temperature, and mixing ratios of water vapor and cloud drops are diagnosed. Leapfrog time differencing with an Asselin filter and time-splitting scheme (Klemp and Wilhelmson, 1978) is used to advance the velocity while a second order advection scheme is used for all other predicted variables. The model top boundary condition prevents mass flux across the boundary which requires damping of gravity waves. When the model timestep was on the order of 90 seconds, Rayleigh friction was applied to the top five model levels to dampen gravity waves (Heckman, 1991). For model simulations in which the timestep was on the order of 15 minutes, the Rayleigh friction was not necessary. Cyclic lateral boundary conditions created a large-scale infinite domain, in essence, a 1D model. The radiation model is as described in section 1.1. The soil model was developed by Tremback and Kessler (1985) with 11 vertical levels. The bottom boundary condition was treated as homogeneous soil type and moisture to create a 1D version of RAMS. For further details of RAMS, a general description of the model can be found in Tripoli and Cotton (1982), Cotton *et al.* (1982), Tremback *et al.* (1985), Tripoli (1986), Tremback (1990), Pielke *et al.* (1992), and Walko *et al.* (1994).

Changes to the standard RAMS configuration were needed to create a psuedo-1D format. The microphysics was set up to allow a general cloud water and ice category with diagnosed rain and snow to mimic a GCM with limited microphysics. RAMS is an established, proven model with physics that can be easily adapted for use in this cloud parameterization. Several important design decisions can be made before implementing the model in a GCM where each sensitivity test and modification is more expensive.

### 3.2.1 Grid Configuration

RAMS was developed as a limited-area or regional model. Therefore, to be used as a large-scale, host model, a special set up is required. For the psuedo-1D format, RAMS has 5 grid points of 1000 km grid spacing in the horizontal direction using cyclic boundary conditions. Cyclic boundary conditions create an infinite domain with characteristics of the large-scale climate of interest. A range of 11-170 vertical layers with 2000 m - 175 m grid spacing was used for various simulations. This grid configuration is ideal to force the physics to behave one dimensionally. The surface vegetation, surface moisture, and terrain were specified as homogeneous to maintain a psuedo-1D environment.

RAMS is a flexible model which allows various configurations for testing this parameterization. Vertical and temporal resolution of the host model can be modified to determine the minimum requirements needed by a GCM using a cloud parameterization to include the effects upper-level clouds. RAMS cannot be used to measure the actual cloud feedback on the large-scale circulation, but the relative importance of the cloud feedback can be estimated by calculating the magnitude of the radiative feedback and water budget tendency. RAMS provides a useful framework to develope a cloud parameterization but must eventually be replaced by a true GCM.

### 3.2.2 Microphysics parameterization

The microphysics described for the cloud model was taken from RAMS and so a detailed description will be omitted here. However, some slight changes were necessary to create two general categories of cloud water and ice to mimic a hypothetical, optimal scheme in a GCM. The mixing ratios of both total water and ice were predicted as well as the ice crystal number concentration. Cloud water is diagnosed as discussed earlier. The shape parameter for the ice category ($\nu_h$) was assumed to be unity. To divide the one host model ice category into the two nested model ice categories of pristine ice and snow, a bounding diameter, $D_b = 125\ \mu m$, was selected. All ice below this diameter is placed into the pristine ice category; likewise, all ice larger than $D_b$ is assigned to the snow category. The division of ice can conserve two of the three properties of mass, total number concentration, and characteristic diameter. The expressions for placing the host ice into the lower (smaller) and upper (larger) ice categories is as follows:

$$
\begin{aligned}
N_l &= \int_0^{D_b} n(D)dD && (3.29)\\
N_u &= N_h - N_l && (3.30)\\
r_l &= \frac{1}{\rho_{air}}\int_0^{D_b} m(D)n(D)dD &&\\
&= \frac{1}{\rho_{air}}\int_0^{D_b} \alpha_l D^{\beta_l}\frac{N_h}{\rho(\nu_h)}\left(\frac{D}{D_b}\right)^{\nu_h-1}\exp\left(-\frac{D}{D_h}\right)d\frac{D}{D_h} && (3.31)\\
r_u &= r_h - r_l && (3.32)\\
D_l &= \frac{\int_0^{D_b} Dn(D)dD}{\int_0^{D_b} n(D)dD} && (3.33)\\
D_u &= \frac{\int_{D_b}^{\infty} Dn(D)dD}{\int_{D_b}^{\infty} n(D)dD} && (3.34)
\end{aligned}
$$

where $N$ is total number concentration, $n$ is number concentration for a given diameter, $D$ is the diameter, $r$ is the mixing ratio, $\rho_{air}$ is the dry air density, $m$ is the mass, $\alpha$ and $\beta$ are power law parameters for the mass relationship, and $\nu$ is the shape parameter for the gamma distribution. The subscripts $h$, $l$, and $u$ represent the host, lower, and upper ice category regions respectively.

For this research, the mixing ratio and characteristic diameter are conserved to maintain the behavior of each portion of the original one category ice distribution. Number is re-diagnosed for pristine ice and snow. The one category exponential distribution of ice is redistributed onto a smaller ice category also with a exponential distribution and the larger ice category with a shape parameter of 4. RAMS microphysics has been modified to represent the limited abilities of a GCM to model microphysics.

### 3.2.3 Radiation parameterization

The radiation scheme in RAMS is the same broadband model presented in the 1D cloud model section. As described earlier, the model was originally developed by Chen and Cotton (1983) but modified to differentiate between ice and liquid water. For these simulations, the radiation was called once an hour. The scheme also has the potential to include the effect of partially-cloudy grid volumes using cloud fraction. Within the 1D cloud model, the radiation balance was computed assuming a cloud fraction of 1. For the host model, the upper-level cloud does not necessarily cover the entire grid volume. Several cloud fraction schemes are available but are not developed specifically for ice clouds. One cloud fraction scheme by Ek and Mahrt (1991) which was developed for boundary-layer clouds has potential with modification for use in this application. The scheme is discussed below.

The fractional cloudiness function (FC) developed by Ek and Mahrt (1991) for boundary-layer clouds in models with 10 to 100 km grid spacings is dependent on the grid average relative humidity with respect to liquid (RH), and its standard deviation or

$$\mathrm{FC} = F(\mathrm{RH}, \sigma_{\mathrm{RH}}) \tag{3.35}$$

where $F()$ is the percentage area under a Gaussian curve greater than 1.0. If either the grid averaged relative humidity or the standard deviation were increased, the fractional cloudiness would be greater. To compute $\sigma_{\mathrm{RH}}$, Ek and Mahrt assumed a contribution from a turbulent and mesoscale component expressed by

$$\sigma_{\mathrm{RH}} = [\sigma^2_{\mathrm{RH}turb} + \sigma^2_{\mathrm{RH}meso}]^{1/2} \tag{3.36}$$

where $\sigma^2_{\mathrm{RH}turb}$ and $\sigma^2_{\mathrm{RH}meso}$ are the turbulent and mesoscale variance respectively.

By dividing the $\sigma_{\mathrm{RH}}$ into two components, the fractional cloudiness becomes a function of the grid size and turbulent nature of the grid volume. Given the moisture variance ($\overline{w'q'_t}$), standard deviation of vertical velocity ($\sigma_w$), and the saturation specific humidity ($\overline{q_s}$), the $\sigma^2_{\mathrm{RH}turb}$ can be expressed as:

$$\sigma^2_{\mathrm{RH}turb} = C_1 + C_2[\overline{w'q'_t}/(\sigma_w \overline{q_s})]^2 \tag{3.37}$$

while $\sigma^2_{\mathrm{RH}meso}$ was defined by:

$$\sigma^2_{\mathrm{RH}meso} = a_0 + a_1(\Delta x) + a_2 \ln(\Delta x) \tag{3.38}$$

where $\Delta x$ is the grid spacing. Both expressions include coefficients which were determined from a data set taken for boundary-layer clouds. By expanding Ek and Mahrt's data set to include upper level clouds and larger grid spacings, this fractional cloudiness scheme could be used in conjunction with the nested cloud model. The cloud fraction dependance on RH could be modified to include a dependance on relative humidity with respect to ice. The diagnosed cloud fraction could then be used in the radiation model and in area weighted average of the parameterization tendencies to improve the accuracy of the upper-level cloud feedback. However, at this stage of development, the cloud fraction is assumed to be unity.

## Chapter 4

## SENSITIVITY TESTS

To make informed decisions when developing the nested 1D cloud model, several types of cirrus were simulated using RAMS to explore the behavior for various model configurations. A range of cirrus altitudes at both tropical and midlatitude locations were simulated to understand the scope of cirrus behavior. Several degrees of freedom are available when choosing the model configuration in such areas as vertical resolution, timestep, complexity of microphysics, and radiative feedback. By comparing these sensitivity tests, the optimal choices for the resolution, microphysics, and radiation can be determined and used when developing the nested 1D cloud model.

### 4.1 Initialization

A range of altitudes (125 mb to 450 mb) were selected for initializing various cirrus clouds to get a general idea of model performance for different situations. The cases are presented in Table 4.1 with their descriptions for reference. The cirrus altitudes were chosen based on the findings of Platt *et al.* (1986) for cirrus at Aspendale and Victoria Australia. Average cirrus depths measured by Platt *et al.* (1986) were around 2 km. Liou (1986) also reported a climatological average value of 2 km depth for both tropical and midlatitude cirrus. Most of the clouds were initialized in the same manner; the water vapor mixing ratio ($r_v$) was increased above ice saturation in a 2 km depth. The relative humidity was also slightly increased above and below the cloud layer. The relative humidity and wind profiles for the tropical clouds are shown in Fig. 4.1. An ice supersaturation ($SS_i$) of 50% was chosen as representative of supersaturations a cirrus may experience in cloud drafts (Starr and Cox, 1985a). The temperature profile in the cloud was also adjusted to the psuedo-moist adiabat which at these temperatures is pratically the dry adiabat lapse rate.

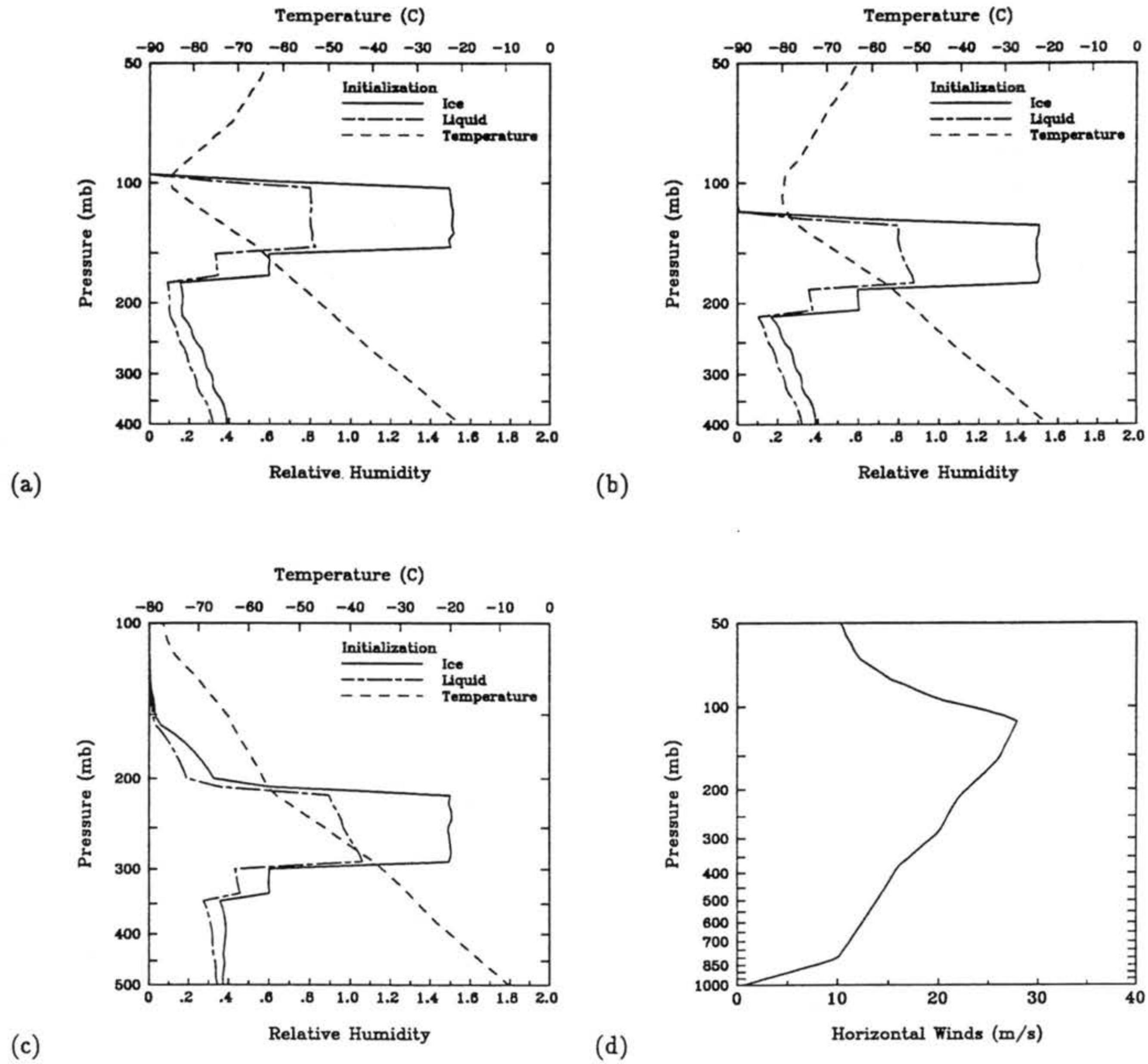


Figure 4.1: Tropical cirrus initialization for (a) 125 mb cirrus (b) 150 mb cirrus (c) 250 mb cirrus and (d) the horizontal wind profile for each simulation.

Table 4.1: Description of each cirrus simulation.

| Case | Location | Altitude | Initialization | Mid-cloud Temperature |
|---|---|---|---|---|
| 1 | tropics | 125 mb | $SS_i = 50\%$ | $-70°C$ |
| 2 | tropics | 150 mb | $SS_i = 50\%$ | $-60°C$ |
| 3 | tropics | 250 mb | $SS_i = 50\%$ | $-40°C$ |
| 4 | midlatitudes | 250 mb | $SS_i = 50\%$ | $-42°C$ |
| 5 | midlatitudes | 350 mb | $SS_i = 50\%$ | $-28°C$ |
| 6 | midlatitudes | 450 mb | $SS_i = 50\%$ | $-15°C$ |
| 7 | tropics | 125 mb | $0.5g/kg$ added mass | $-70°C$ |
| 8 | tropics | 150 mb | $0.5g/kg$ added mass | $-60°C$ |
| 9 | tropics | 250 mb | $0.5g/kg$ added mass | $-40°C$ |

For the midlatitude cirrus located at 350 mb and 450 mb, a $SS_i$ of 50% results in a liquid supersaturation ($SS_l$) of 20% to 30% which produces an unrealitic initial cloud water amount. The excess cloud water quickly collected into rain and fell out of the cloud. For these two cases, $r_v$ was limited to values in the cloud layer to create a maximum $SS_l$ of 10%. The initial relative humidities and wind profile are shown in Fig. 4.2. The 450 mb midlatitude cloud initialization may not be classically defined as cirrus at a temperature of $-15°C$ but the case will provide useful information about the interaction of liquid and ice water species.

A different initialization was explored to mimic the situation of cirrus created from storm outflow or cloud venting for the three tropical cases. In this case, 0.5 g/kg of mass in the 2 km depth were added to the total water mixing ratio ($r_t$) which is equivalent to adding the mass as cloud water. The $SS_i$ was also increased to 10% in the cloud layer (Fig. 4.3). The temperature profile was not modifed to decrease the stability.

The RAMS grid was setup in the same manner described before to achieve a pseudo-1D format: a 2D model option with 5 horizontal grid points at a spacing of 1000 km. Between 11 and 170 model layers were used at a spacing ranging from 2000 m to 175 m to investigate the effect of vertical resolution on the cloud development. The daytime simulations began at 1400h local time, and the nighttime simulations were initiated at 0200h local time. Generally, each case was run for 3 hours at a 90 second timestep.

In the microphysics scheme, the categories of pristine ice, snow, aggregates, cloud, and rain were included. Graupel and hail were never observed in early studies so are excluded

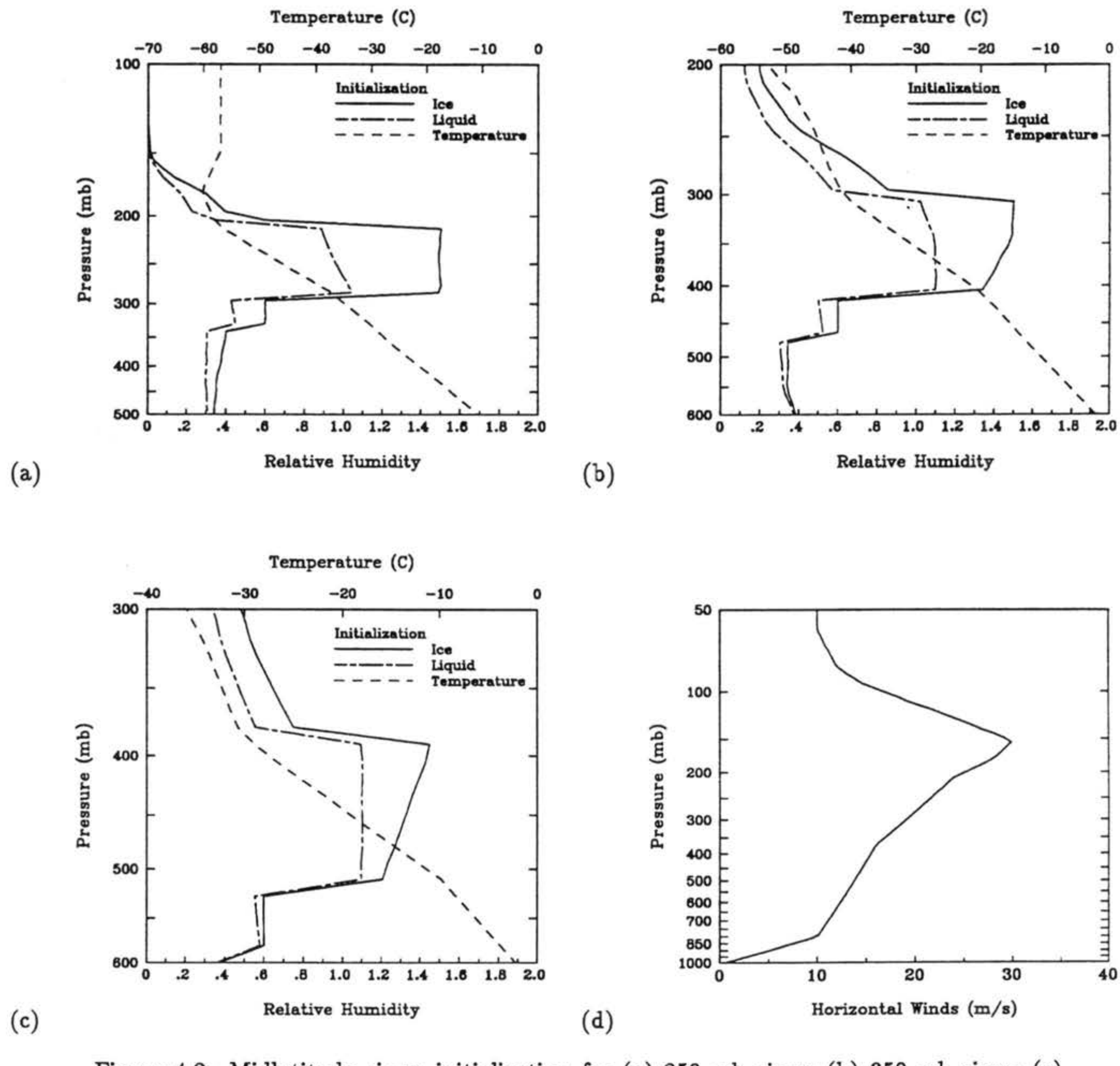


Figure 4.2: Midlatitude cirrus initialization for (a) 250 mb cirrus (b) 350 mb cirrus (c) 450 mb cirrus and (d) the horizontal wind profile for each simulation.

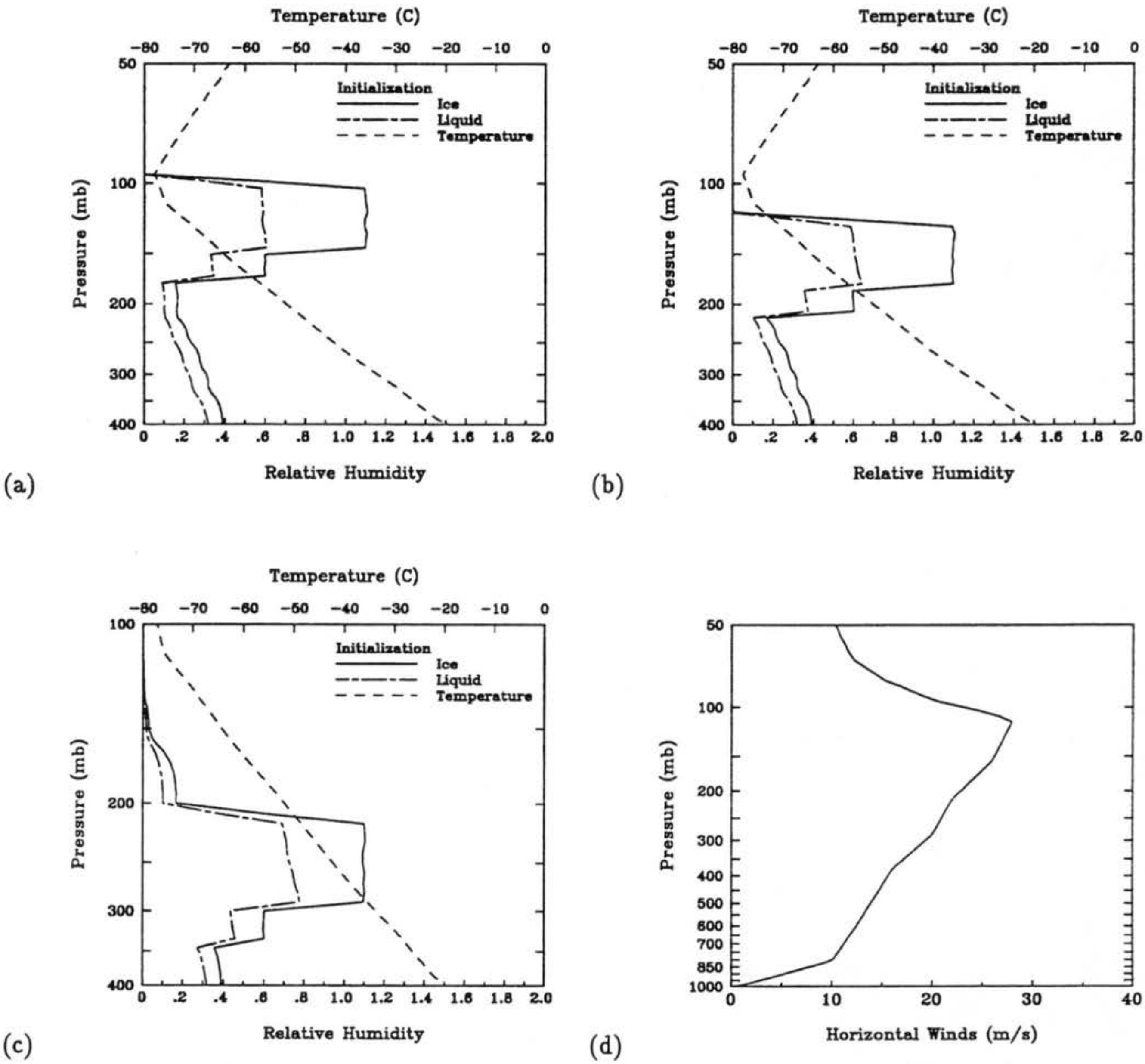


Figure 4.3: Storm outflow tropical cirrus initialization for (a) 125 mb cirrus (b) 150 mb cirrus (c) 250 mb cirrus and (d) the horizontal wind profile for each simulation.

in these simulations. The specification of hydrometeor characteristic diameter are the same as the setup for the cloud model described in Chapter 3. To differentiate between the two locations, the specified cloud water total number concentrations could be altered to represent tropical maritime and midlatitudinal continental values. For simplification at this stage of model development, cloud water concentration was held constant. The pristine ice nucleation scheme will more likely be the dominant source of hydrometeors. For comparison, the host model microphysics (described in section 3.2.2) which uses a two categories of cloud ice and water was also employed to investigate the impact of microphysical complexity on the cirrus simulations.

### 4.1.1 Tropical

The standard tropical summer atmosphere is shown in Fig. 4.4 before the addition of water vapor mass to create the cirrus cloud. The relative humidity with respect to ice is originally below 30% for the three tropical cirrus cases. The primary difference between the midlatitude and tropical simulations is the solar zenith angle. The tropical case is also located over the Atlantic ocean at 30° west and 5° north with a sea surface temperature prescribed at 298 K. Unlike other clouds, cirrus are not directly created by surface fluxes of moisture and heat; therefore, it is unlikely the surface boundary condition will make significant impact on the simulation.

### 4.1.2 Midlatitude

The standard dry midlatitude summer atmosphere is presented in Fig. 4.5. The grid is located at 93° west and 40° north (central Iowa). The soil type was selected to be sandy loam at a moisture level of 10% water capacity and an initial temperature of $2°C$ colder than the lowest layer of the atmosphere. As mentioned above the choice of soil type, moisture, and temperature is probably not relevant in these simulations.

## 4.2 Resolution

The primary goal of developing a nested cloud model to use with large-scale models is to provide the resolution necessary for simulating cirrus with as little computational

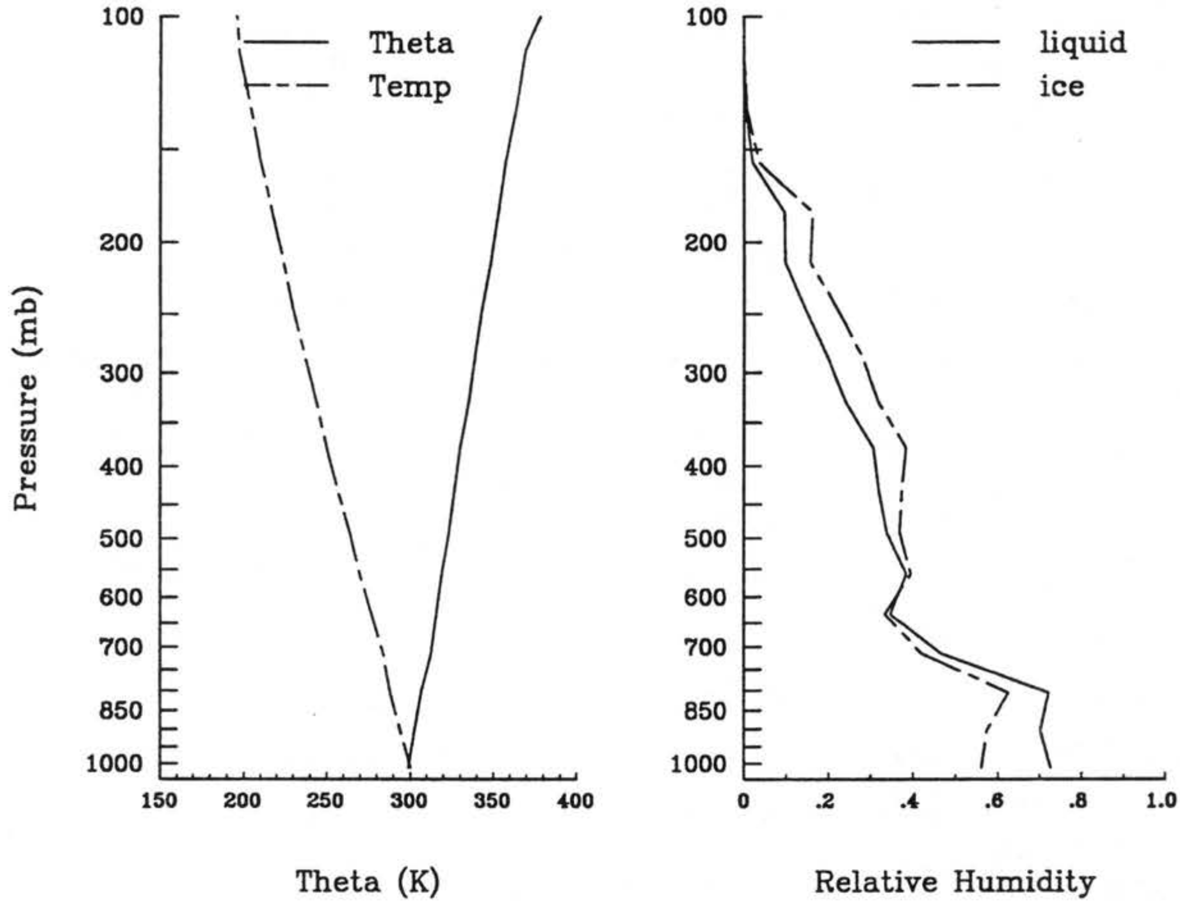


Figure 4.4: Standard tropical summer atmosphere.

cost as possible. The required vertical resolution will be dictated by the need to resolve collection and sedimentation of hydrometeors. A finer vertical resolution will also allow better definition of heating rate peaks at cloud top and cloud base. The relatively short timescale of the microphysical properties of nucleation, deposition, evaporation, and melting will limit the maximum timestep that can be used. To determine what resolution is adequate for capturing the essential features of a cirrus cloud, several simulations were run at various timesteps and vertical resolutions.

### 4.2.1 Timestep

To investigate the effect of timestep on the cirrus simulation, 5 timesteps of 45, 90, 180, 450, and 900 seconds were used to compute the mixing ratios of pristine ice ($r_i$), snow ($r_s$),

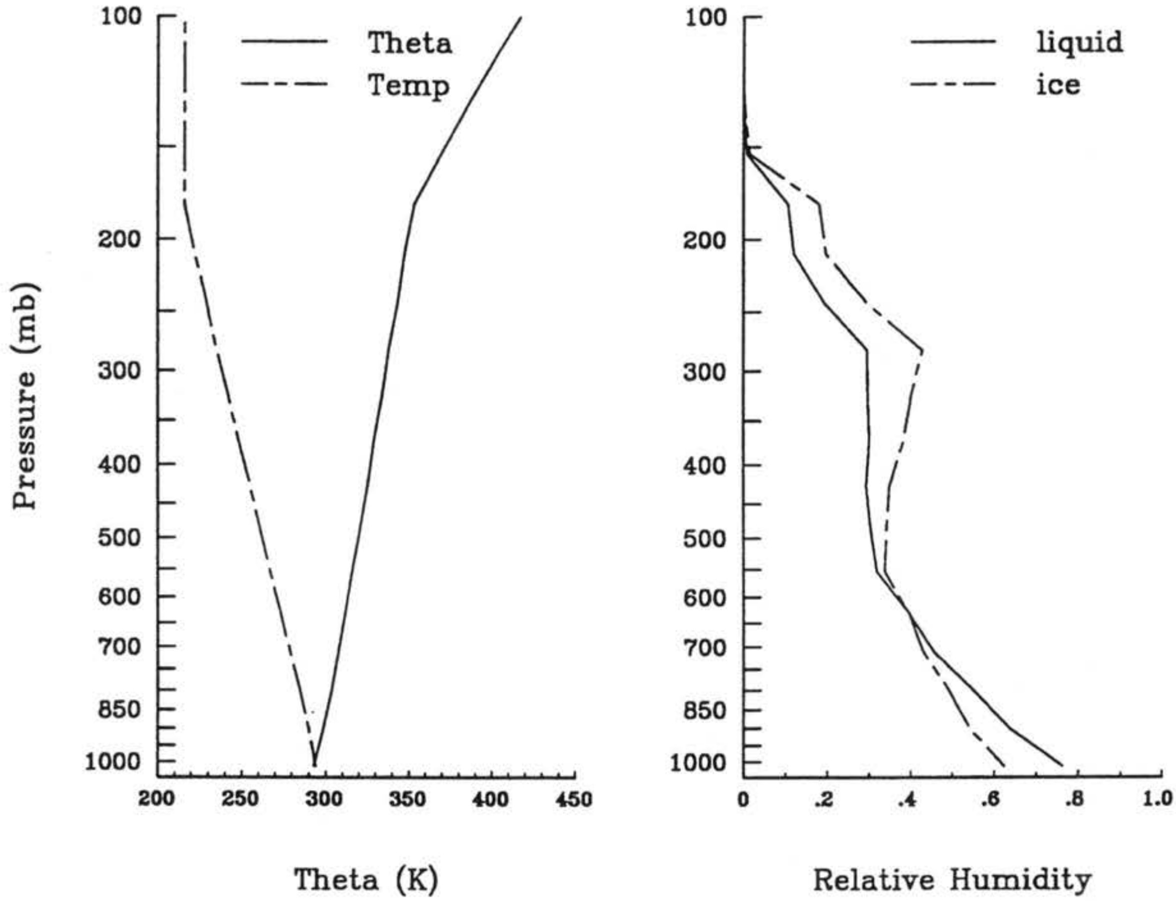


Figure 4.5: Standard midlatitude summer atmosphere.

and aggregates ($r_a$) at 900 seconds (Fig. 4.6). The cirrus cloud was initiated by increasing $r_v$ beyond ice saturation from approximately 400 mb to 200 mb at a vertical spacing of 500 m. The 900 second timestep output has been calculated once by the microphysical scheme; whereas, the 45 second timestep results have looped through the calculation 20 times to reach the final time of 900 seconds. This difference creates a discrepancy in the mixing ratios of ice. The 900 second timestep creates the largest amount of pristine ice and smallest amount of snow. Pristine ice nucleation is computed first by the microphysics routine before the calculation of vapor growth of pristine ice to snow. For the shortest timestep, the final pristine ice mass is smaller while snow mass has increased. The largest computed aggregate mixing ratio is for the 900 second timestep which corresponds with the large amount of pristine ice available to collect itself to form aggregates. These results illustrate the linear nature of the microphysics scheme. Inappropriate, longer timesteps will create erroneous results. The physical processes in the cloud in reality occur simultaneously; vapor is removed by nucleation and deposition at the same time. Therefore, the smaller the timestep used, the closer the routine will model the competing processes of microphysics. As the timestep is decreased, the solutions do converge to a single solution. Fig. 4.6 and another study with 100 m vertical resolution (not shown) indicate a maximum timestep between 90 seconds and 180 seconds is required. This result is critical when typical GCM timesteps can be as large as an hour. *Nesting in time becomes a necessity to model microphysics in a GCM.*

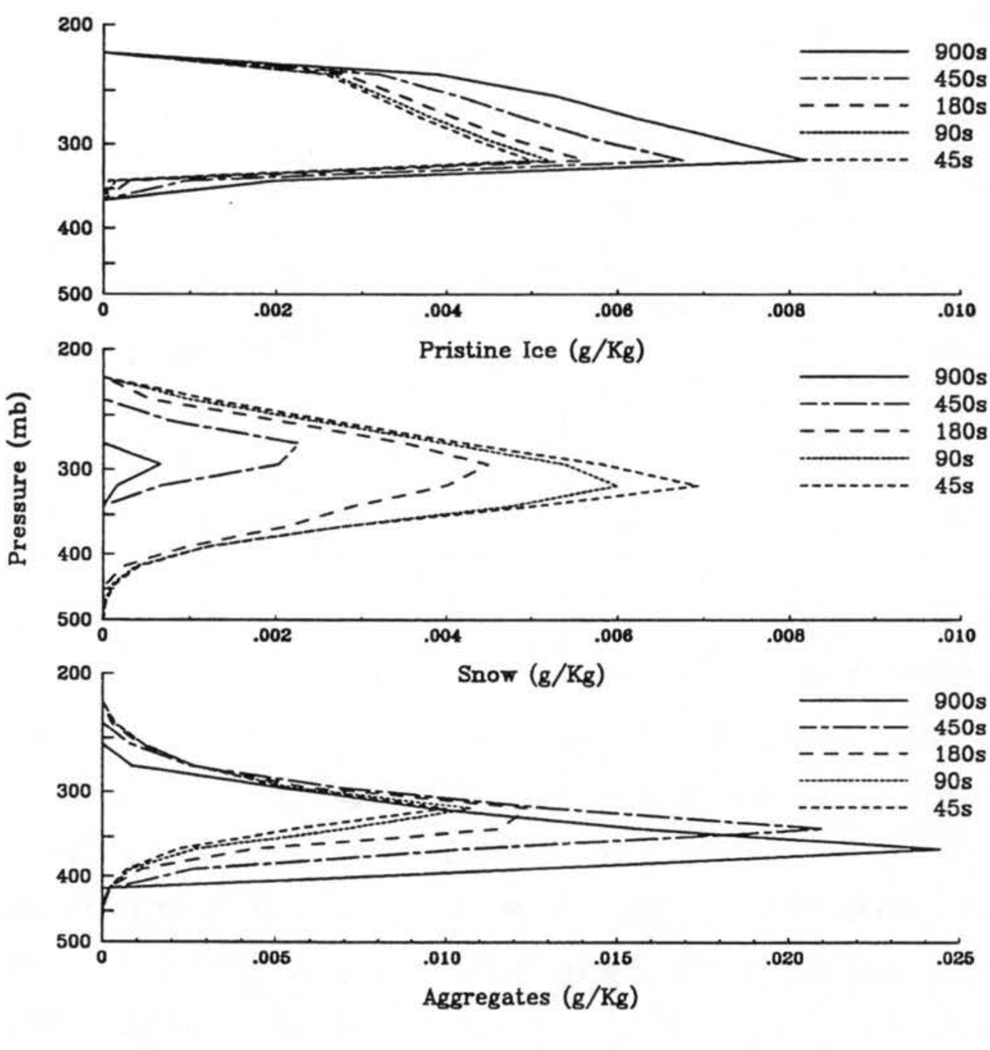


Figure 4.6: Impact of timestep on mixing ratios of ice species.

### 4.2.2 Vertical resolution

Even though a 1D cloud model will not explicitly model cloud-scale circulations, vertical resolution on the order of 500 m is still necessary to resolve the interactions of hydrometeors collecting and falling through the cloud. A higher resolution will also accurately capture the important peaks in the radiative heating profile. Two cases, the 250 mb tropical and 350 mb midlatitude cirrus, are presented for vertical spacing ($\Delta z$) ranging from 175 m to 2000 m. This comparison of vertical resolution will determine the optimal choice for the nest ratio in the cloud model.

By examining the tropical 250 mb cirrus simulations (Fig. 4.7), the progression of total ice mixing ratio at 15 minutes, 30 minutes, 1 hour, and 3 hours reveals the effect of vertical resolution on the cloud development. The 175 m and 250 m $\Delta z$ consistently capture the peak in ice mixing ratio at about 250 mb throughout the 3 hour simulation. The 500 m $\Delta z$ also resolves this peak but at 1 hour over-predicts the mass. The 1000 m $\Delta z$ has over-predicted the deepening of the cloud and the magnitude of the precipitation trails. The 2000 m $\Delta z$ is only able to resolve the general presence of the cirrus cloud with one grid point actually containing cloud ice.

The impact of the different resolutions of cloud mass is quickly seen by examining the radiative heating rates (Fig. 4.8) of the same cirrus. The location and magnitude of the cloud ice mixing ratio has a direct impact on the location of heating and cooling by radiation. At 1 hour, only the 175 m and 250 m $\Delta z$ have the strong cloud top cooling of $20°C/day$. The 1000 and 2000 m $\Delta z$ capture the correct sign of the overall heating in the cloud layer but place the maximum/minimum at a different heights. The shift from cloud base warming to a dominant cooling in the cloud layer can be explained by the decrease in the solar zenith angle from 1400h to 1700h local time. For this particular case, a $\Delta z$ of 500 m appears to be sufficient to contain the basic cirrus features but the spacings of 250 m and 175 m are the more ideal choices for $\Delta z$.

To make an informed decision about vertical resolution, another simulation with different characteristics should also be considered. The warmer, 350 mb midlatitude cirrus is shown in Fig. 4.9. For this case, there is a larger discrepency between the solutions. Except

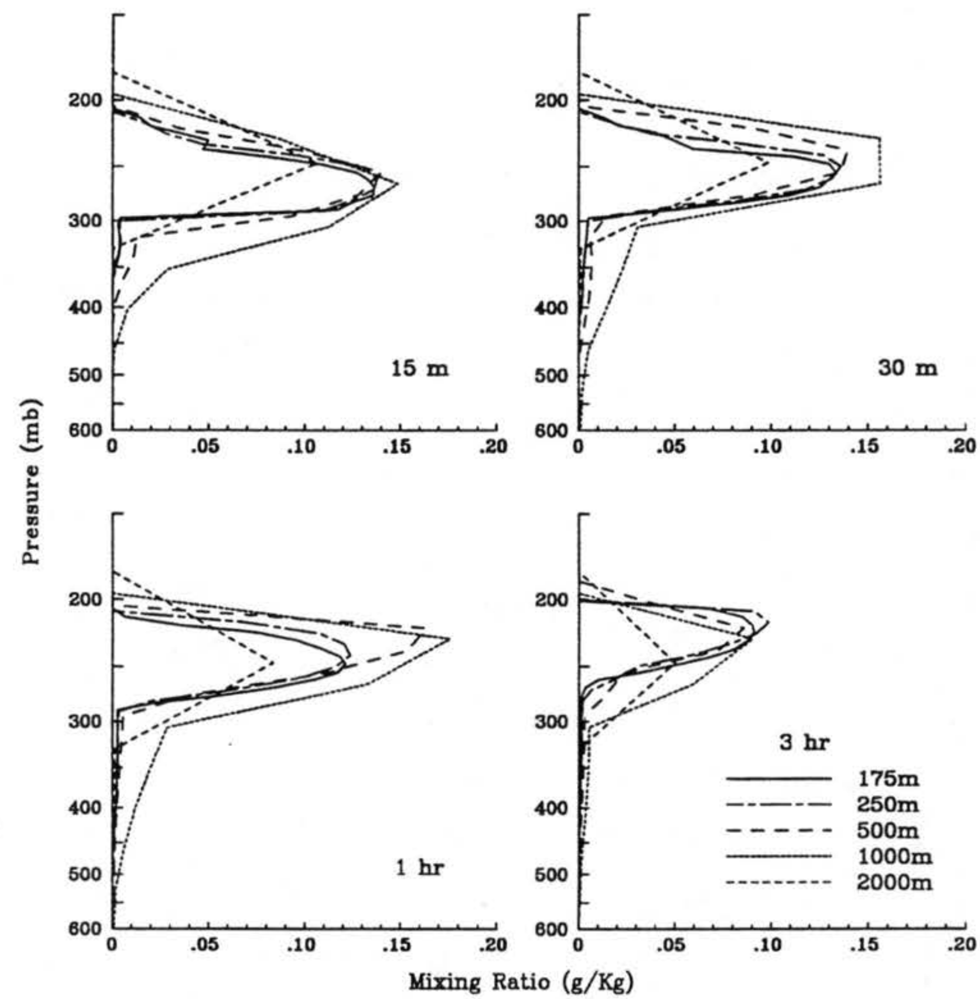


Figure 4.7: Impact of vertical resolution on ice amounts in the 250 mb tropical cirrus simulation.

for the 2000 m case, increasing the vertical spacing increases the ice mixing ratio by a factor of 2 in some cases. Interestingly, the coarsest resolution consistently under-predicts the ice mixing ratio; the coarser resolution has less vertical layers with an initial increased $r_v$. The 2000 m resolution has simply captured the presence of the cirrus but not any detailed features.

For the 350 mb cirrus, the 175, 250, and 500 m $\Delta z$ have very similar heating rate profiles (Fig. 4.10). Only the 1000 m and 2000 m grids fail to capture the profile details. The strongest cloud top cooling is shown at 1 hour which is primarily a result of the shallower

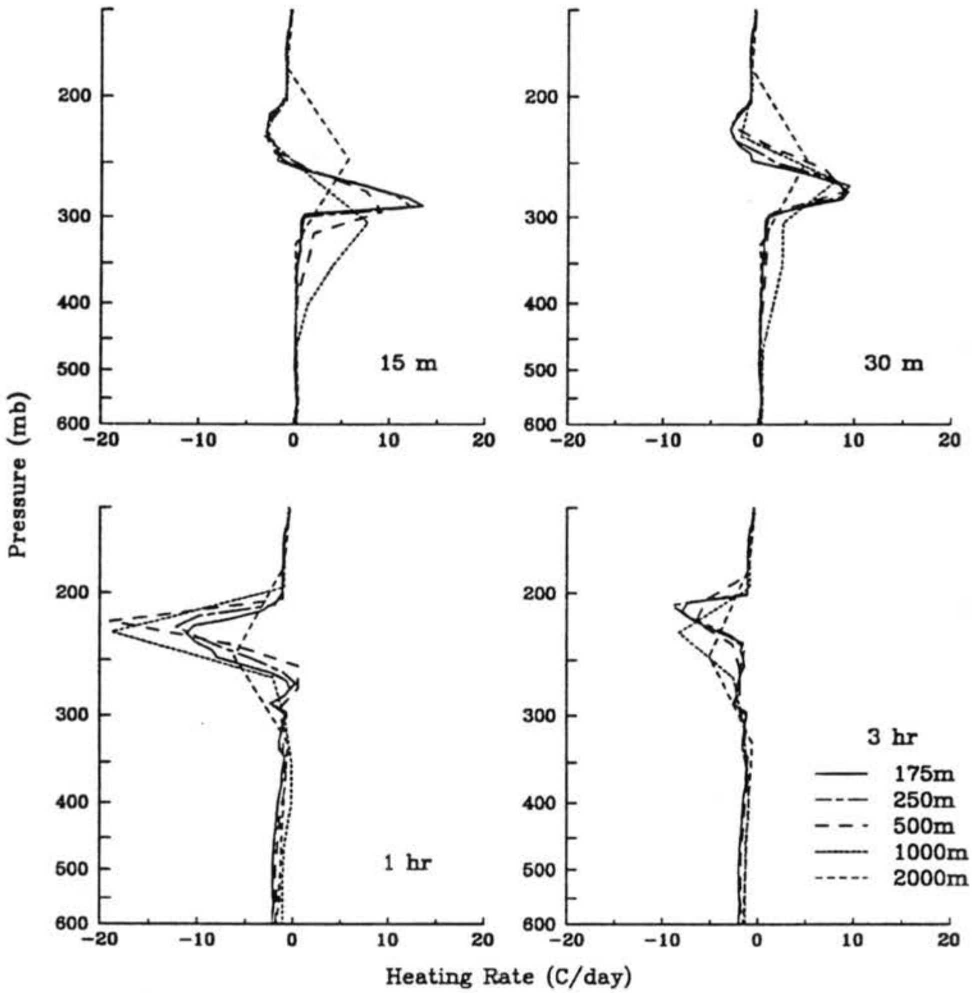


Figure 4.8: Impact of vertical resolution on heating rates in the 250 mb tropical cirrus simulation.

cloud structure at this time; the cloud top cooling has dominated over the solar heating through out the cloud layer.

By examining these two types of cirrus, one can conclude that vertical resoltion like the temporal resolution has a significant impact on the model results. The actual impact of the vertical spacing on the mixing ratio and heating rates will vary for each specific cirrus simulation but it can be concluded that a coarser grid spacing will not resolve the actual minimums and maximums. The finest grid spacing of 175 m will hopefully be possible by using a nested cloud model but these results suggest a $\Delta z$ of 250 m may be adequate. This conclusion is obviously dependent on the parameterizations used in the cloud model.

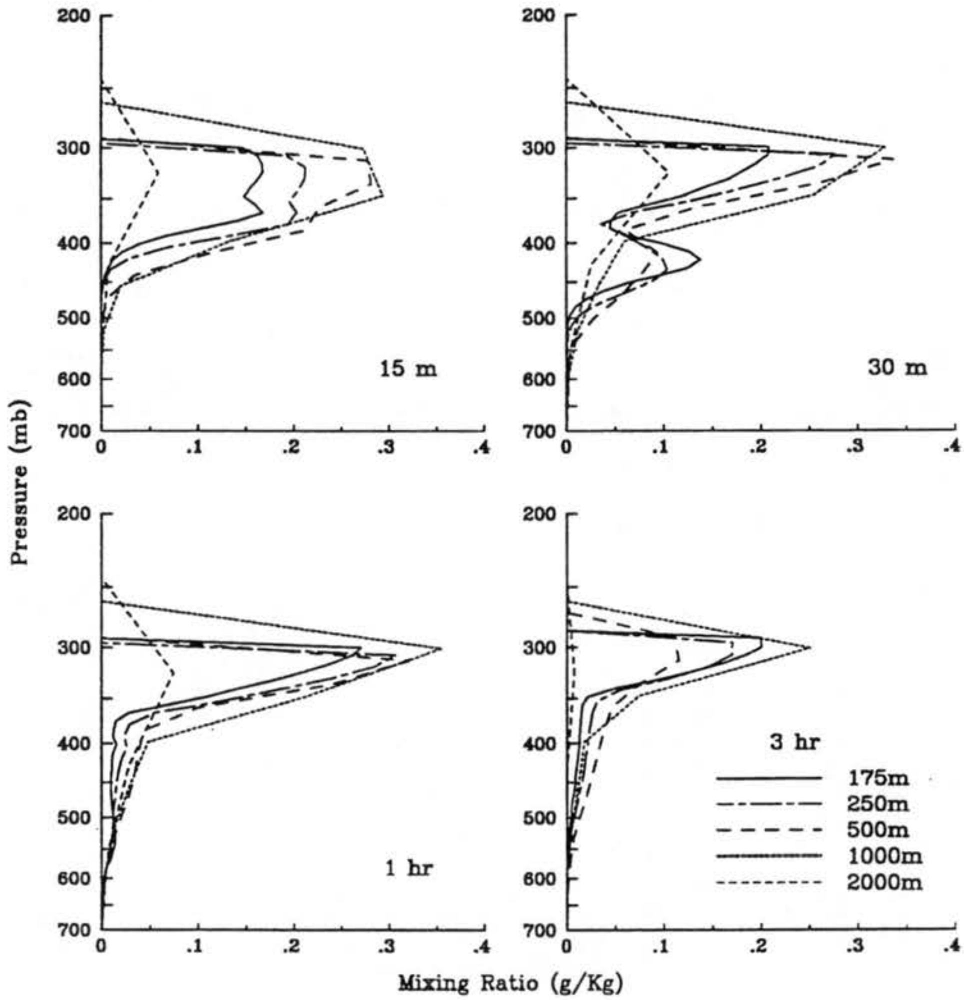


Figure 4.9: Impact of vertical resolution on hydrometeor amounts in the 350 mb midlatitude cirrus simulation.

## 4.3 Results

To understand the possible requirements of the 1D cloud parameterization, a range of cirrus simulations are used to explore possible situations. As described earlier, 6 tropical and 3 midlatitude cirrus cases were used to determine the impact of temperature on the development of cirrus. Several perturbations to the standard simulations allows the effects of microphysical complexity and radiation on the results to be examined. These simulations will provide information about what role various physical mechanisms play in the development of cirrus as modeled by the parameterization.

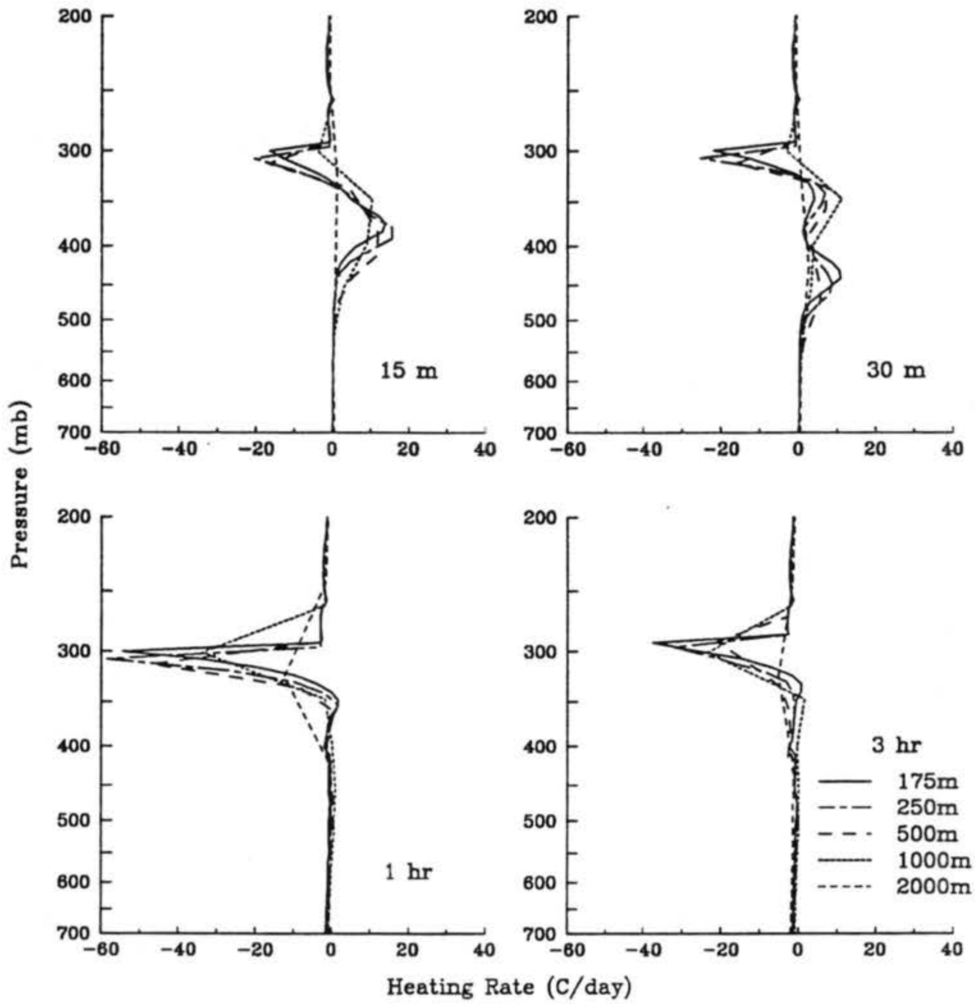


Figure 4.10: Impact of vertical resolution on heating rates in the 350 mb midlatitude cirrus simulation.

### 4.3.1 The effect of altitude on ice development

The primary effect of altitude on ice development is cloud temperature. As shown in the previous chapter, pristine ice nucleation is highly dependent on temperature, relative humidity with respect to ice and liquid, and the presence of cloud water. The temperature will also affect the collection efficiencies of ice crystals. The nucleation in turn will impact the available water vapor for growth of small ice into the snow category. The presence of liquid water in the cloud is dependent on the $RH_l$. Therefore, the initial height of the cirrus will determine the characteristics of the cirrus cloud. A brief discussion of each cirrus case is shown for a $\Delta z$ of 250 m and a timestep of 90 seconds.

#### 125 mb tropical cirrus

The highest, and therefore coldest, cirrus case is the 125 mb tropical initialization. Cloud temperature is approximately $-70°C$ with only ice species present. Fig. 4.11 displays the time series of the three ice categories, pristine ice, snow, and aggregates for the 250 m $\Delta z$ simulation. Because of the cold temperature of the cloud, the dominant ice category is pristine ice with a maximum amount of 0.008 $g/kg$ at the base of the cloud. The only mechanism of nucleation active at this temperature is depositional freezing. A miniscule amount of snow and aggregates are created but fall out of the cloud and evaporate by 3 hours.

Because the amount of ice nucleated is so small, the cloud radiative impact is nonexistant (Fig. 4.12). The ice water content is only at most 2 $mg/m^3$, and optical depth is 0.01. This 125 mb cirrus will have little affect on the large-scale circulation according to this radiation parameterization. Liou (1986) computed heating rates for various cirrus cloud thickness with the same mean ice content of 13 $mg/m^3$. The optically "thinnest" cloud presented by Liou was a 0.1 km deep cloud at about 8 km. This cirrus which is optically thicker than the 125 mb tropical cirrus, had heating rates no greater than ±2°C/day. Reasonably, a cloud with less ice mass would create an even smaller feedback.

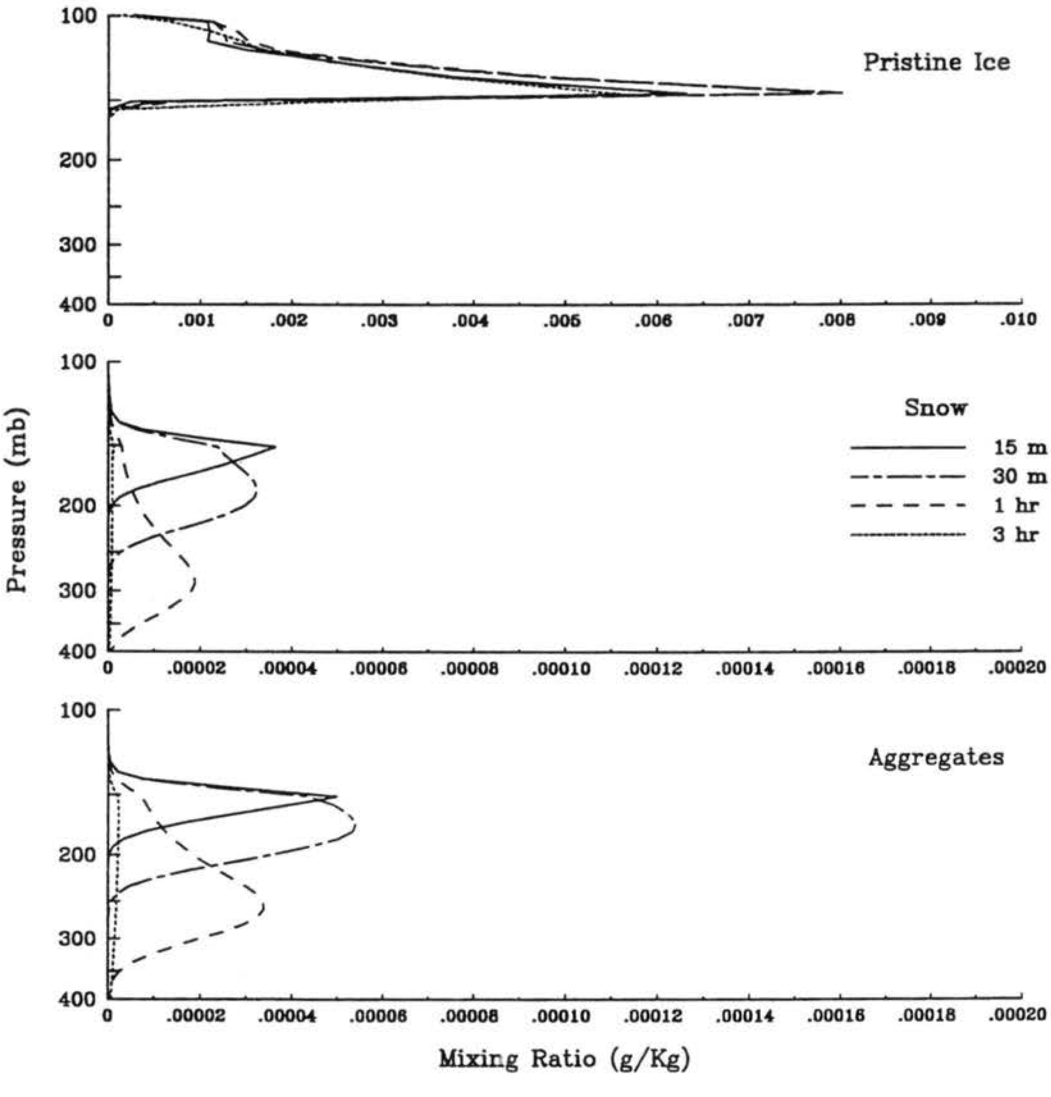


Figure 4.11: Development of the ice water mixing ratio for the 125 mb tropical cirrus.

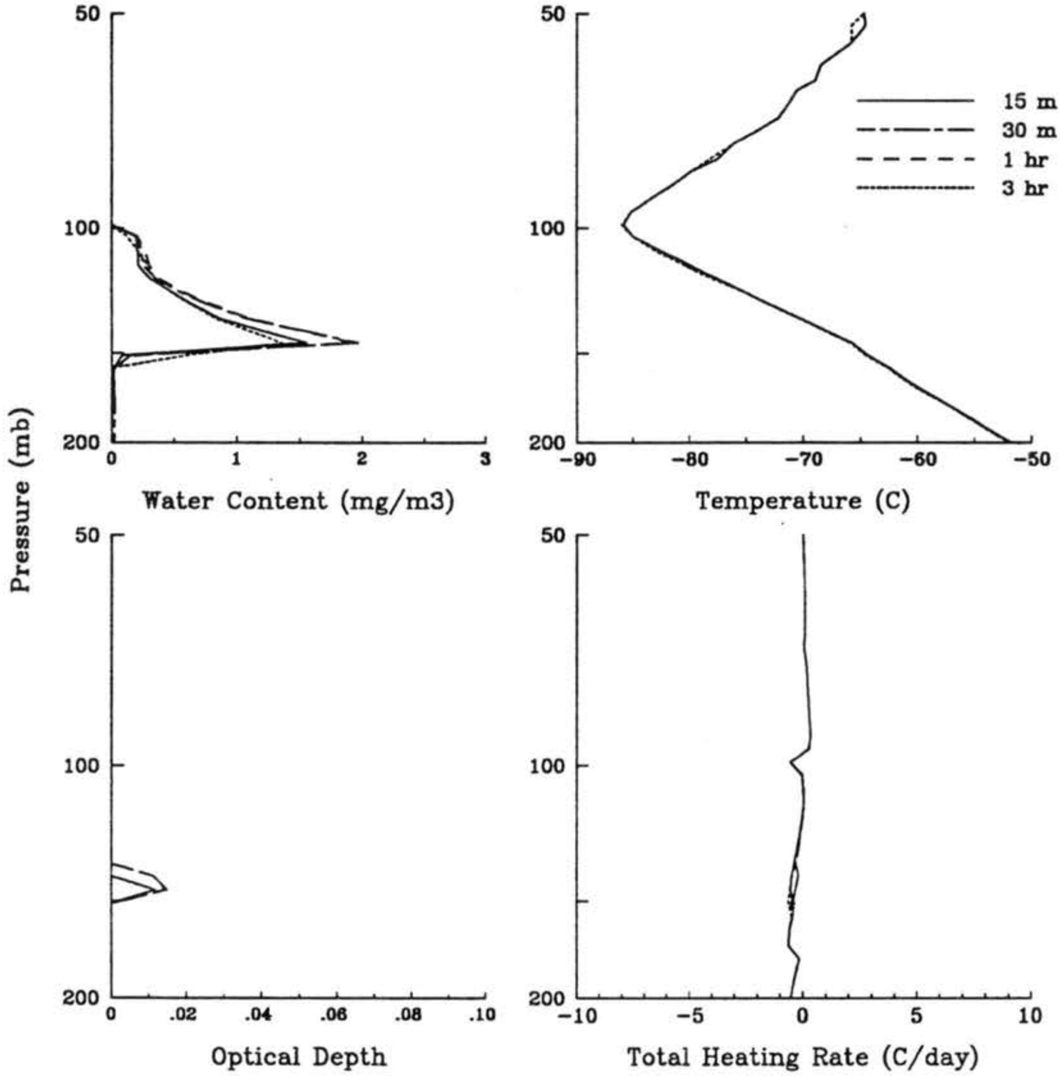


Figure 4.12: Radiative properties for the 125 mb tropical cirrus using a vertical spacing of 250 m.

### 150 mb tropical cirrus

For the 150 mb tropical cirrus (Fig. 4.13) the nucleated mass is larger than the 125 mb cirrus because of the increase in temperature to $-65°C$; more water vapor exists at a given $SS_i$. Snow mixing ratio is also larger but not nearly as increased as aggregates. The 5° increase in temperature has increased the collection effeciency of the 3 ice categories.

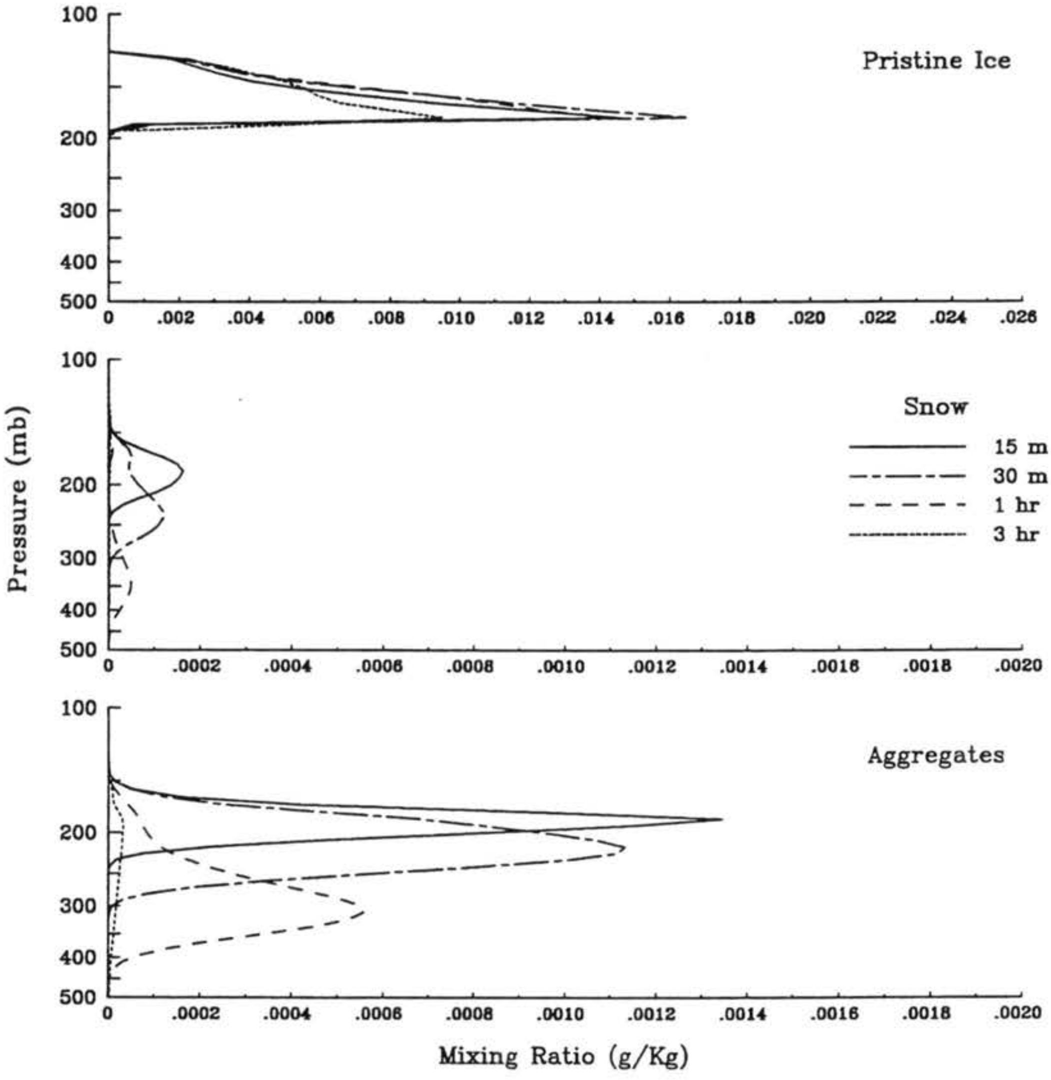


Figure 4.13: Development of the ice water mixing ratio for the 150 mb tropical cirrus.

The increase in aggregates can also be seen in the water content (Fig. 4.14) as precipitation trails. By 3 hours, only pristine ice is present in significant amounts. The cloud top cooling and cloud base warming can be seen in the heating rate but examining the time series of the temperature profile reveals that like the 125 mb cirrus, this cirrus will not impact the large-scale circulation significantly.

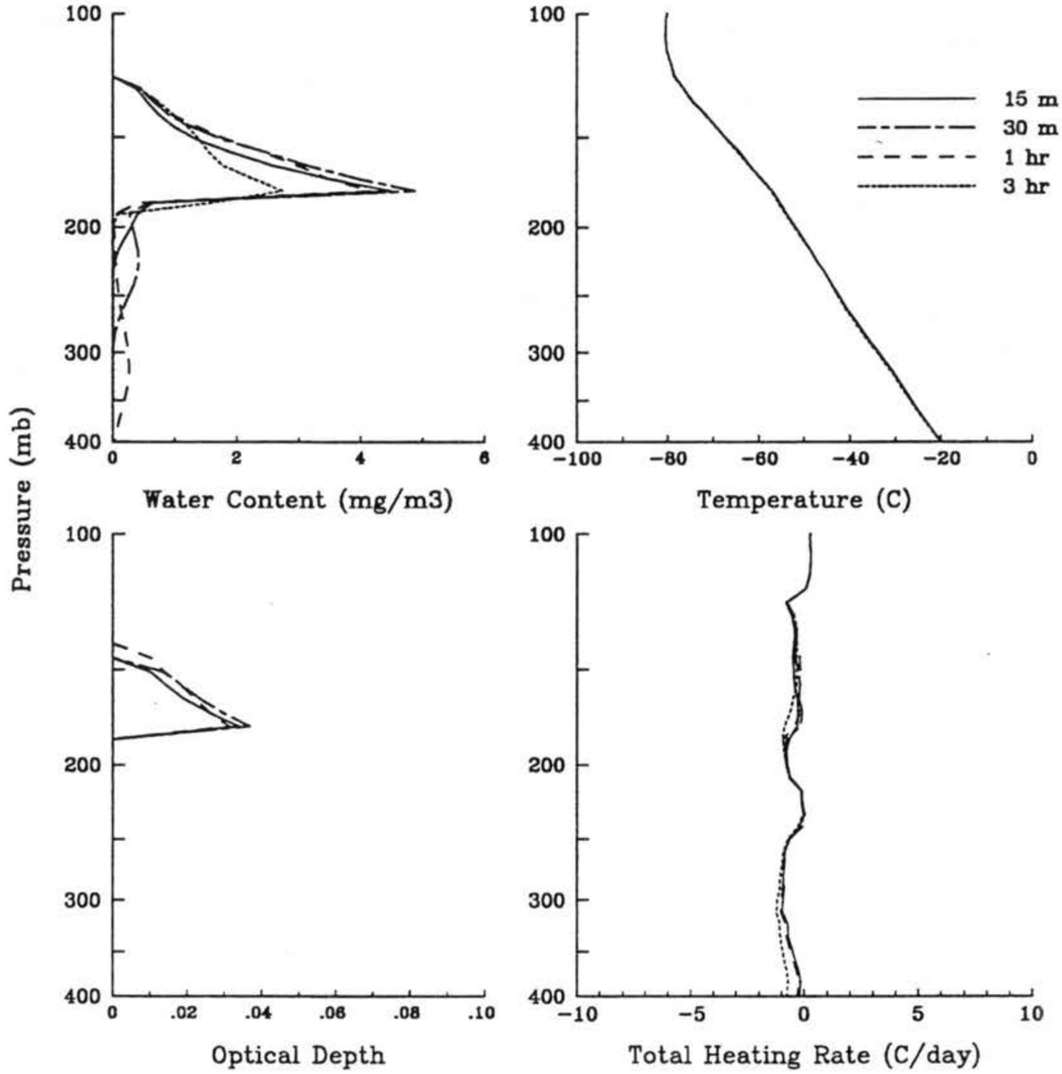


Figure 4.14: Radiative properties for the 150 mb tropical cirrus.

### 250 mb tropical cirrus

For the 250 mb tropical cirrus, the cloud temperature ranges from $-50°C$ to $-30°C$ which causes an order of magnitude increase in the amount of pristine ice (Fig. 4.15). At this temperature for a $SS_i$ of 50% the $RH_l$ has increased above 82% which permits homogeneous nucleation of haze can occur. Such a high number of ice particles are nucleated (Fig. 4.16) that the mean diameter is decreased. This increase in number reduces the amount of ice crytals that can grow to the larger snow category. Therefore, no snow is present for this cirrus. Aggregates created by pristine ice colliding with itself, are still only present in a small amount. The mass of pristine ice removed by collection and radiative heating can be seen by the decrease in the maximum amount by 3 hours.

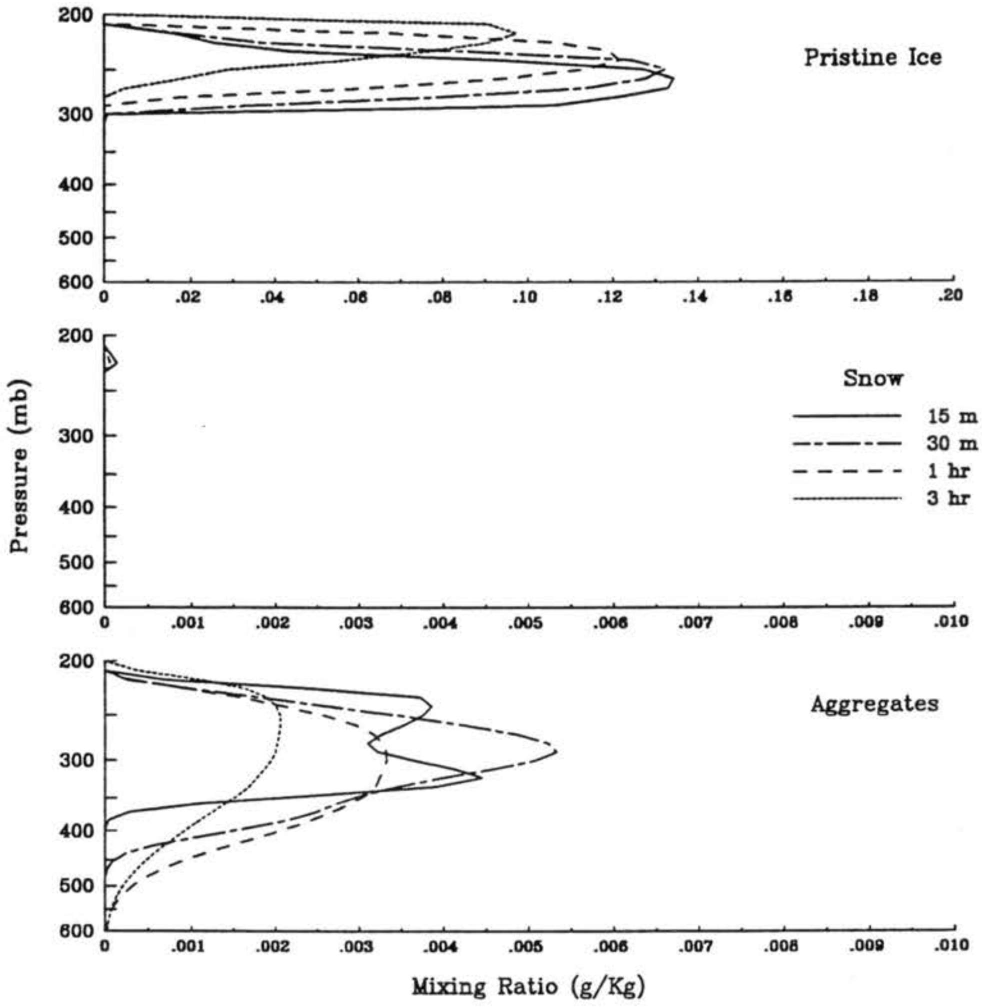


Figure 4.15: Development of the ice water mixing ratio for the 250 mb tropical cirrus.

The larger ice mixing ratio of this cirrus corresponds with larger water content as shown in Fig. 4.17. The maximum optical depth is still below 1 but is large enough to make a noticable change in the temperature profile. The heating rate has a distinct cloud top cooling/cloud base warming structure that decreases in magnitude as the cloud ice thins.

The warming in the lower half of the cloud is responsible for the sublimation of the pristine ice layer seen at 3 hours, an example of feedback between microphysics and radiation.

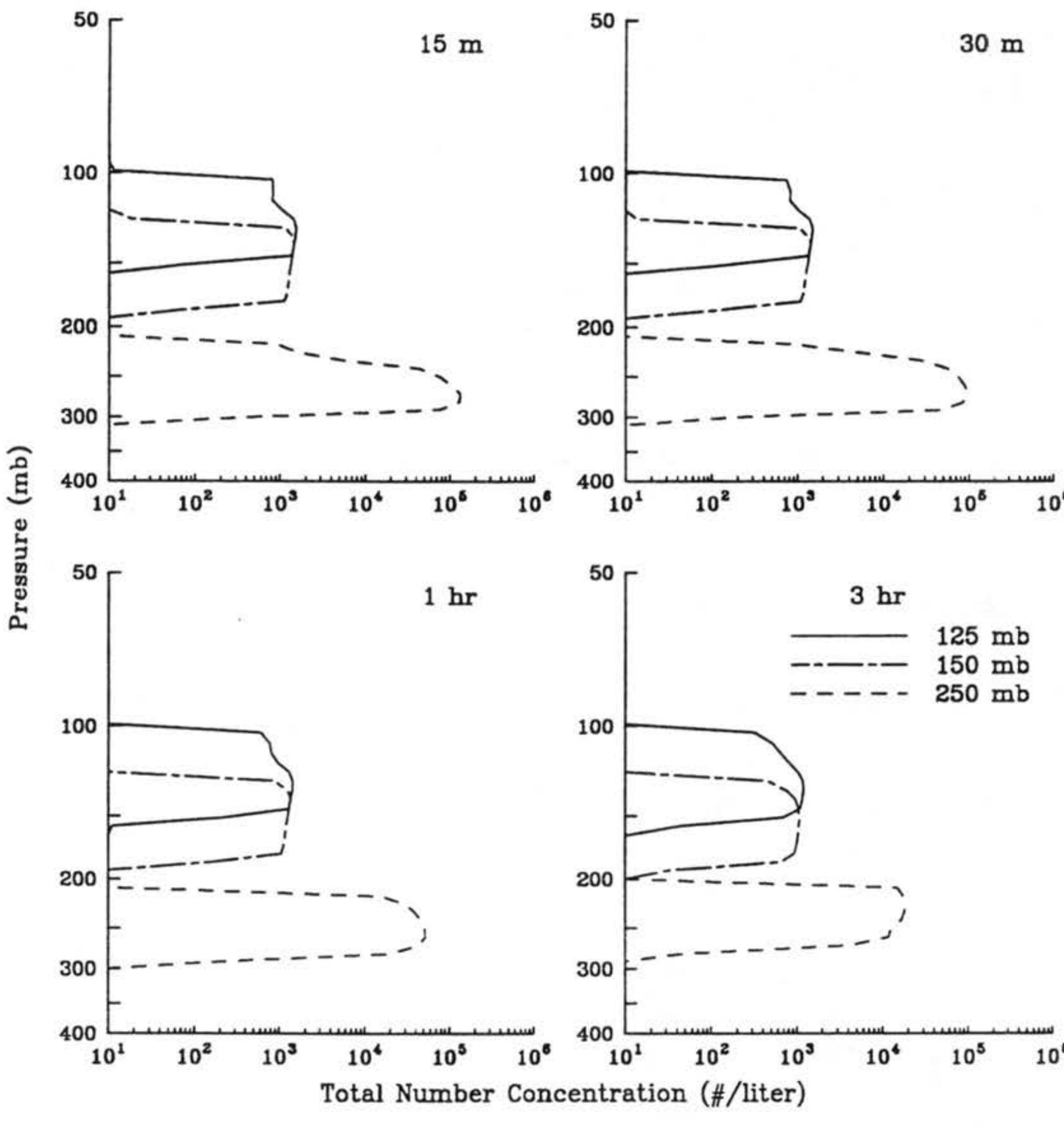


Figure 4.16: Pristine ice crystal concentration for 125 mb, 150 mb, and 250 mb tropical cirrus simulations.

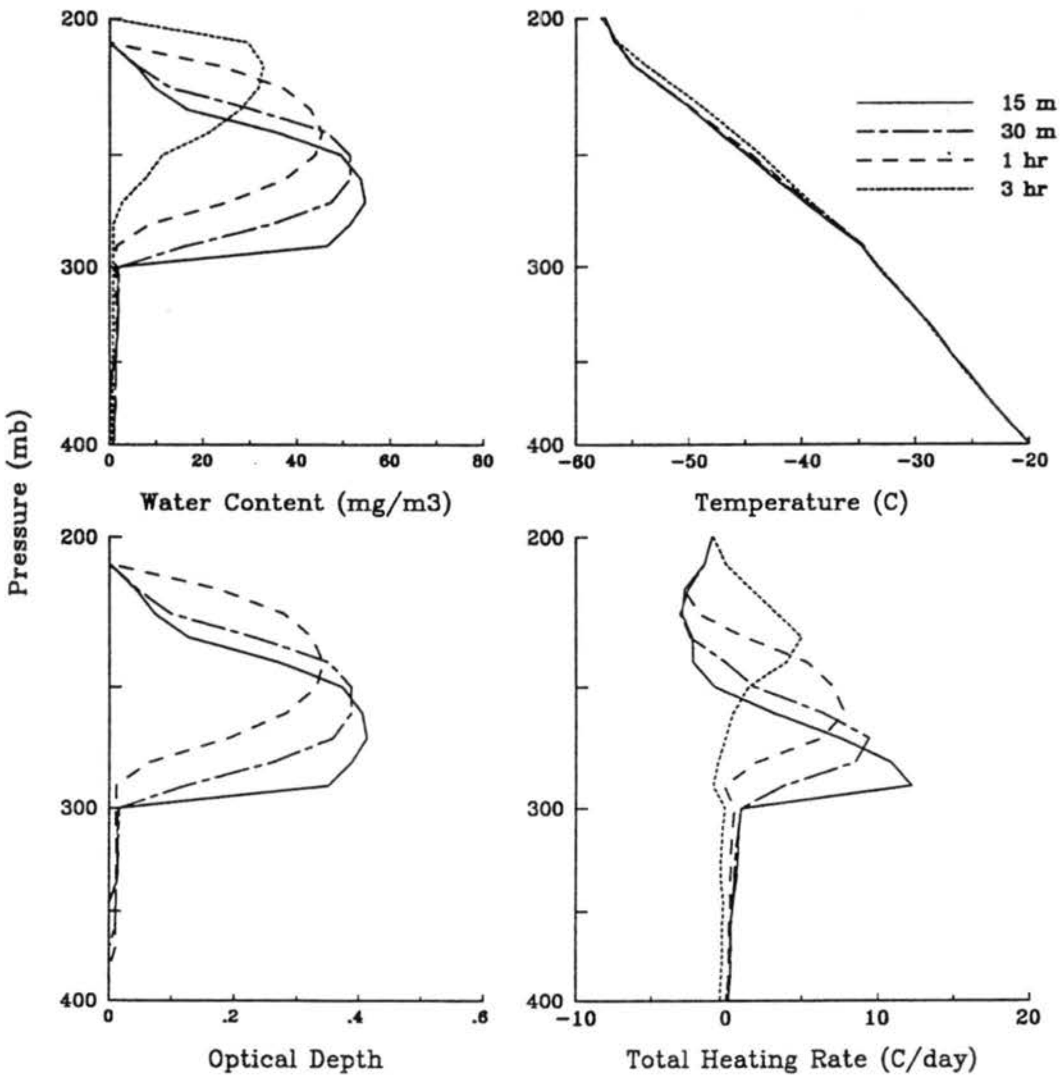


Figure 4.17: Radiative properties for the 250 mb tropical cirrus.

**250 mb midlatitude cirrus**

The 250 mb midlatitude cloud is approximately the same temperature as the 250 mb tropical cloud. The main difference between these two cases is the change in solar zenith angle and $RH$ in the vertical column. When compared to the tropical atmosphere (Fig. 4.4), the midlatitude atmosphere (Fig. 4.5) has a higher humidity above 600 mb but is drier in the lower levels between 850 mb and 600 mb. At the surface, the midlatitude atmosphere is about 5% more humid. This difference will affect the radiation balance in the atmosphere.

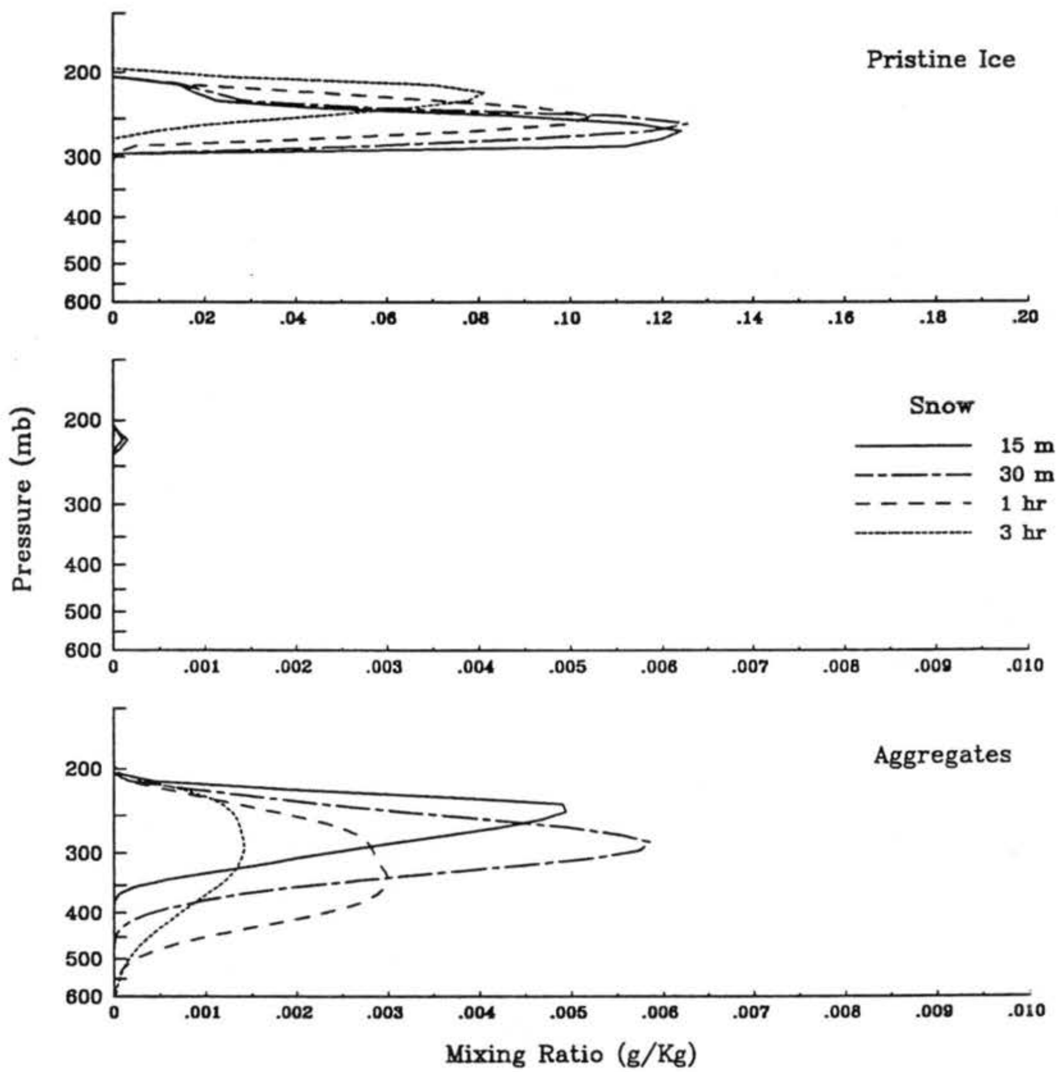


Figure 4.18: Development of the ice water mixing ratio for the 250 mb midlatitude cirrus.

The pristine ice mixing ratio (Fig. 4.18) is just slightly less than the tropical case with the largest difference at the final time of 3 hours. The amount of aggregates is about the same amount as the tropical aggregates. Basically, the two cases are fairly close; the difference in pristine ice mixing ratio at 3 hours can be attributed to the initially stronger heating and cooling for the tropical cirrus (Fig. 4.19).

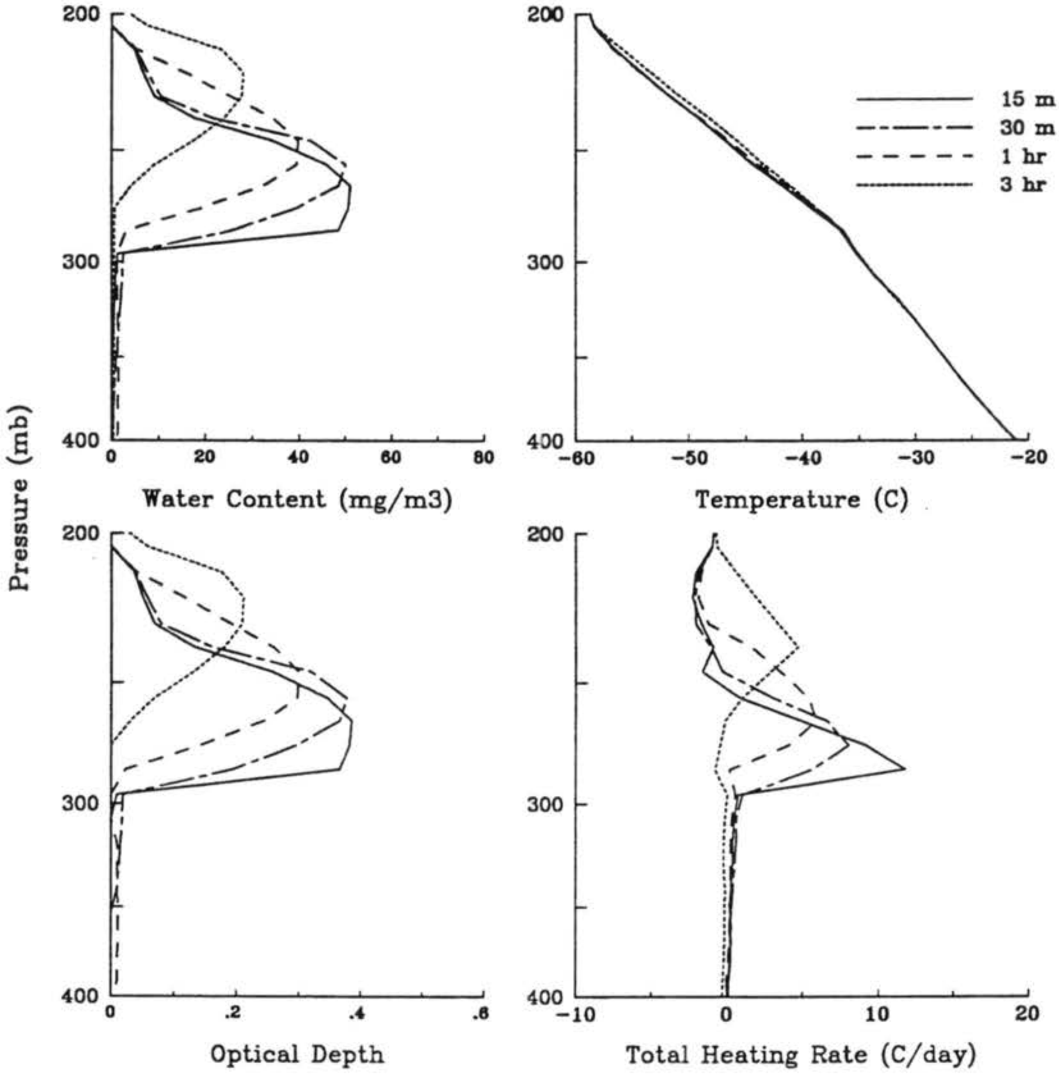


Figure 4.19: Radiative properties for the 250 mb midlatitude cirrus.

### 350 mb midlatitude cirrus

The 350 mb midlatitude cirrus cloud has more than twice the pristine ice amount than the 250 mb case due to the increase in water vapor at the warmer temperature (Fig. 4.20).

Initially, a smaller amount of snow is formed but collection quickly converts the ice to aggregates. Early in the simulation, aggregates mixing ratio is the same order of magnitude as pristine ice until sedimentation and evaporation remove the majority of the mass.

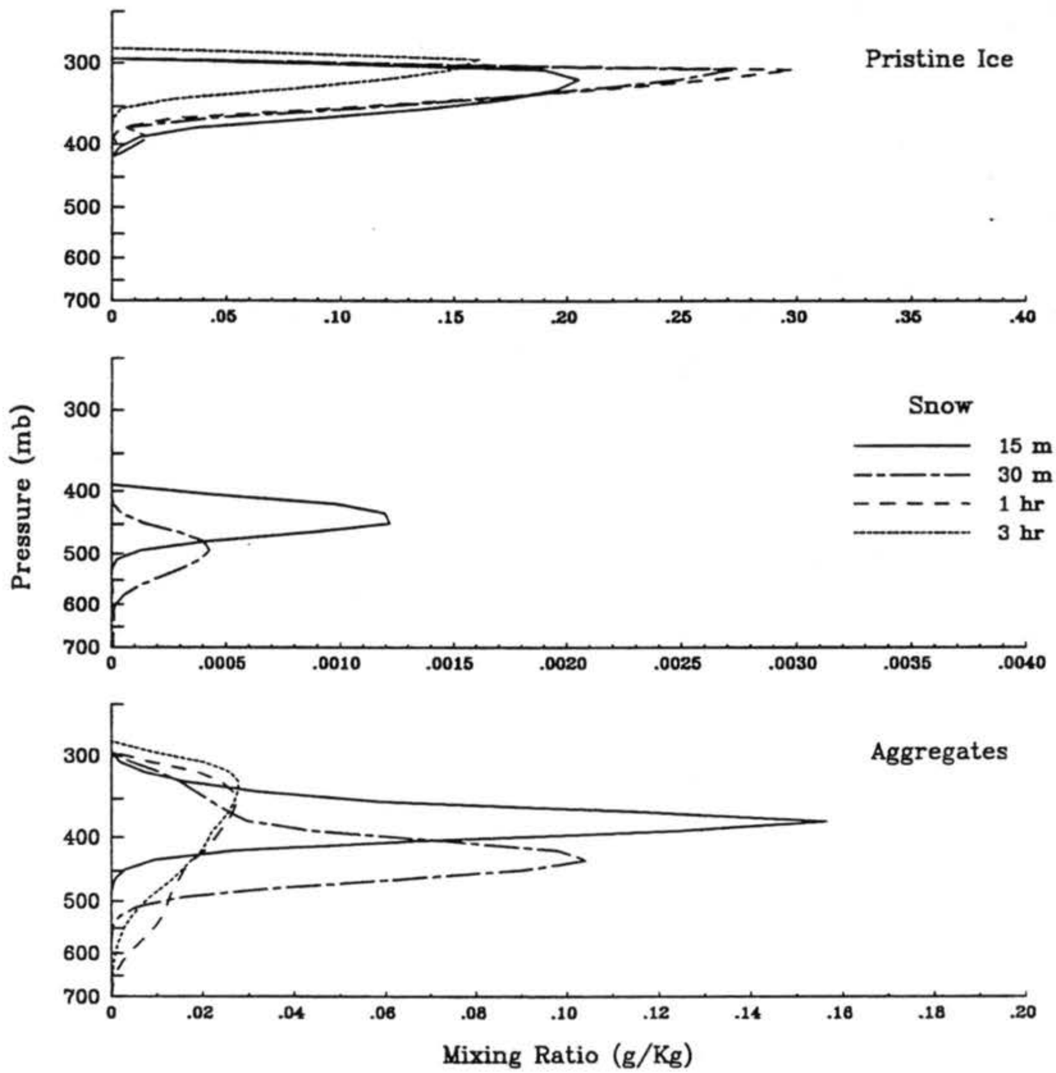


Figure 4.20: Development of the ice water mixing ratios for the 350 mb midlatitude cirrus.

The doubling of pristine ice for the 350 mb cirrus also results in a doubling of optical depth (Fig. 4.21). As expected, the cloud top cooling and cloud base warming have increased to $20°C/day$. As mass is lost through sedimentation, the cloud layer becomes more shallow and the cloud warming ascends with time.

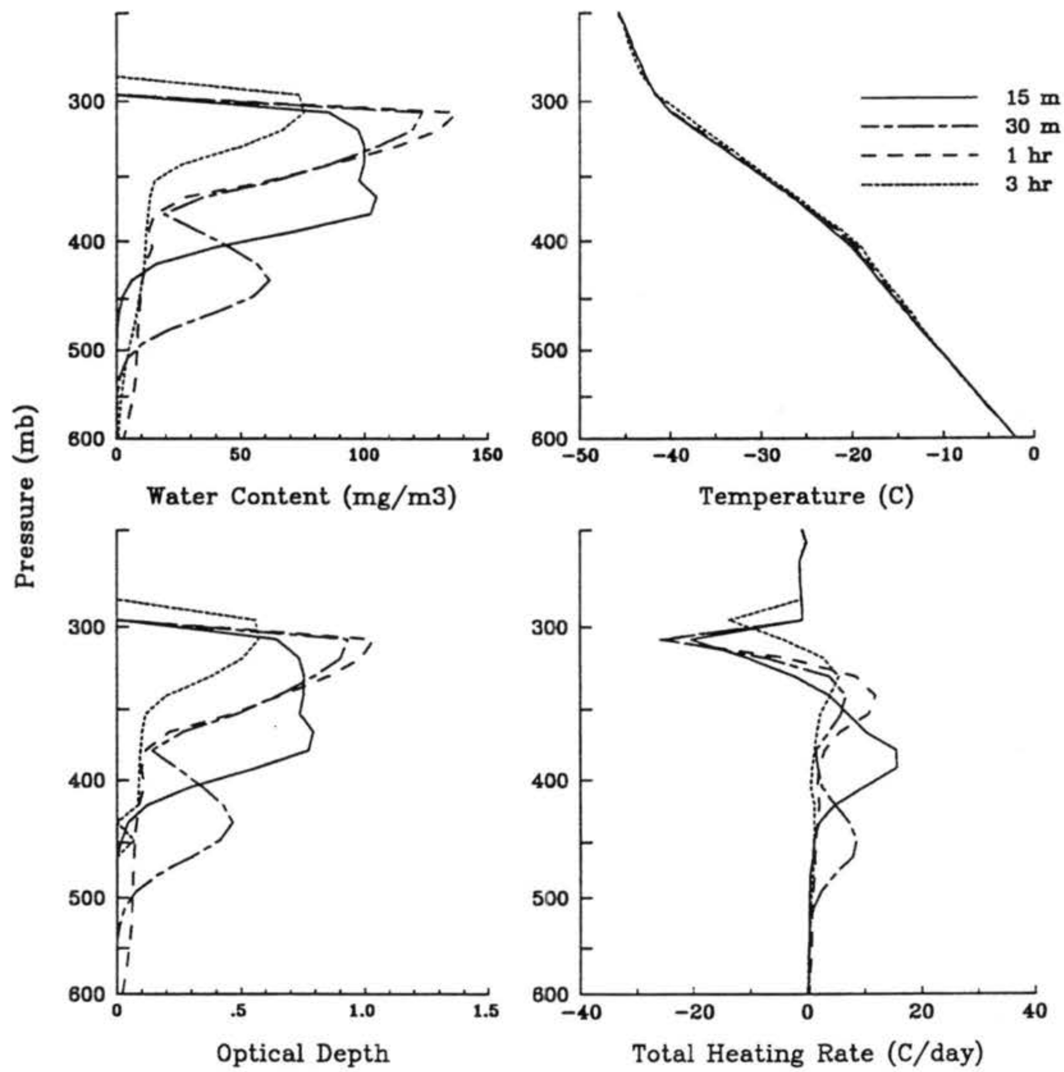


Figure 4.21: Radiative properties for the 350 mb midlatitude cirrus.

### 450 mb midlatitude cirrus

The 450 mb midlatitude cloud has a mid-cloud temperature of $-15°C$. This cirrus is too warm for homogeneous freezing of haze which dominated over the other ice nucleation mechanisms in the other simulations. Homogenous nucleation of cloud water is also not possible at this temperature. As a result, the dominant hydrometeor for this cirrus is cloud water (Fig. 4.22). Aggregates are next largest mass amount but are an order of magnitude smaller than cloud water. By 3 hours, all the cloud water has evaporated by solar heating or been collected by aggregates leaving a small amount of ice ($\sim 0.015 g/kg$) in the cirrus cloud. Pristine ice is able to increase with time as the cloud top becomes subsaturated with respect to liquid but remains supersaturated with respect to ice.

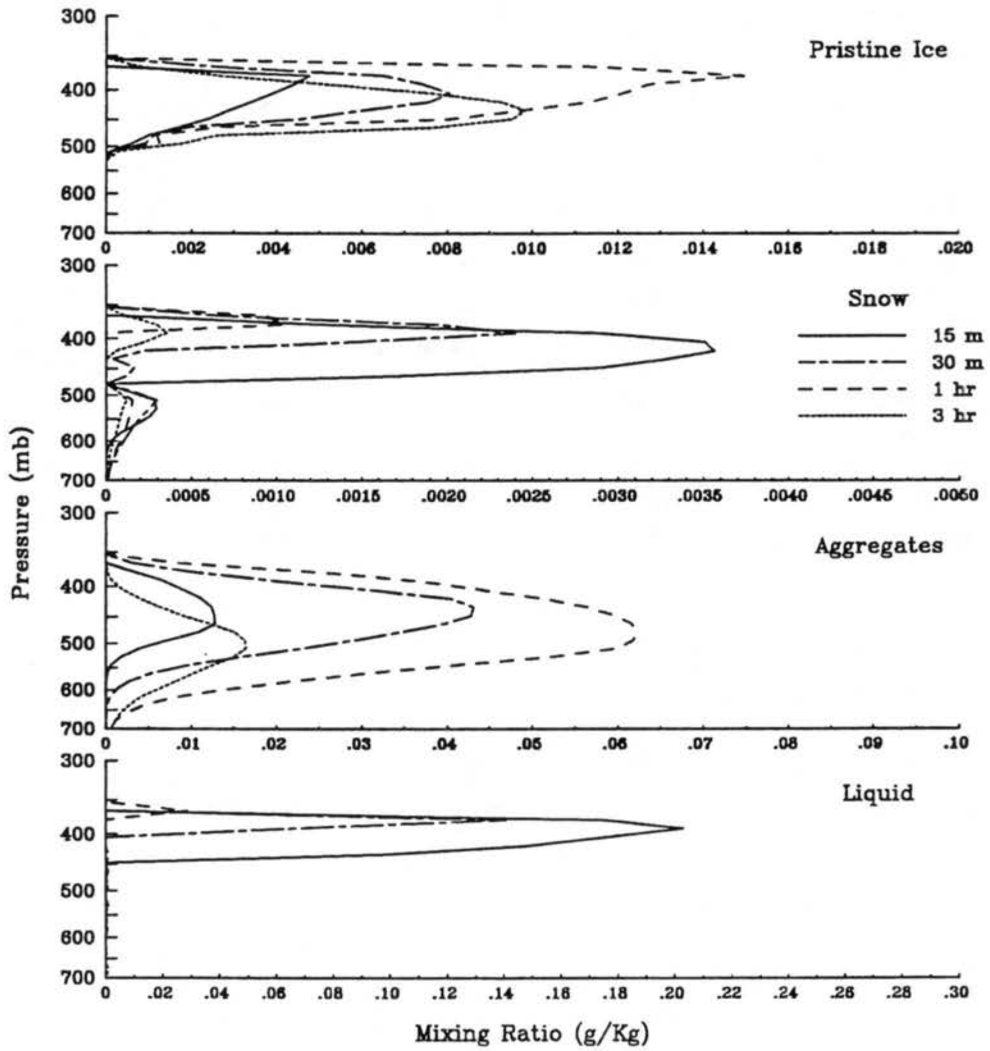


Figure 4.22: Development of the cloud water mixing ratios for the 450 mb midlatitude cirrus.

As expected when liquid water is present, the optical depth and heating rate profiles (Fig. 4.23) are dictated by the cloud water. Before 15 minutes, the cloud water created a strong raditive heating which caused the cloud water mass to be moved back into the water vapor category. The cooling in the cloud never grows larger than $\sim 5°C/day$; solar heating of liquid water initially dominates. At 3 hours, when no cloud water is present and the cloud has become optically thin, the whole cloud layer is cooling. This mixed-phase cirrus indicates the importance of distinguishing ice from liquid in the radiation scheme.

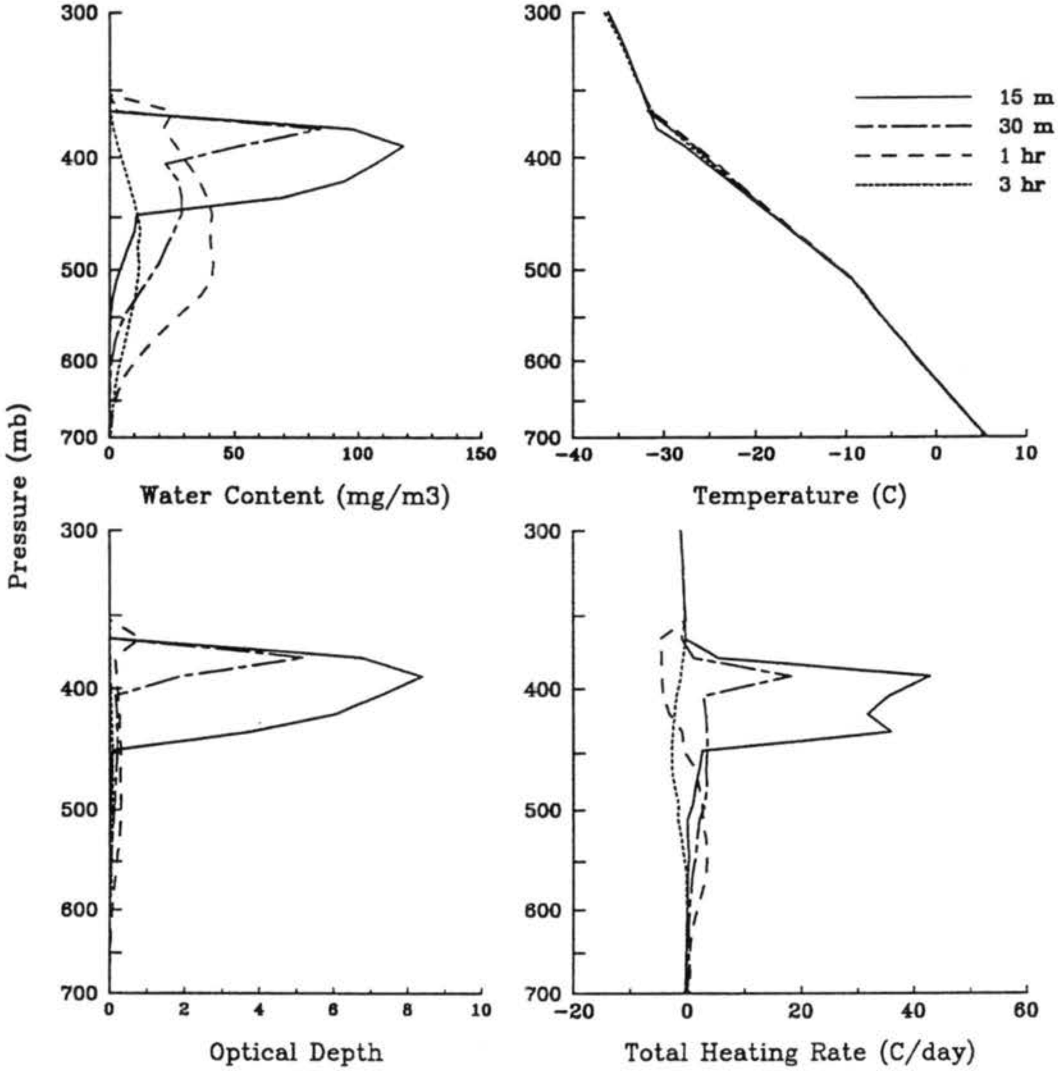


Figure 4.23: Radiative properties for the 450 mb midlatitude cirrus.

### 125 mb storm outflow tropical cirrus

To simulate a cirrus which is created by storm outflow instead of large-scale weather disturbances, the three tropical cirrus cases are repeated with a mass of 0.5 $g/kg$ directly added to the total water mixing ratio category which is equivalent to adding cloud water. Fig. 4.24 indicates that the added mass is completely nucleated into pristine ice through the mechanism of homogeneous freezing of cloud drops. Aggregates are formed through pristine ice collection but no snow develops. If cloud water is advected to relatively dry, cold conditions, it is unlikely that the frozen water would gain mass through vapor deposition.

The sublimation of pristine ice seen at 3 hours is caused by the radiative warming in the cloud layer (Fig. 4.25).

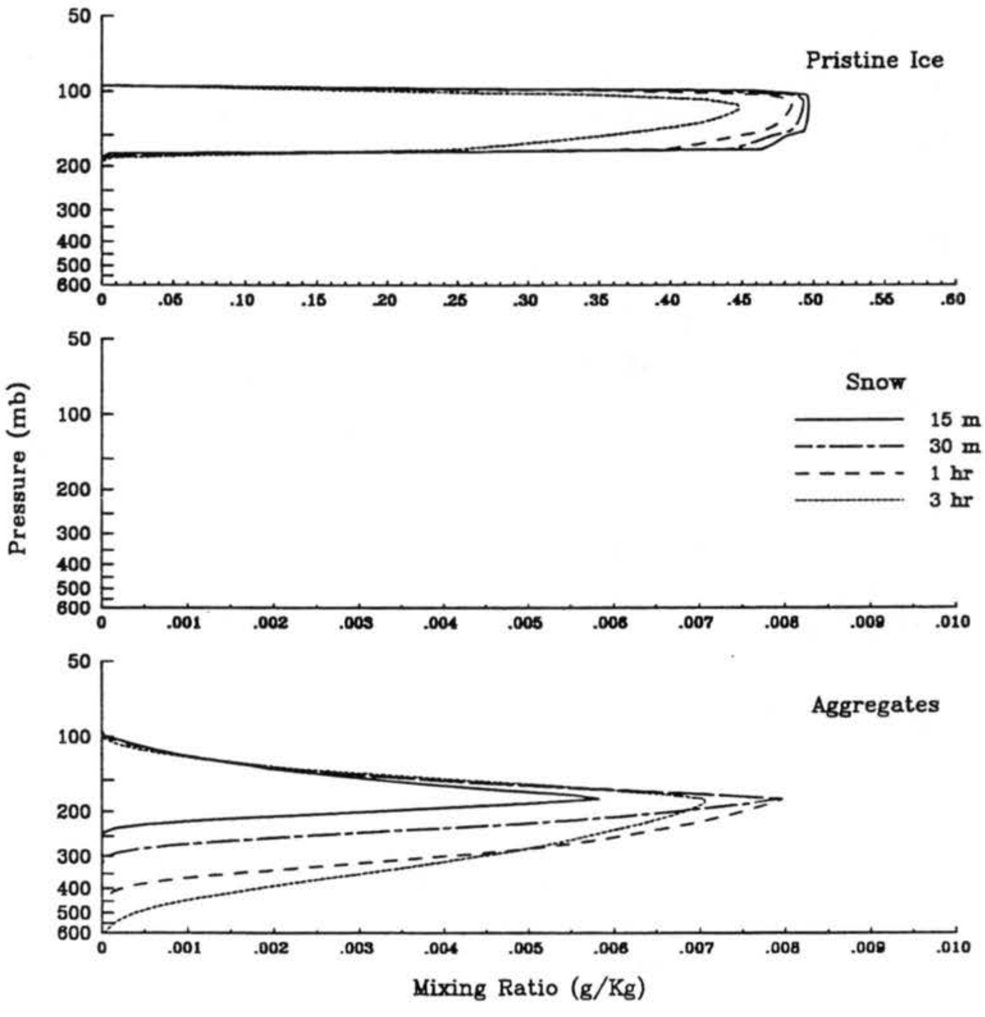


Figure 4.24: Development of the ice water mixing ratio for the 125 mb storm outflow tropical cirrus.

For the elevated $RH_i$ cirrus at 125 mb, there was pratically no contribution to the radiative heating rate from the cloud. For the storm outflow initialization, strong warming is evident throughout the cloud layer with a maximum heating at the cloud base. No cooling is present because the cirrus is at such a cold temperature. The temperature profile shows a drastic increase by 3 hours; thick cirrus created by storm outflow could significantly heat the upper troposphere.

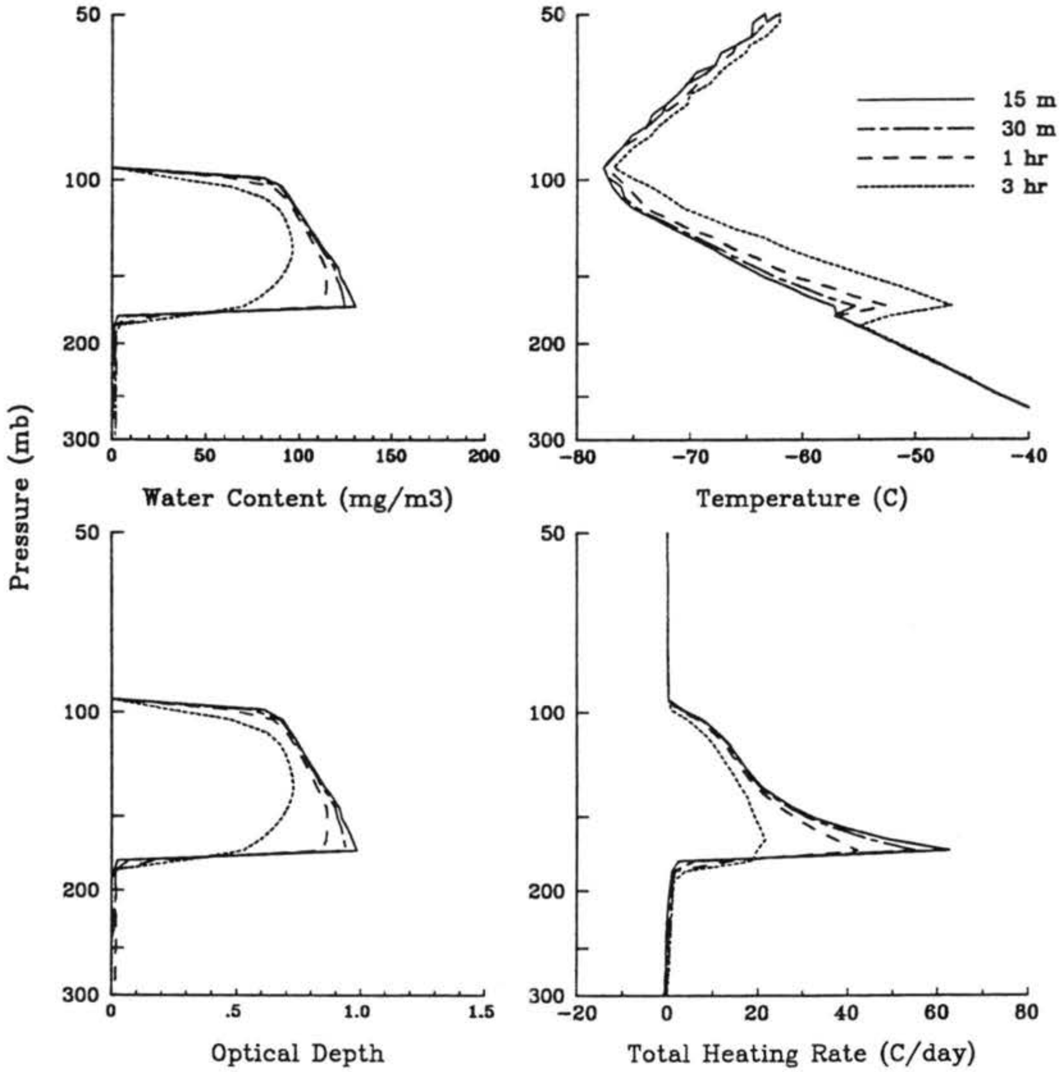


Figure 4.25: Radiative properties for the 125 mb storm outflow tropical cirrus.

### 150 mb storm outflow tropical cirrus

The 150 mb storm outflow cirrus is almost identical to the 125 mb cirrus. Because the main source of pristine ice is homogeneous freezing of cloud drops, the warmer nature of this cloud as compared to the 125 mb cirrus has little impact on the resulting ice categories (Fig. 4.26). The mass of the aggregates is double at 15 and 30 minutes due to improved collection effeciencies but the final mass at 3 hours is identical to the 125 mb cirrus.

The radiative heating rate in Fig. 4.27 is also similar to the 125 mb cirrus except for the small cloud top cooling at 125 mb. This cirrus is warmer than the 125 mb cloud allowing a very small amount of cooling to space.

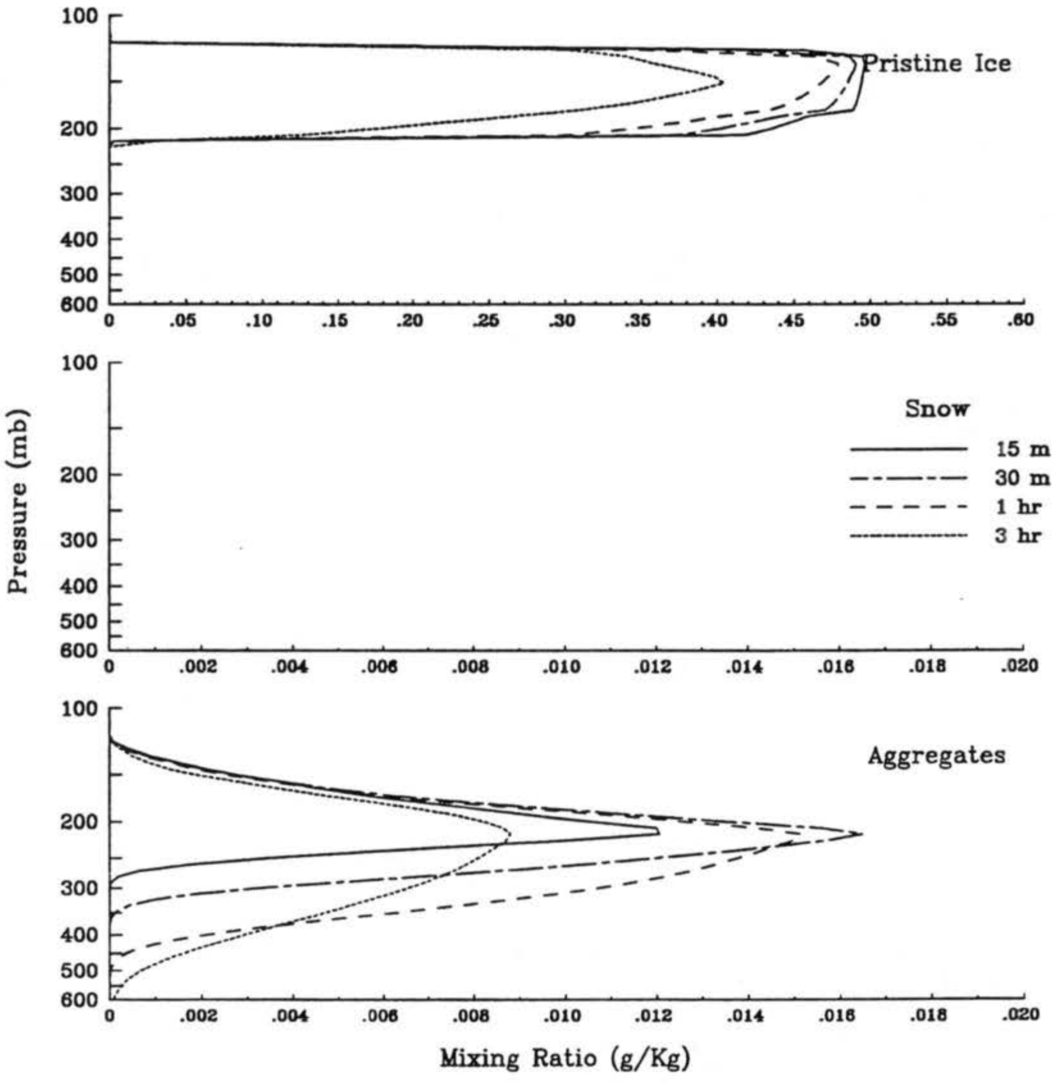


Figure 4.26: Development of the ice water mixing ratio for the 150 mb storm outflow tropical cirrus.

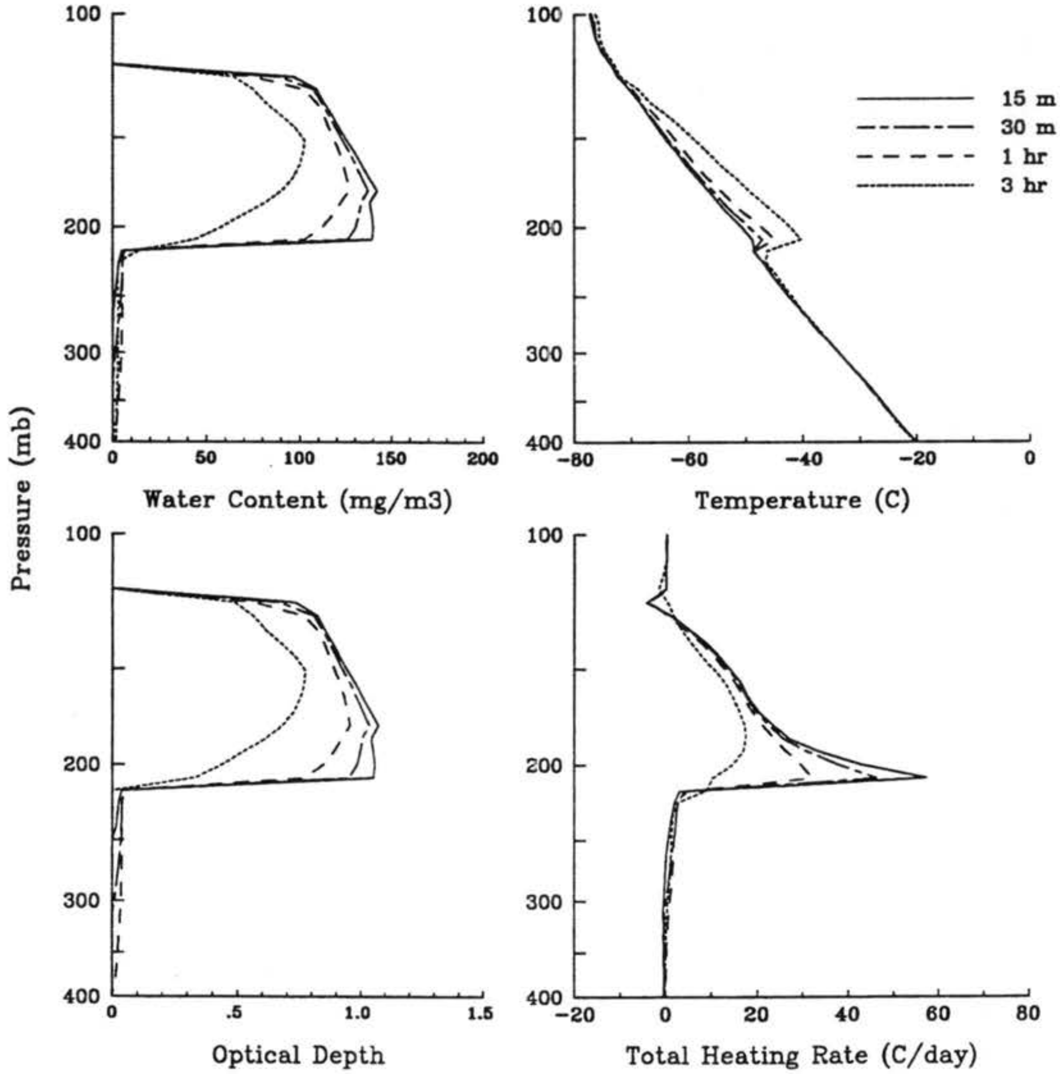


Figure 4.27: Radiative properties for the 150 mb storm outflow tropical cirrus.

**250 mb storm outflow tropical cirrus**

Unlike the previous two cirrus cases, the 250 mb storm outflow cirrus has a significant amount of aggregates (about 20% of the magnitude of pristine ice) in the first half hour (Fig. 4.28). Even snow exists in a small amount. This indicates that more water vapor is avaiable for the same $RH_i$ because of the warmer temperature of this cloud. The final mass of pristine ice at 3 hours exists in a shallower layer than the previous cases because of loss to collection and sublimation from the radiative heating.

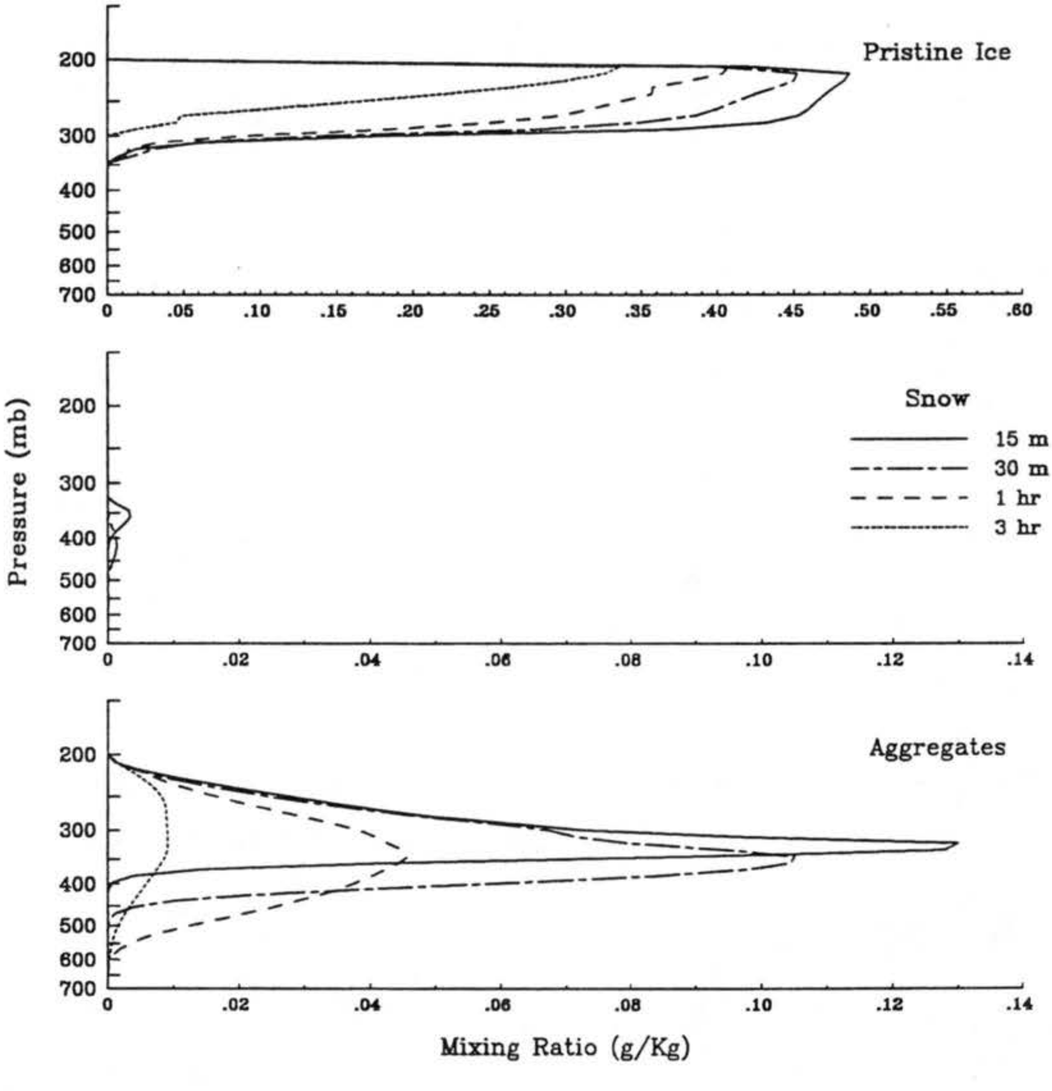


Figure 4.28: Development of the ice water mixing ratio for the 250 mb storm outflow tropical cirrus.

The character of the heating profile is also changed from the other cirrus cases (Fig. 4.29) due to both the fallout of aggregates and the warmer cloud temperature. The cloud top cooling is now as large as $-30°C/day$ and quite distinct. Warming is present from 250 mb to 500 mb depending on the sedimentation of aggregates.

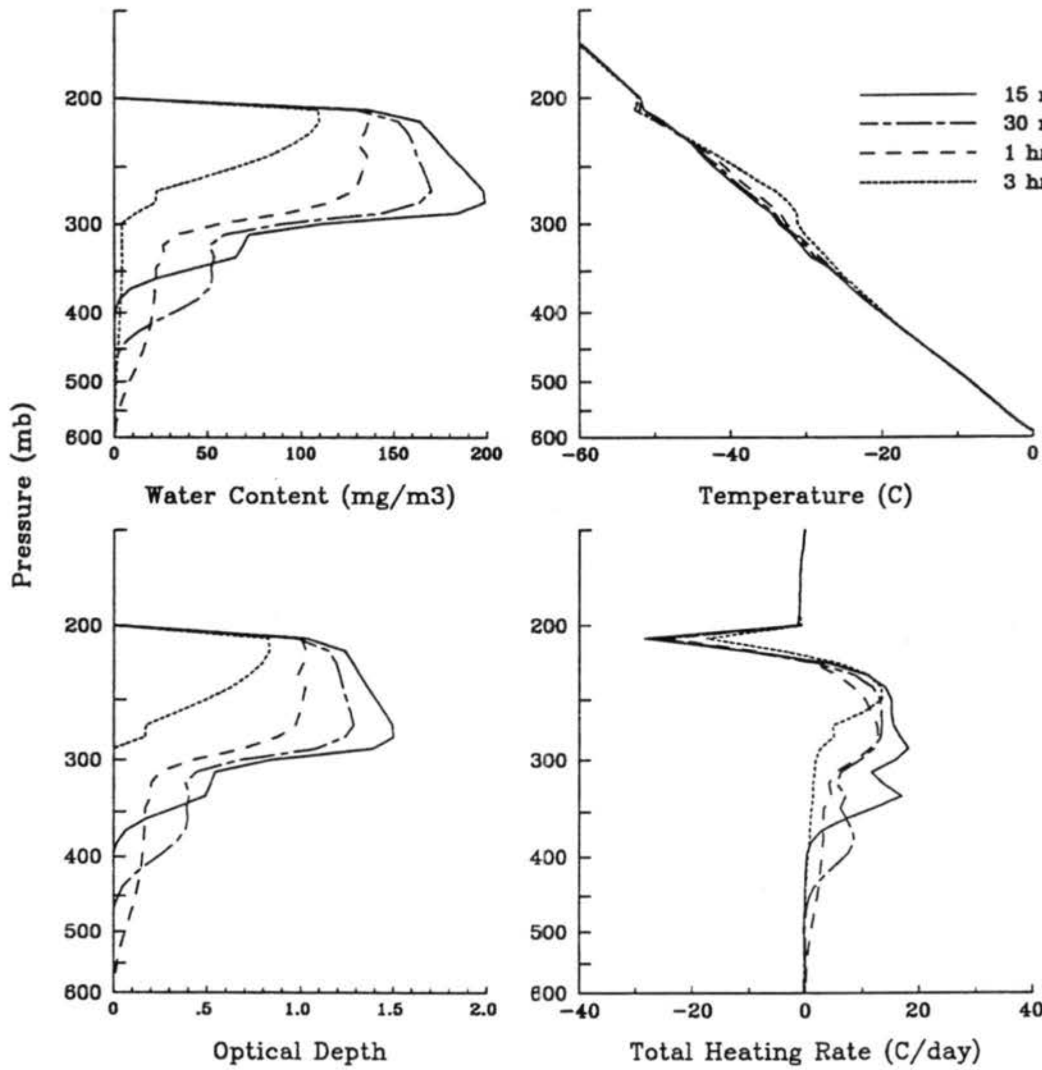


Figure 4.29: Radiative properties for the 250 mb storm outflow tropical cirrus.

As can be seen from the 9 simulations discussed in this section, the character of a given cirrus cloud will be strongly dependent on temperature as well as the method of initialization. The production of cirrus can be generalized into three regimes, colder than $-50°C$, between $-50°C$ and $-30°C$, and warmer than $-30°C$. These temperature ranges approximately correspond to depositional freezing, haze/cloud homogeneous nucleation, and heterogeneous depositional/condensational freezing respectively. The warmest temperature range will also likely have cloud water present. The storm outflow cirrus results are less dependent on temperature except for aggregate production and cloud top cooling. The various characteristics of these cirrus must be modeled by a single 1D cloud parameterization.

### 4.3.2 One category vs. three categories of ice

To illustrate the importance of modeling more than one ice category for a cirrus cloud, two cirrus simulations were repeated using the one generic ice category described in section 3.2.2 for the RAMS large-scale model setup. Fig. 4.30 displays the 150 mb tropical cirrus total ice for the original simulation with pristine ice, snow, and aggregates compared to the one ice category results. The most obvious difference between the two simultations is the lack of precipitation trails for the one ice category case. The one category case has therefore over-predicted the maximum ice mixing ratio.

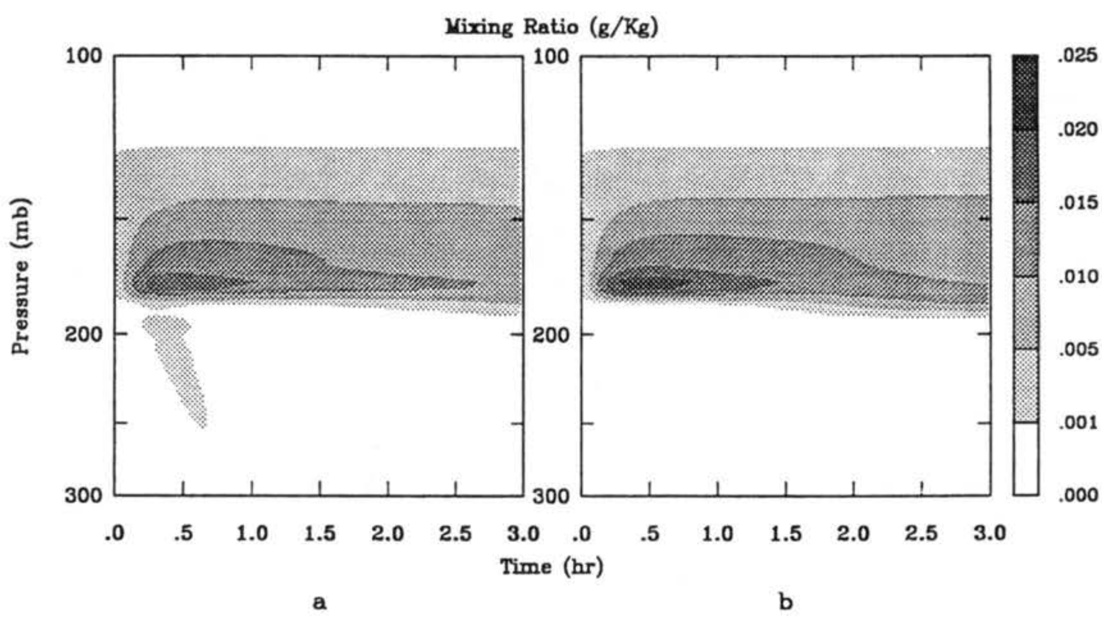


Figure 4.30: Comparison of ice mixing ratios for the 150 mb tropical cirrus for (a) 3 ice categories and (b) 1 ice category simulations.

The 350 mb midlatitude cirrus shown in Fig. 4.31 shows a larger discrepency than the previous comparison. The one category ice simulation consistently over-predicts the total hydrometeor mixing ratio in a shallower cloud layer. The one ice category fails to capture the deepening of the cirrus caused by creation of larger crystals by collection which acquire a larger terminal velocity than the smaller ice crystals.

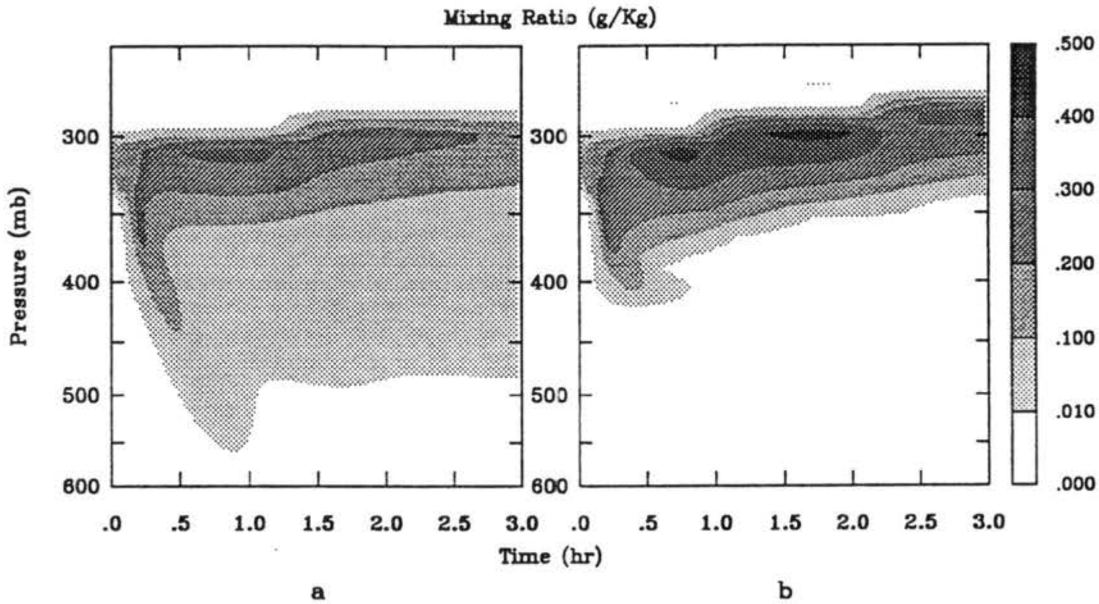


Figure 4.31: Comparison of ice mixing ratios for the 350 mb tropical cirrus for (a) 3 ice categories and (b) 1 ice category simulations.

These results indicate the three ice category microphysical scheme is necessary to correctly model the sedimentation of large particles which either create precipitation trails or deepening. By applying a 1D cloud parameterization which models the hydrometeor categories of pristine ice, snow and aggregates as well as cloud water and rain, the desired microphysical complexity is possible without compromising the host model effeciency.

### 4.3.3 The effect of solar heating on ice development

The simulations presented so far all began at 1400h local time. To determine the effect of solar heating on the cirrus, each simulation was repeated at 0200h local time. To summarize, for the cirrus cases which were optically thinner with little to no solar heating show pratically no difference between the day and night simulations. For the cirrus clouds at 250 mb, the ice mixing ratio for pristine ice and aggregates do not decrease in time as seen with the day simulations because of sublimation from solar heating. The final mixing ratio of pristine ice is actually about 10% larger for the night simulation from cloud top cooling.

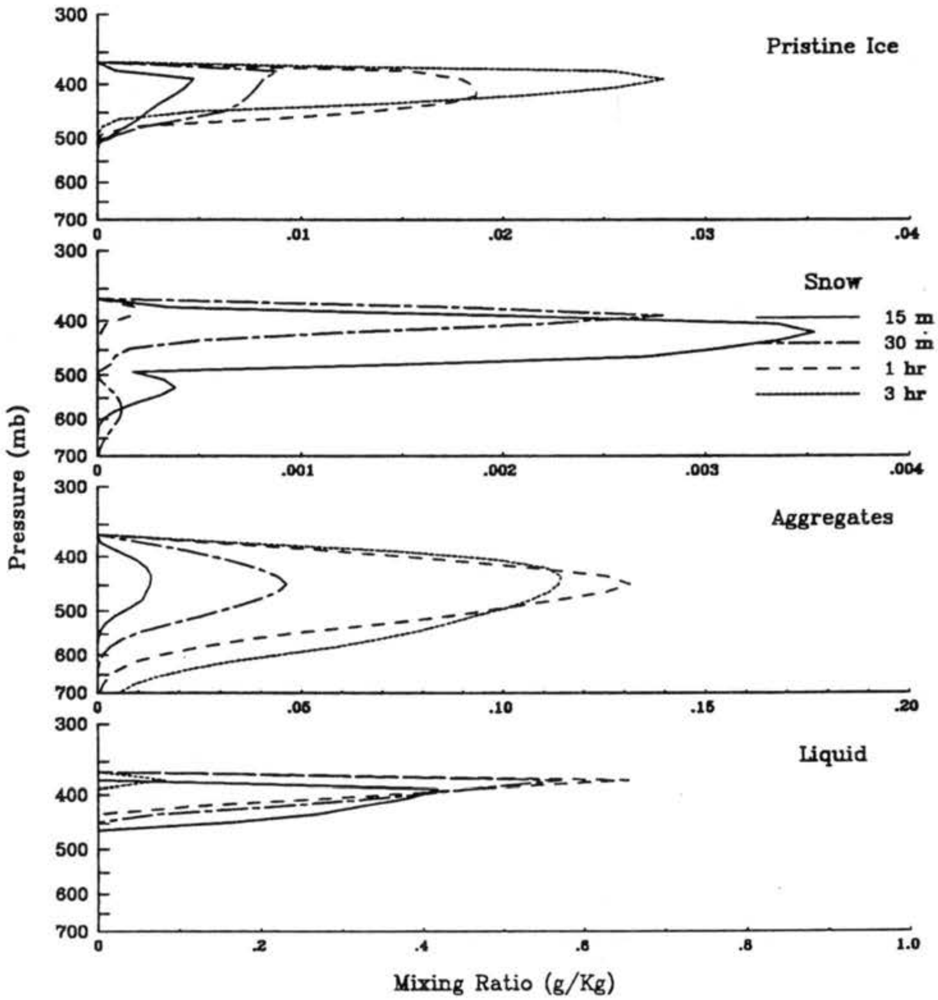


Figure 4.32: Development of the cloud water mixing ratios for the night simulation of the 450 mb midlatitude cirrus.

The most dramatic change in mixing ratio is for the 350 mb and 450 mb midlatitude cirrus. Fig. 4.32 displays the results for the 450 mb simulation. Comparing this figure to Fig. 4.22, the threefold increase in pristine ice and tenfold increase in aggregates at 3 hours are immediately apparent. Cloud water has also increased to 10 times the daytime simulation at 1 hour.

The heating rate profile for the night simulation shown in Fig. 4.33 explains the increase in cloud water mixing ratio. The lack of strong solar heating results in a large increase of cloud water instead of evaporation as seen in the daytime simulation. The strong cloud top cooling also allows more in pristine ice nucleation and vapor growth of snow. The combination of all these factors causes the large increase in aggregates by 3 hours.

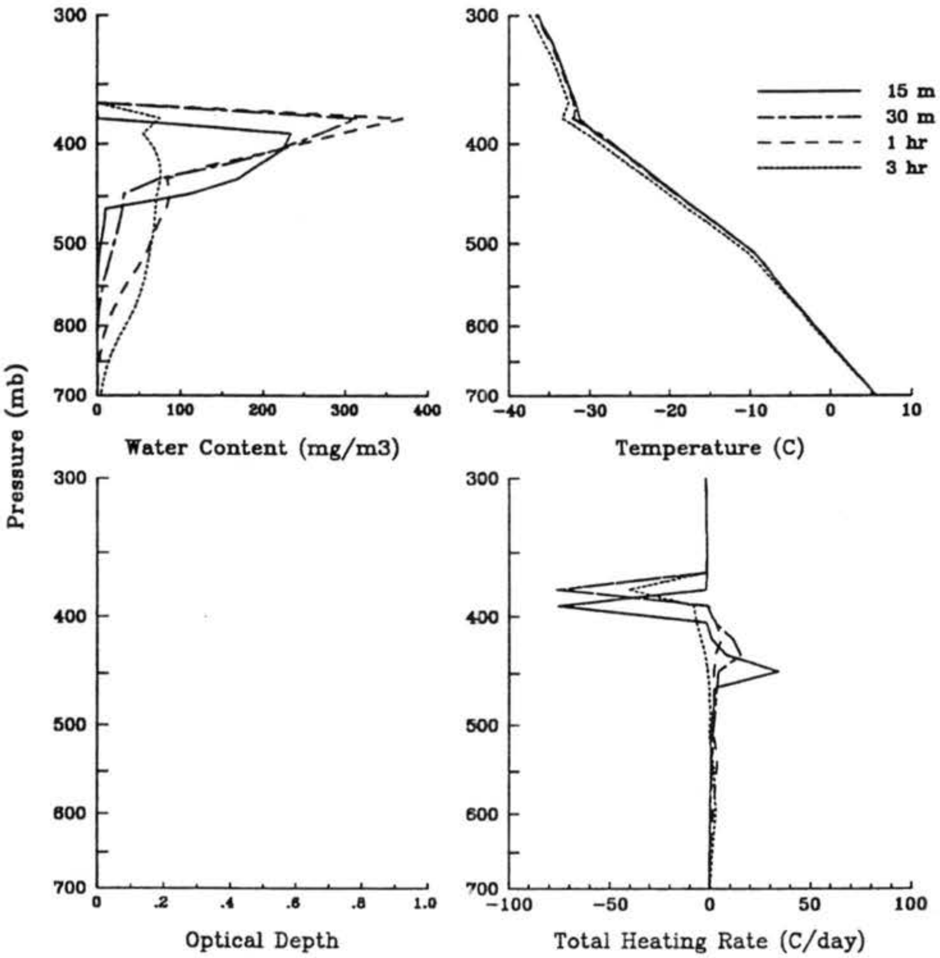


Figure 4.33: Radiative properties for the night simulation of the 450 mb midlatitude cirrus.

The comparison of day versus night simulations easily illustrates the importance of solar heating feedback on the development of the cirrus. As can be expected, the optically thinner clouds are less affected by solar heating. Therefore, an accurate radiative scheme is necessary to determine whether or not a significant radiative feedback will modify the development of the cloud.

### 4.3.4 The effect of cloud heating or cooling on ice development

To investigate the total radiative feedback on the cirrus development, two cases were simulated without any condensate included in the radiation parameterization. The results for the 250 mb tropical cirrus is shown in Fig. 4.34. With no radiative feedback, the mixing ratio of pristine ice and aggregates are slightly larger than the original simulation (Fig. 4.15) at all times. The cloud develops in the same way with a deepening by aggregates at 3 hours. The pristine ice peak in mixing ratio is slightly lower in height due to the lack of nucleation from the cloud top cooling when radiation interacts with the cloud development.

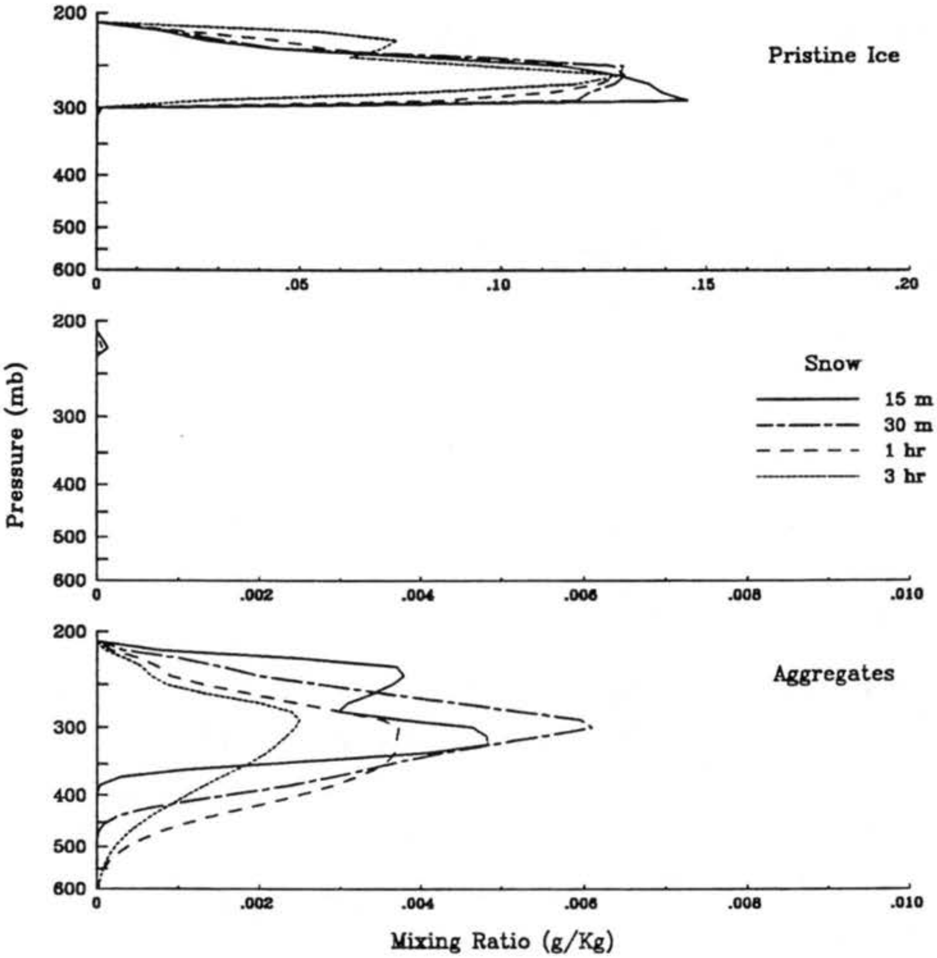


Figure 4.34: Development of the cloud water mixing ratios with no radiative feedback of the 250 mb tropical cirrus.

The effect of radiation on mixing ratio for the 450 mb midlatitude cirrus (Fig. 4.35) is primarily determined by the larger amount of cloud water present in the first hour. The lack of cloud warming which had previously removed the cloud water (Fig. 4.22) has instead allowed the liquid water to remain. The diffusion mixing of the pseudo-adiabatic layer has increased the amount of water vapor in the top portion of the cloud and likewise decreased water vapor in the lower half of the cloud. The cloud water therefore increases until it reaches a maximum around 1 hour. At this point enough ice particles exist to begin to effectively collect the cloud droplets through riming. As the crystals aquire mass, the aggregate ice category grows. The large crystals with faster fallspeeds then settle out of the saturated cloud deck and evaporate in the layers below. The collection and sedimentation is so efficient that the final mixing ratios of the cloud species is smaller than the simulation including radiation feedback. The most significant difference between the two cases may not be the final state of the cloud but the cloud development during the 3 hours in which the cloud grows and decays.

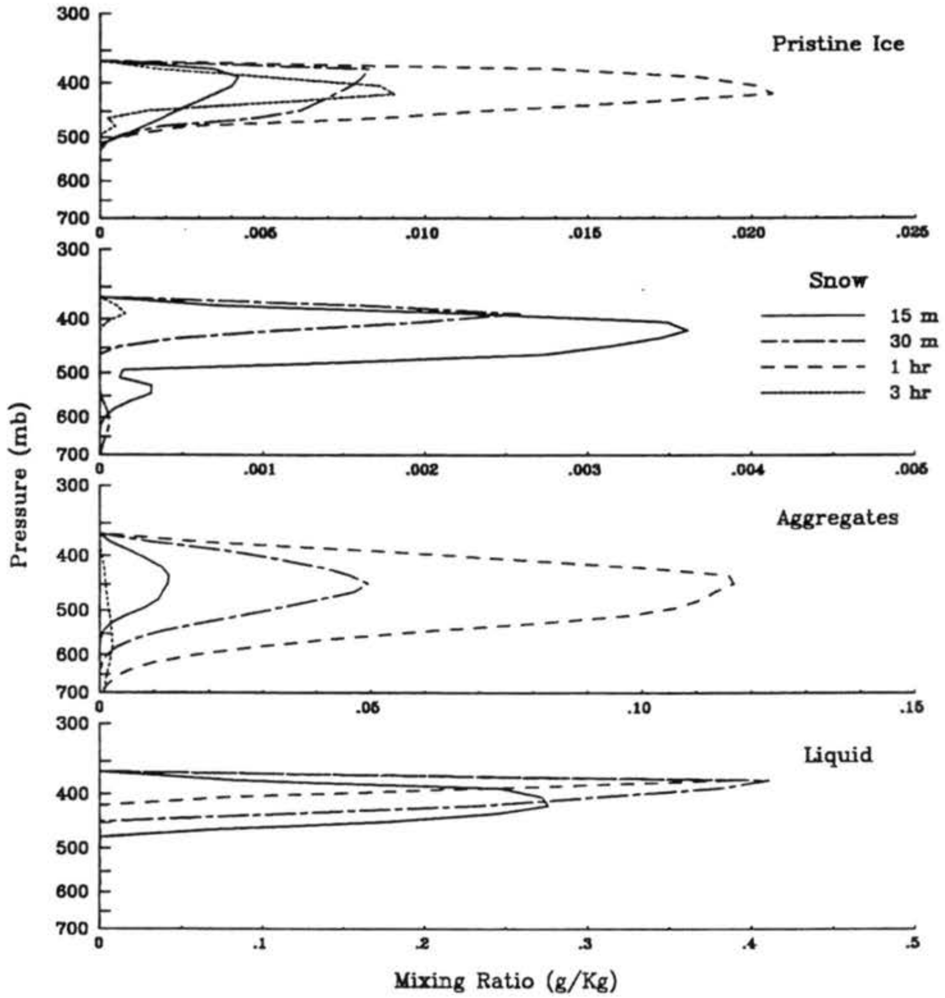


Figure 4.35: Development of the cloud water mixing ratios with no radiative feedback of the 450 mb midlatitude cirrus.

The radiative feedback appears to be a subtle effect on the development of the hydrometeors. The effect on the temperature and surface flux is easier to evaluate. Fig. 4.36 shows the time series of the surface flux for both the tropical and midlatitude cirrus compared to the clear sky values. The initial decrease in the shortwave flux is about 200 $W/m^2$ and larger for the case where liquid water was present (450 mb midlatitude cirrus). Likewise, the increase in longwave surface flux ranges from 10 to 40 $W/m^2$. So for all the cirrus cases but 125 mb and 250 mb tropical cases, the presence of the cirrus significantly impacts the surface radiation budget.

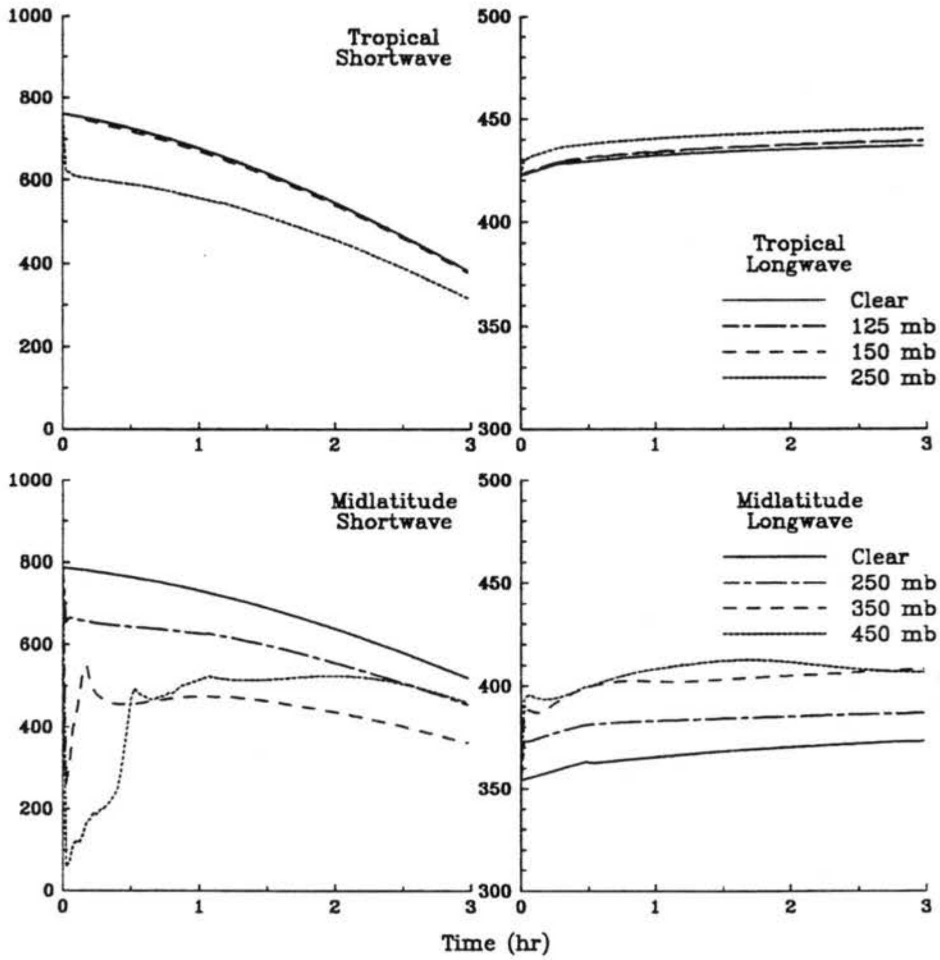


Figure 4.36: Surface flux of radiation at the ground for each cirrus simulation.

### 4.3.5 Conclusions

To adequately model the cirrus cloud in a 1D format, the following conclusions were made which should be applied to the design of a cloud parameterization. A timestep of 90 or 180 seconds is necessary to capture the relatively fast processes of nucleation, collection, and sedimentation. A $\Delta z$ of 250 m or smaller is needed to resolve the magnitude of the primary and secondary maximum of mixing ratios. Initialization with either $SS_i$ or direct addition of cloud water will significantly impact the development of the cirrus cloud. Three categories of cloud ice are needed to generate the precipitation trails and deepening of cirrus clouds caused by large size particles. The cloud radiative feedback strongly interacts with the temperature profile and surface flux when the cloud optical depth is greater than 0.1. The radiative feedback also affects with the development of hydrometeors but is a more complex interaction. By examining these sensitivity studies, the initial configuration for the 1D cloud parameterization has been determined as well as gaining a basic understanding of what results to anticipate for the cirrus simulations by the nested cloud model.

# Chapter 5

# RESULTS

To determine the success of using a 1D nested cloud parameterization to resolve cirrus in a large-scale numerical model, several cirrus cases used for the sensitivity tests were repeated using the psuedo-GCM RAMS configuration and the nested 1D cloud model. Four cirrus cases were selected and include the 150 mb and 250 mb tropical cirrus, the 350 mb midlatiude cirrus, and the 250 mb storm outflow tropical cirrus. For the cirrus created by large-scale forcing, the host RAMS model initializes the cirrus using the elevated relative humidity described in Chapter 4. The storm outflow cirrus was initialized by introducing cloud water to represent the advection of cloud species from convective towers.

The nested cloud model is triggered by the second host timestep and called every host timestep for the remainder of the 3 hour simulation. These simulations will be refered to as the nested simulations while the sensitivity studies shown in the previous chapter will be denoted as the explicit simulations. The results presented for each cirrus case include the development of ice species as resolved by both the host and nested grids, the radiative heating rates, the impact of the host model resolution on the results, and a discussion of the cloud layer stability. These results will provide a preliminary evaluation of the performance of the 1D cloud parameterization.

## 5.1 150 mb tropical cirrus

The 150 mb tropical cirrus simulation was repeated using the psuedo-GCM RAMS configuration with the nested 1D cloud model. The cirrus was initialized by increasing the relative humidity with respect to ice ($RH_i$) to 150% in the cloud layer as descibed in Chapter 4. The host model has 22 vertical levels with a spacing ($\Delta z$) of 1000 km and a timestep of 900 seconds. Radiation tendencies are updated every host timestep. The nested cloud model had a timestep ratio of 10 which allows a 90 second timestep for the nested grid. The vertical nest ratio was also set to 10 which achieved a 100 m spacing in the nested model. Radiation tendencies were updated every 450 seconds for the nested grid. This model configuration was used for all the cirrus simulations presented here.

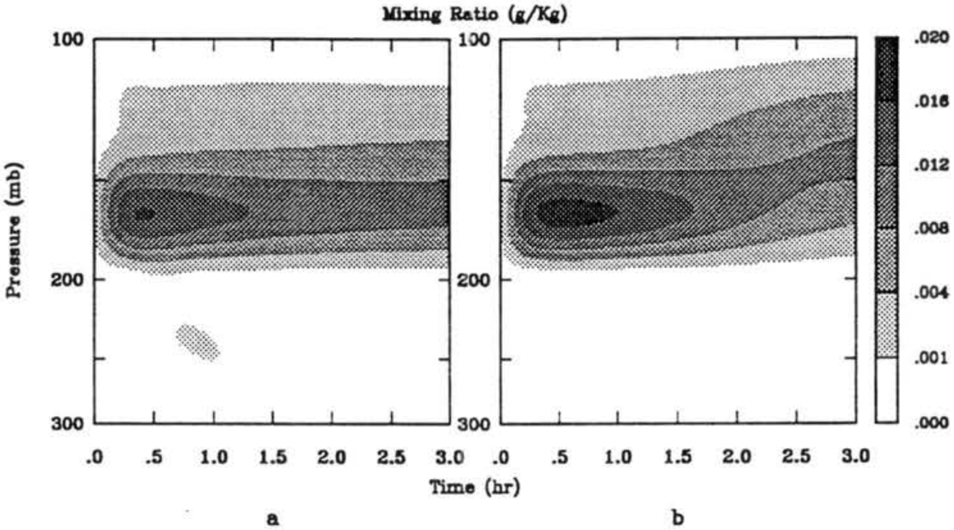


Figure 5.1: Ice species in the 150 mb tropical cirrus when (a) the nested cloud model is used and (b) the nested model is not used.

The 150 mb tropical cirrus ice mixing ratio time series are shown in Fig. 5.1. Presented are the values as interpolated to the host model grid. Shown are two simulations, one in which the nest model is triggered by the second host timestep and the other where the nested model is never used. When the nested grid model is not called the ice mixing ratios are over-predicted while the maximum amount ascends by the end of the simulation. The model also fails to resolve the small amount of large ice fallout. Comparing this figure to the simulation in Chapter 4 (Fig. 4.13), the performance of the nested cloud model can be judged. Note that when the nested model has computed the cirrus development for each host timestep, the cloud variable tendecies are interpolated back to the host cloud model resolution. By replacing the explicit simulation of the cirrus on the host grid with a nested grid, some small scale detail is lost. For this particular case, the nested results compare well with the explicit simulation. Both cases computed a maximum ice mixing ratio around 0.16 g/kg initially which tapers off to 0.12 g/kg. The nested simulation also shows the small amount of ice falling out of the cloud around 1 hour.

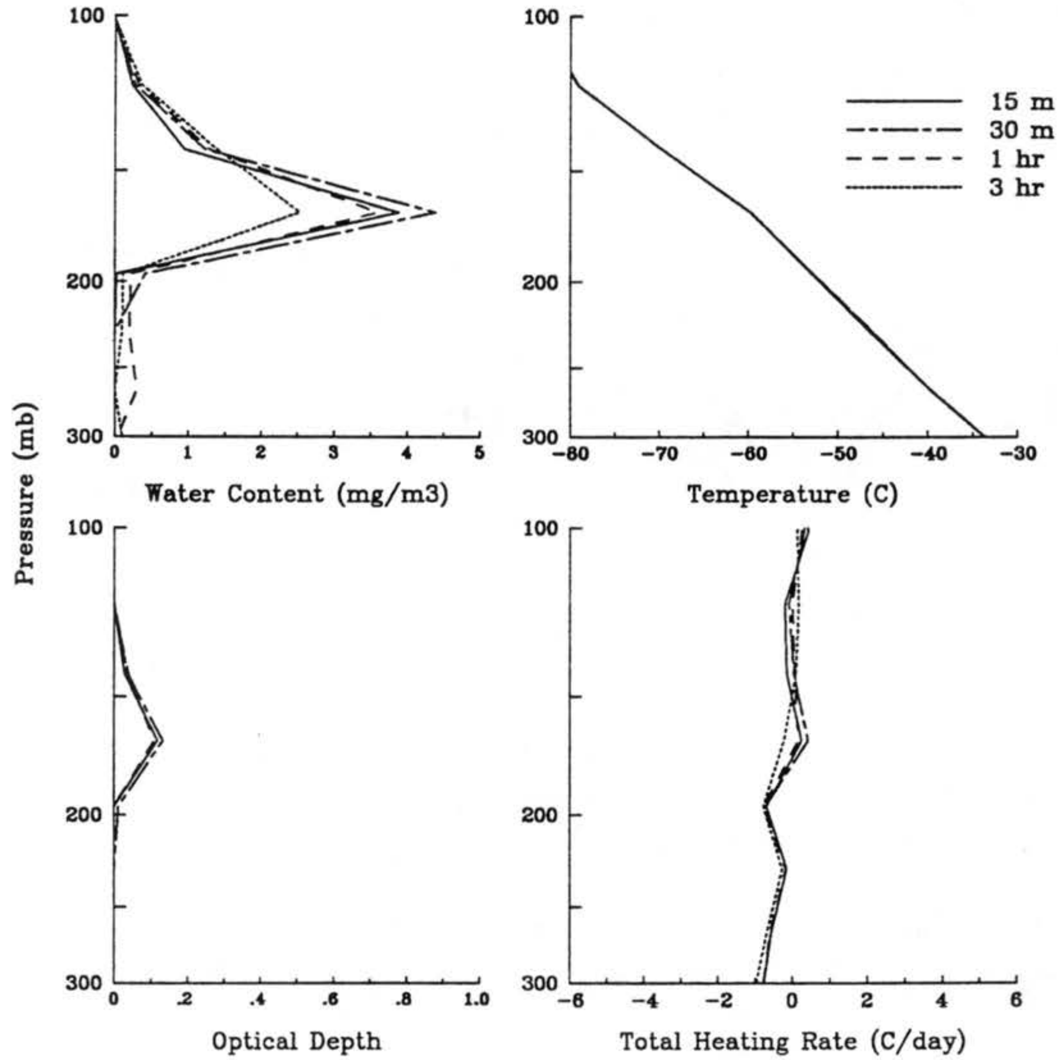


Figure 5.2: Radiative properties for the 150 mb tropical cirrus.

As seen in the explicit simulation (Fig. 4.14), the 150 mb tropical cirrus does not generate large heating rates ($1°/day$) from this radiation parameterization. The nested simulation shown in Fig. 5.2 also produced little to no radiative impact from this cirrus. For this particular cirrus, the improvement in the GCM simulation by using the nested cloud model may not be large enough to justify using the parameterization.

### 5.1.1 Ice development in the nested 1D cloud model

To examine the behavior of the nested cloud model, the time series for the ice species before interpolation back to the host grid is shown in Fig. 5.3. The 15 minute ice mixing ratios actually corresponds to the initialization of the nested model at the beginning of the 2nd host timestep. The development of pristine ice is similar to the explicit simulation with the initial amount at 15 minutes growing and then decreasing by 3 hours due to collection.

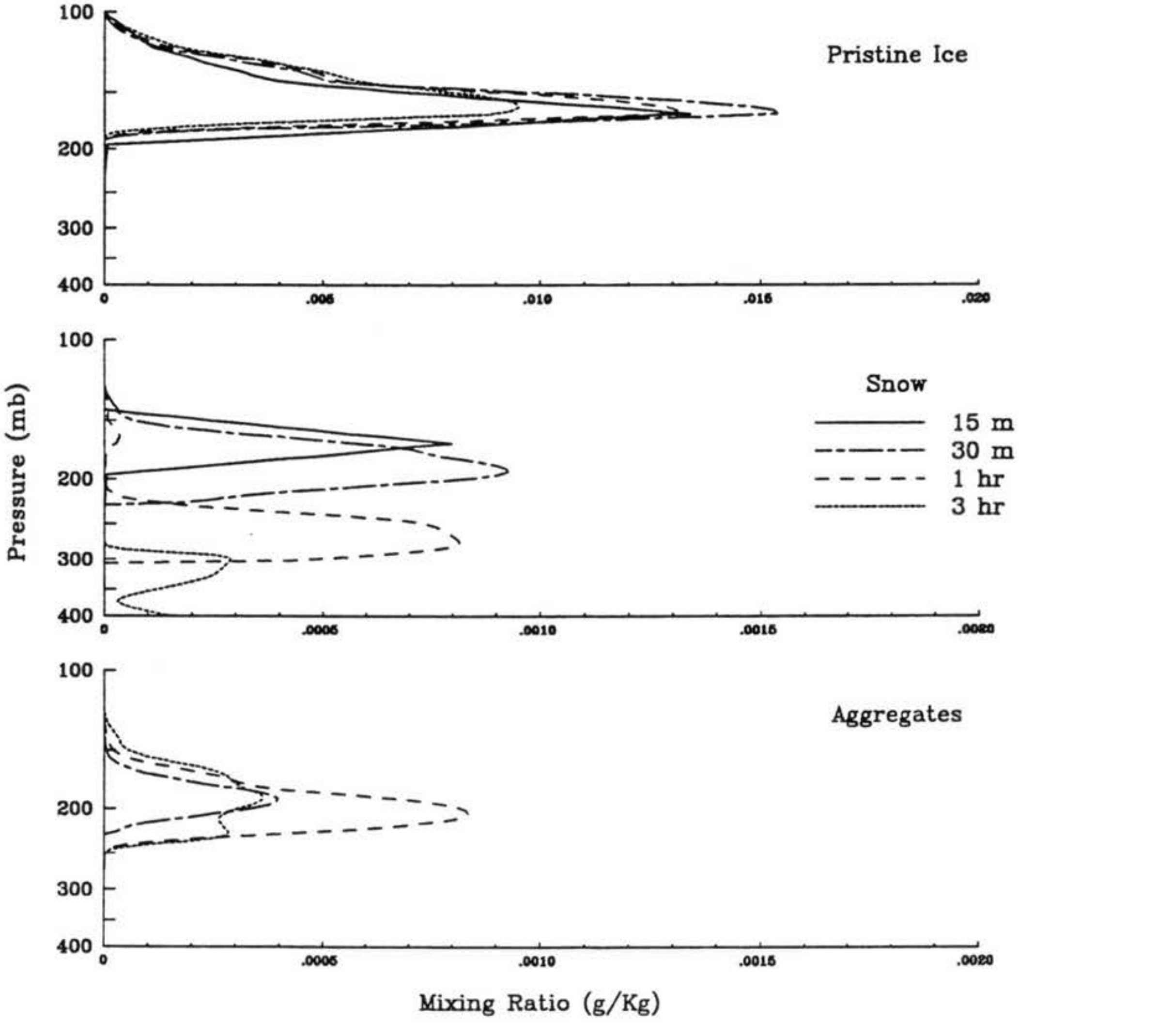


Figure 5.3: Ice species in the nested model for the 150 mb tropical cirrus.

The main difference between the explict and nested simulations is the amount of snow and aggregate species. Because of the conversion from one ice category in the host model to the nested model pristine ice and snow categories, the amount of snow is larger than computed by the explicit simulation. As discussed earlier, the only significant difference between the snow and aggregate categories is their method of formation. Terminal velocity and characteristic diameter are fairly similar. So the two categories will practically behave in the same manner. The nested model does convert the snow into aggregates through collection but for this case, the majority of the precipatation trails are composed of snow. The mass of the ice fallout is only about half of the amount computed by the explicit simulation.

### 5.1.2 Host model resolution

The initilization of the nested cloud model is only as accurate as the host model resolution will provide. To test the dependancy of the cloud simulation on the host model resolution, the 150 mb tropical cirrus case was repeated using a vertical spacing of 2000 m. The vertical nest ratio was increased to 20 to maintain a nested vertical spacing of 100 m. The dramatic impact of increasing the host vertical spacing is shown in Fig. 5.4. The mixing ratio of ice for both simulations with and without the nested cloud model was less than half the amount computed by the 1000 m $\Delta z$ grid. The simulation with the nested cloud model fails to resolve any precipitation trails.

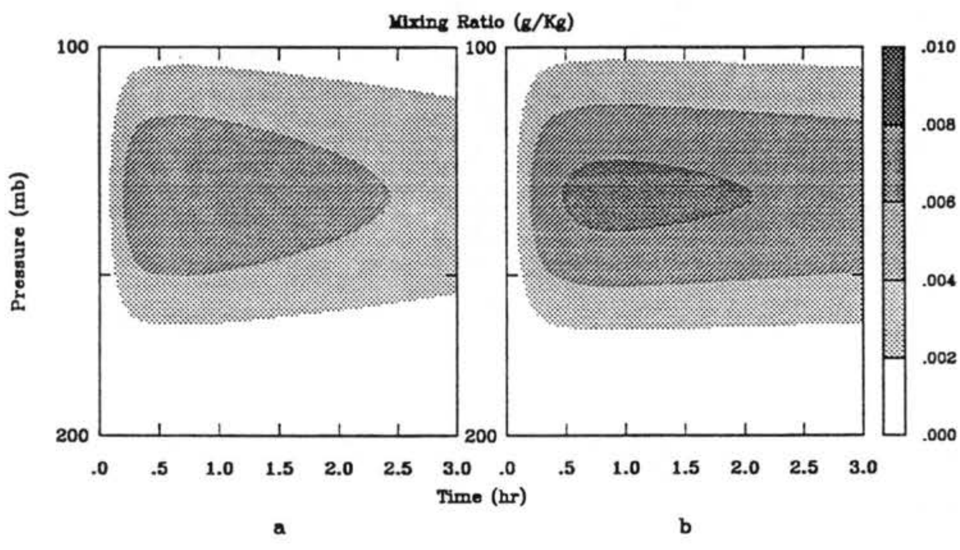


Figure 5.4: Ice species in the 150 mb tropical cirrus with 2000 m $\Delta z$ vertical spacing when (a) the nested cloud model is used and (b) the nested model is not used.

From this comparison, the results indicate that calling the nested cloud model does not improve the modeling of this cirrus. Similar conclusions were found for the the 250 mb tropical cirrus. In general when the host model did not use the cloud parameterization, the ice amounts were only slightly larger. The 350 mb midlatitude cirrus did show an improvement by using the nested model even at this low a resolution so those results will be presented. Large-scale models with small vertical resolution may only benefit from a nested cloud model if the host model does not predict cloud species. To apply a cirrus cloud model in this manner would require an additional parameterization to initiate the cloud model from the available large-scale model variables.

### 5.1.3 Cirrus layer stability

The initial design of the 1D cloud model includes the three schemes for.microphysics, radiation, and turbulence. To examine the interaction of the three components, the tendency of potential temperature ($\theta$) computed by each scheme is presented in Fig. 5.5 as the change in $\theta$ over the three hour simulation. Because of the optical thinness of the 150 mb tropical cirrus, the radiation does not significantly alter $\theta$.

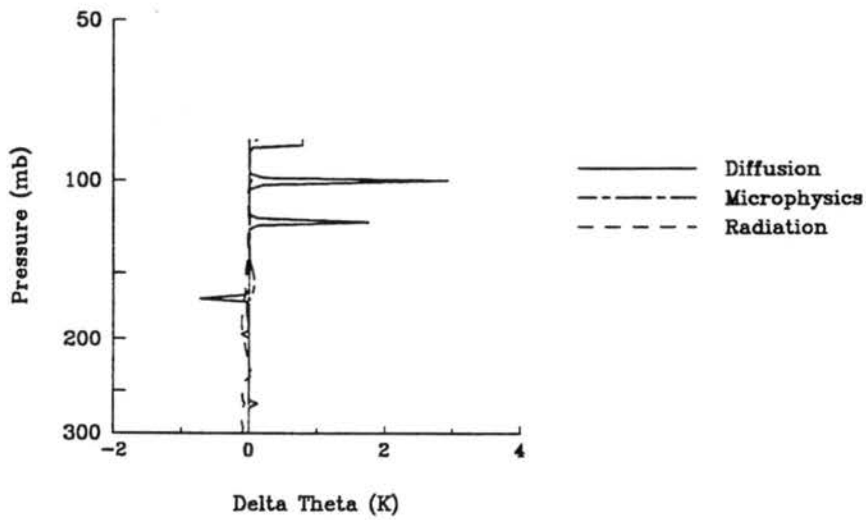


Figure 5.5: Change of potential temperature due to radiation, turbulence, and microphysics in the 150 mb tropical cirrus over the 3 hour simulation.

The diffusional mixing from the turbulence model does slightly change $\theta$ in such a way as to remove the pseudo-moist adiabatic layer used to initialize the cloud simulation. Impact on $\theta$ from the phase change of water does not change the stability of this cirrus cloud layer. In general, as a result of the small amount of ice present, the cirrus is not dynamically active.

### 5.2 250 mb tropical cirrus

The 250 mb tropical cirrus which is initiated at a warmer temperature has an order of magnitude larger amount of ice compared to the previous 150 mb cirrus simulation. Fig. 5.6 shows the total ice mixing ratio for both the host/nest and host only model simulations. Comparing both figures to the explicit simulation (Fig. 4.15), only the results using the nested model show a deeping of the cloud layer and precipitation trails. The initial maximum ice amount of 0.24 g/kg is greater than the 0.14 g/kg from the explicit simulation. As a result of the discrepancy at 15 minutes, a much larger amount of ice settles out of the cloud at 30 minutes for the host/nest simulation. The final mixing ratio of ice at 3 hours for both simulations are 0.02 g/kg smaller than the explicit simulation but are at the correct height.

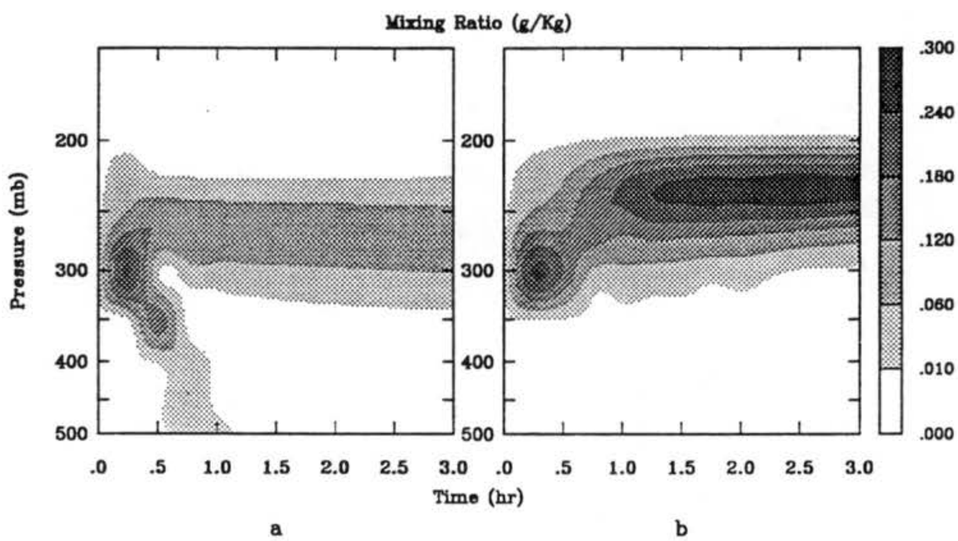


Figure 5.6: Ice species in the 250 mb tropical cirrus when (a) the nested cloud model is used and (b) the nested model is not used.

The consequence of an over-prediction of initial ice amount can also be seen in the radiative heating rates shown in Fig. 5.7. Refering to Fig. 4.19, the maximum heating at 30 minutes is at a lower height due to the large sedimentation of ice. While at 1 hour, the maximum heating has shifted higher to 250 mb and is significantly reduced. Much of the difference between the explicit and the parameterized simulations can be attributed to averaging the detailed nested information to the coarse host grid.

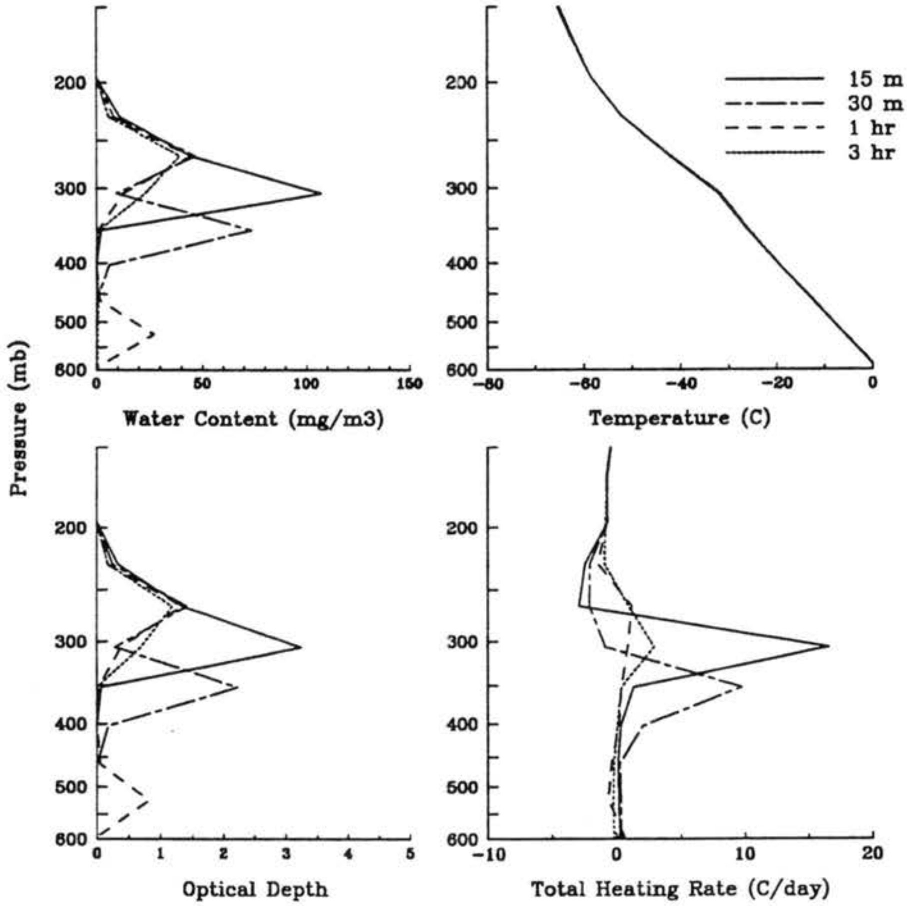


Figure 5.7: Radiative properties for the 250 mb tropical cirrus.

### 5.2.1 Ice development in the nested 1D cloud model

The individual amounts of the nested model ice species (Fig. 5.8) indicate the over-prediction of initial ice is solely attributed to the snow category. The pristine ice amount is actually very close to the amount of pristine ice nucleated in the explicit run (Fig. 4.15). The initialization of snow has created a large amount at 300 mb which is converted to aggregates later in the simulation. The original aggregate amount from the explicit simulation is only 0.006 g/kg.

The error in the nested model initialization is caused by the conversion of the one host ice species with an exponential number distribution to the two categories in the nested model. Because the host ice category allows a range of diameter from 1 $\mu m$ to 1000 $\mu m$, the mass of ice beyond the limiting diameter of 125 $\mu m$ is larger than the amount of ice

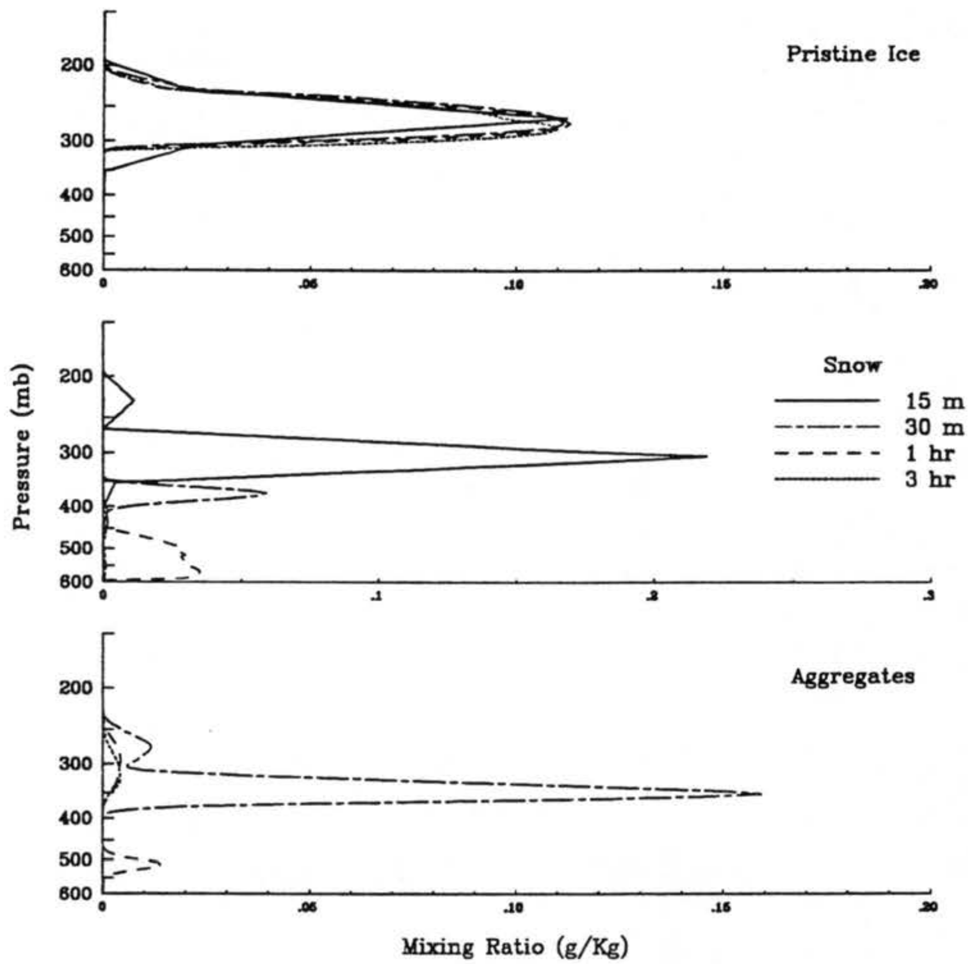


Figure 5.8: Ice species in the nested model for the 250 mb tropical cirrus.

the explicit simulation computed to grow by vapor deposition into the snow category. The easiest solution to this problem is to use a host model which has more than one ice category. This requirement would increase the model memory requirements as well as adding another variable to predict. At this time, the development of this parameterization will assume the host GCM will at most be only able to provide one ice category.

### 5.2.2 Cirrus layer stability

The stability of the 250 mb tropical cirrus is determined by the combination of the radiative forcing, latent heat effects, and the mixing from turbulence. Fig. 5.9 shows the change in the potential temperature ($\theta$) for this cirrus is due mainly to the heating and cooling through radiation. Turbulence mixing is creating a stabilizing tendency of $\theta$ to counteract the radiation tendency. Latent heat effects are significant but are not organized in such away as to dominate the change in $\theta$.

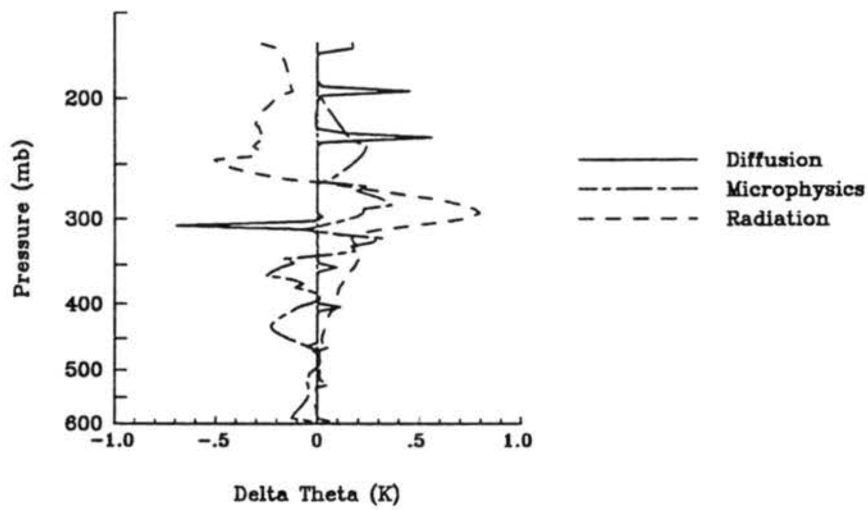


Figure 5.9: Change of potential temperature due to radiation, turbulence, and microphysics in the 250 mb tropical cirrus over the 3 hour simulation.

### 5.3 350 mb midlatitude cirrus

The 350 mb midlatitude cirrus total ice mixing ratio is shown in Fig. 5.10 for both the simulation with and without the nested model. By examining the explicit results (Fig. 4.20), mixing ratios for both simulations are found to be very close to the amount of the explicit simulation at 15 minutes. After 15 minutes, the simulation without the nested model consistently over-predicts the total water mixing ratio and fails to capture the precipitation of the larger ice from the cloud layer through sedimentation.

The decreased host resolution is also apparent when comparing the host radiative heating profiles of the nested simulation (Fig. 5.11) and the explicit simulation heating rates (Fig. 4.21). The resolved maximum cooling has been reduced from 20°C to 5°C. There is also a large difference at 1 hour between the explicit and nest model results. The virga for the nest model simulation did not evaporate as soon as the explicit model simulation causing a significant difference between the heating rates.

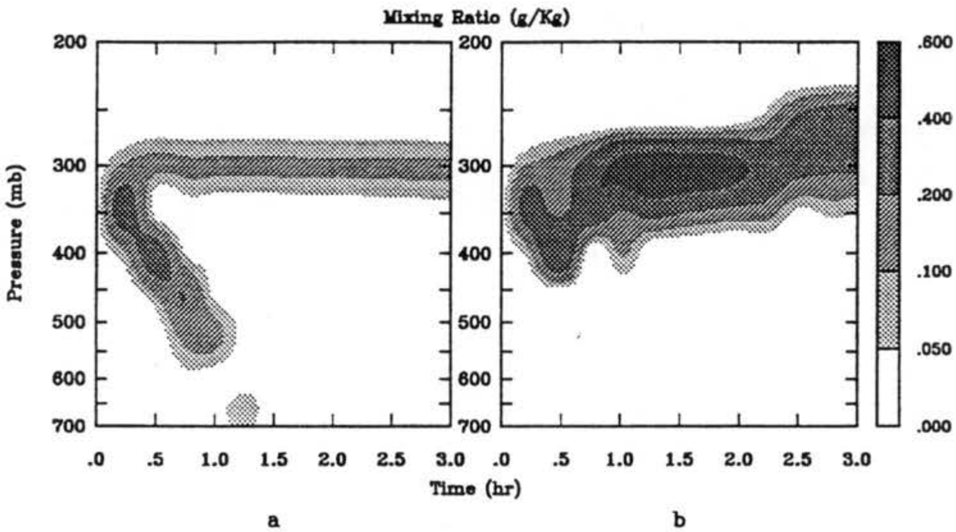


Figure 5.10: Cloud species in the 350 mb midlatitude cirrus when (a) the nested cloud model is used and (b) the nested model is not used.

### 5.3.1 Ice development in the nested 1D cloud model

The nucleation of a large amount of ice in the first host timestep is predominantly converted to the snow category as shown in Fig. 5.12. Pristine ice is less than half the amount of snow initially. The snow is converted to aggregates while both categories fall and evaporate. The total mixing ratio at the end of the simulation (0.12 g/kg) is very close to the explicit simulation (0.15 g/kg). The over-prediction of the one ice category mixing ratio during the first host timestep may indicate that allowing ice crystals to nucleate for diameters greater than 125 $\mu m$ instead of creation by growing to a large diameter through vapor deposition will create erroneous results. The bimodal distribution in the nested model microphysics created by defining two ice crystal categories, pristine ice and snow, removes this problem but errors from initialization by one ice category in the host model can not be avoided.

### 5.3.2 Host model resolution

The large amount of ice mass created in the host model during the first timestep is large enough to create a difference between the 2000 m $\Delta z$ simulations with and without the nested model. In Fig. 5.13, the total water mixing ratio for the host/nest simulation

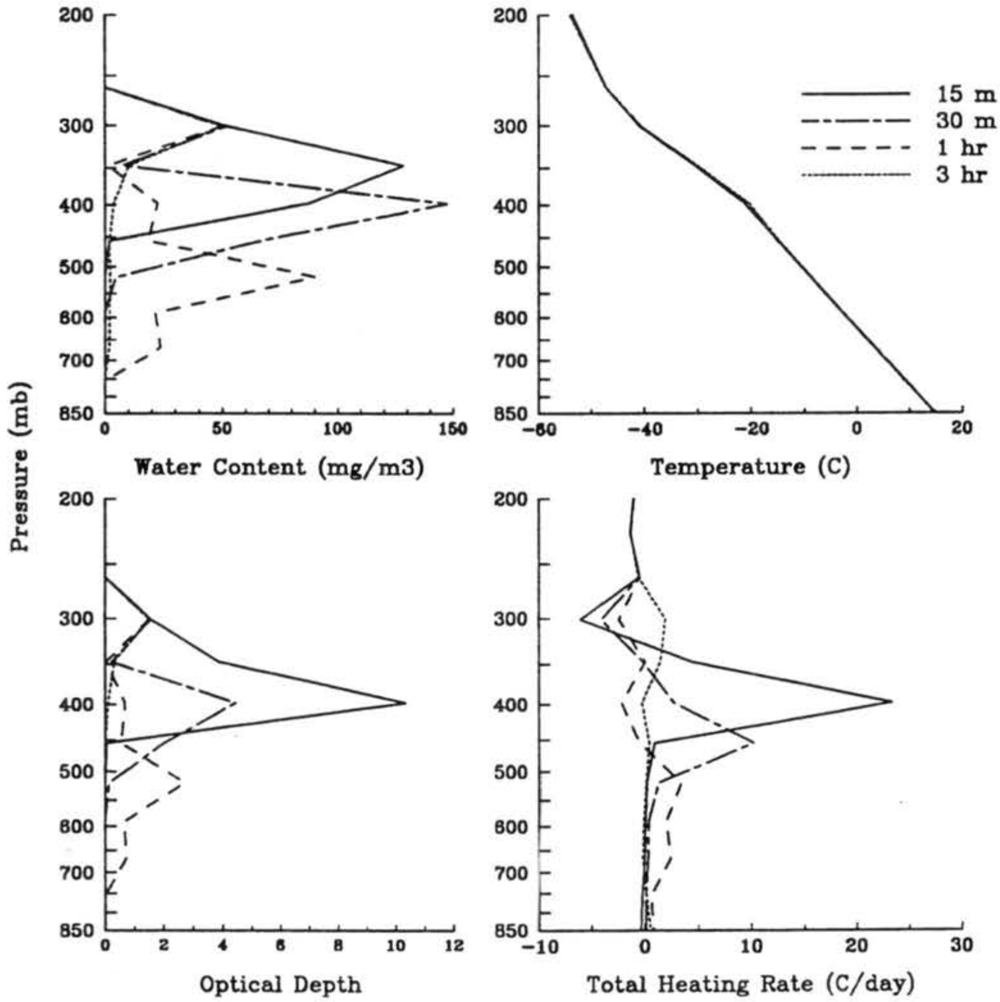


Figure 5.11: Radiative properties for the 350 mb midlatitude cirrus

shows the fallout of a large amount of the ice until at 3 hours only a small amount of the original ice remains. For a large amount of ice sedimentation, the nested cloud model will alter the development of the cirrus even at vertical spacings of 2000 m.

### 5.3.3 Cirrus layer stability

The change in the potential temperature for the 350 mb cirrus is similar to the 250 mb tropical cirrus case with the radiation playing an important role (Fig. 5.14) in destabilizing the cloud layer. But unlike the earlier case, the latent heat release corresponding with the region of radiative heating has the strongest impact on $\theta$. As seen in other cirrus simulations, the turbulent mixing responds with a stabilizing tendency for $\theta$.

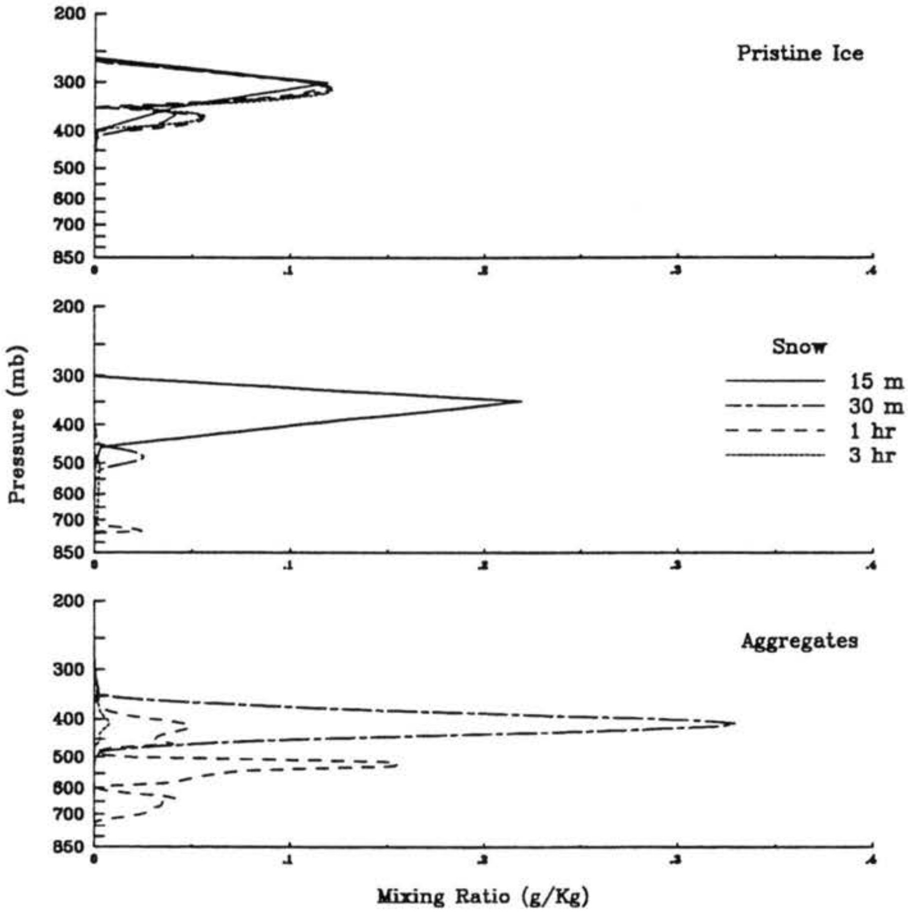


Figure 5.12: Ice species in the nested model for the 350 mb midlatitude cirrus.

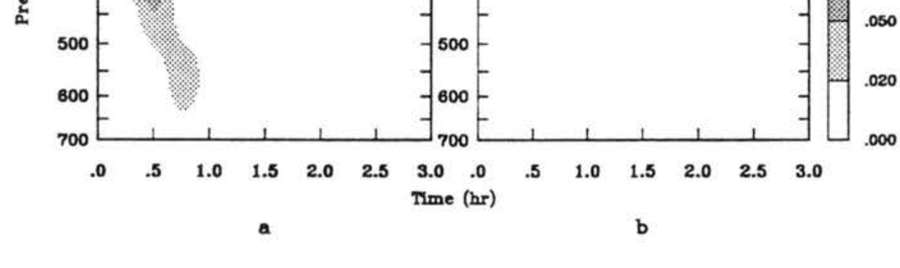


Figure 5.13: Cloud species in the 350 mb midlatitude cirrus with 2000 m $\Delta z$ vertical spacing when (a) the nested cloud model is used and (b) the nested model is not used.

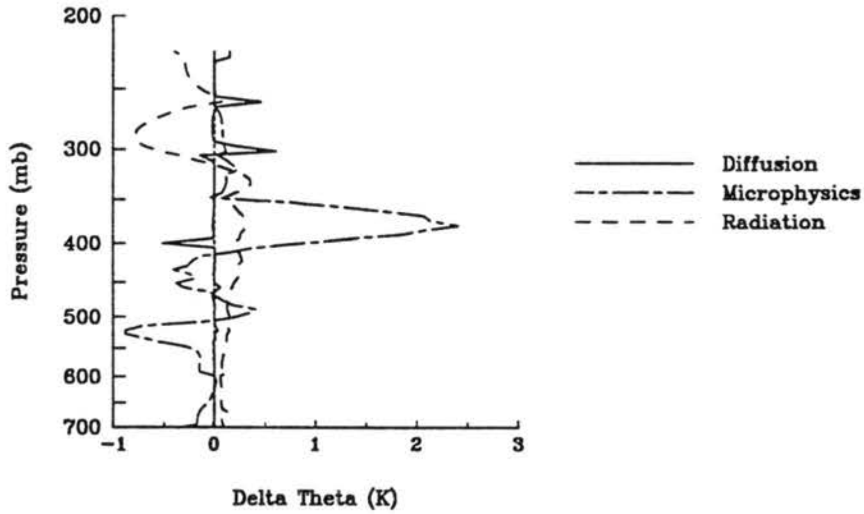


Figure 5.14: Change of potential temperature due to radiation, turbulence, and microphysics in the 350 mb tropical cirrus over the 3 hour simulation.

## 5.4 250 mb storm outflow tropical cirrus

The storm outflow initialization was created by adding 0.5 g/kg mixing ratio of cloud water and elevating the relative humidity with respect to ice 10% above saturation in the cloud layer. As shown before, the 250 mb tropical cirrus created by supersaturation generated a maximum ice mixing ratio of 0.28 g/kg and only 0.14 g/kg in the explicit simulation. By directly introducing cloud water, the primary mechanism for ice formation is homogeneous freezing of cloud droplets. The ice mixing ratios for both the simulations with and without the nested cloud model are shown in Fig. 5.15. Comparing these results to the explicit simulation in Fig. 4.28 shows the initial prediction of ice amount by the host model is just slightly larger (0.02 g/kg) but is at the correct height. At 30 minutes, the host/nest simulation has a large amount of ice falling out of the cloud layer, more than twice the explicit simulation. The precipitation trails are closer to the same value at 1 hour. By 3 hours, the host/nest results show a deeper layer with a final maximum ice mixing ratio of 0.3 g/kg which is the same as the explicit results. The results from the simulation not using the nested cloud model once agin over-predict the mixing ratio and fails to create sedimentation of the larger ice particles.

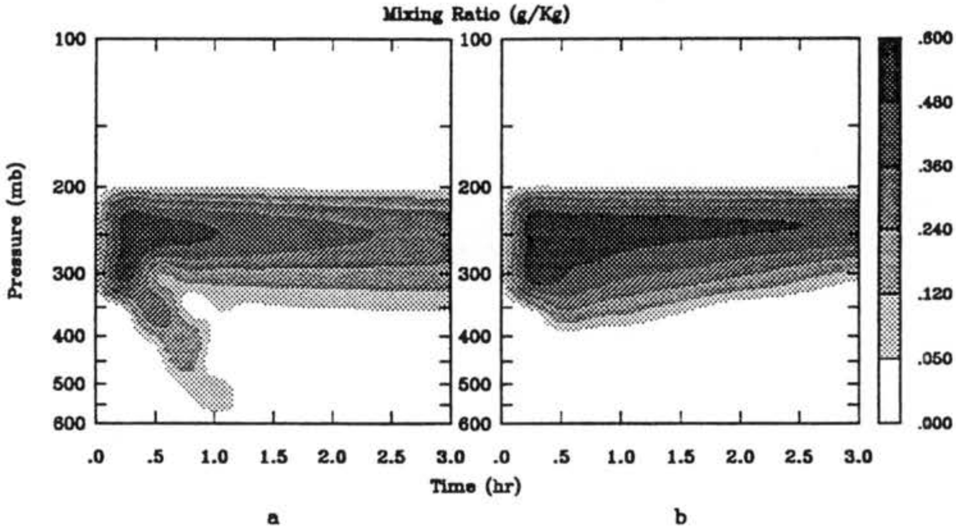


Figure 5.15: Ice species in the 250 mb storm outflow tropical cirrus when (a) the nested cloud model is used and (b) the nested model is not used.

The initial ice amount at 15 minutes is about 50 mb deeper than the explicit results which results in a significant reduction of the cloud top cooling at 200 mb (Figs. 4.29 and 5.16). The cooling at 15 minutes has reduced from $-30°/day$ to $-5°/day$ while the warming at 300 mb has increased by $-2°/day$. The vertical resolution of the host model may be responsible for simply not capturing the cooling peak in this case. The double peaked heating caused by the larger ice crystals falling out of the cloud is present in both the host/nest simulation as well as the explicit results.

### 5.4.1 Ice development in the nested 1D cloud model

The excess of large ice falling out of the host/nest simulation can be understood by examining the individual ice species as predicted in the nest model (Fig. 5.17). The initialization of ice at 15 minutes by the host model has created a snow mixing ratio of 0.4 g/kg. The explicit simulation had generated only 0.13 g/kg of aggregates at the same time. This difference once again indicates the effect of using one ice category in the host model. The snow is converted to aggregates through collection and aggregates are decreased to 0.05 g/kg by 1 hours which is the same amount as computed by the explicit simulation.

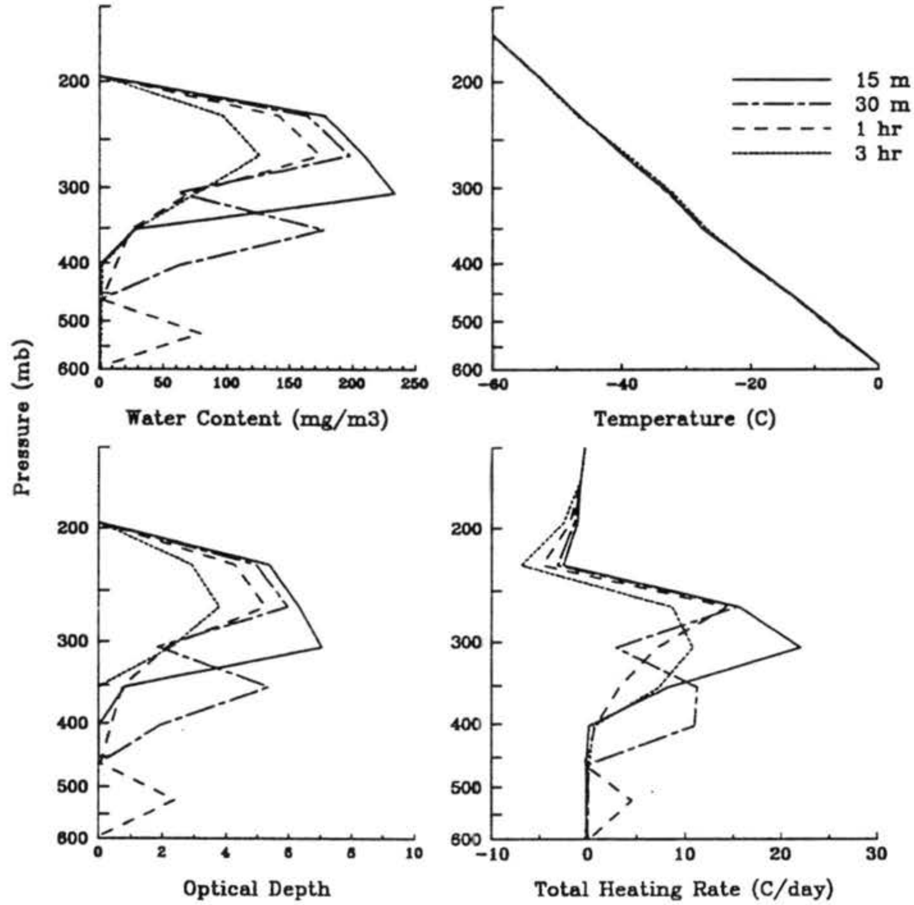


Figure 5.16: Radiative properties for the 250 mb storm outflow tropical cirrus.

### 5.4.2 Cirrus layer stability

The change in $\theta$ over the 3 hour simulation by the nested model tendencies shown in Fig. 5.18 indicate that radiation is once again the dominant component to changing the stability in the layer. The storm outflow cirrus has an initial temperture profile which is stable unlike the elevated RH initializations. Therefore, the turbulence is reponding to the destabilization of the radition but not on the same order of magnitude as seen in the other cirrus simulations. The latent heat effects though smaller than the radiation component also decrease the stability of the cloud layer.

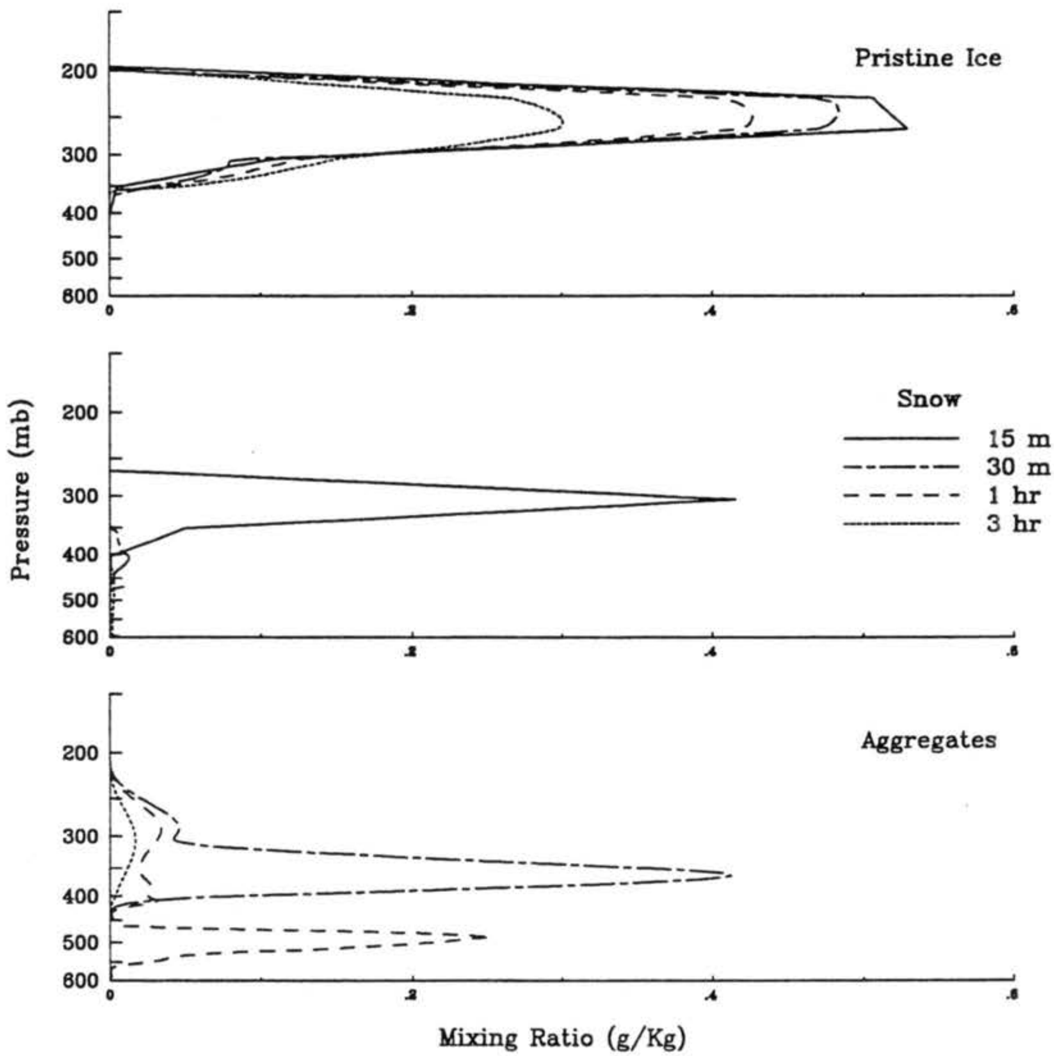


Figure 5.17: Ice species in the nested model for the 250 mb storm outflow tropical cirrus.

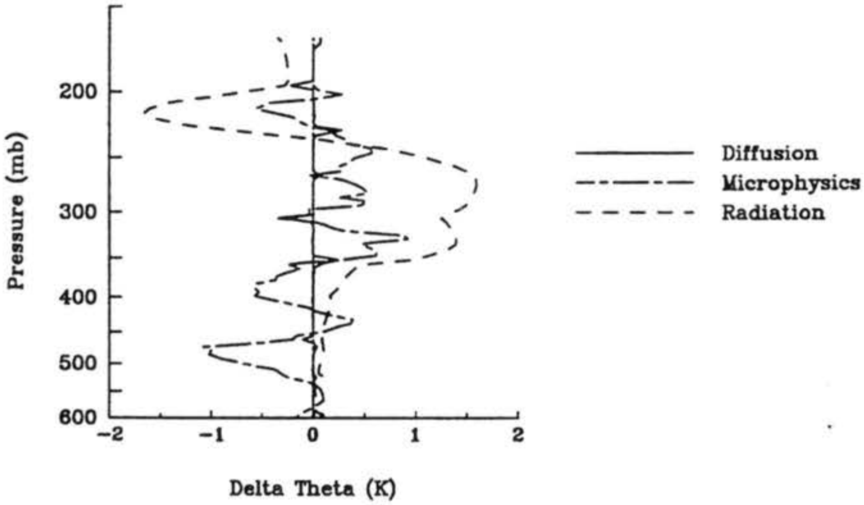


Figure 5.18: Change of potential temperature due to radiation, turbulence, and microphysics in the 250 mb storm outflow tropical cirrus over the 3 hour simulation.

## 5.5 Conclusions

By comparing to the explicit simulations in Chapter 4, the success of the 1D cloud model in accurately modeling the cirrus development can be determined. Several limitations of the combination of the large-scale model with a nested cloud model became apparent. The two most significant restrictions in the physics of the psuedo-GCM are the loss of vertical resolution and one ice category. These limitations were presumed to be realistic features for GCMs in the near future. The nested cloud model is the only viable option for improving cirrus representation in large-scale models.

The host model resolution makes a significant effect on the accuracy of the results even when nesting down to a vertical spacing of 100 m. For host vertical spacing of the order of 2000 m or greater, the impact of calling the nested cloud model is a small change in the maximum ice mixing ratios. Initialization of the cirrus by the host model will also strongly dictate the development of the cirrus. A better application may be to allow the nested cloud model to initialize the cirrus based on host variables. This use of the cloud model may prove more benefitial.

The initialization of the cirrus by the host microphysics seems to generally overpredict the number of large ice particles. This result will be a factor as long as one exponential number distribution is used to describe all ice particles. The nested cloud model does successfully convert the one ice category into pristine ice and snow which then can model the creation of aggregates through collection. The characteristic deepening and fallout of large ice crystals seen in Chapter 4 is only captured by the host model if the nested cloud model is used. Consequently, the heating rates modified by the presence of the cirrus will be applied over a different depth with slightly different magnitudes.

In general, the 1D nested cloud model will improve the large-scale model results for cirrus which have the largest feedbacks. These results indicate that the warmer clouds (above $-50°$C) created by large-scale lifting or any cirrus created by storm outflow with significant amount of ice (0.5 g/kg) will be more likely to create radiative forcing that would impact the large-scale circulation. Using these conclusions, the application of the nested cloud model can be utilized in the most efficient manner.

# Chapter 6

# OPTIMIZATION

The implementation of the 1D nested cloud model has so far been to call the parameterization every host model timestep. This application of the cloud model in a actual GCM simulation would not be desirable. A limited use of the cloud model with a balance between efficiency and accuracy would be ideal to justify the cost of the parameterization. To determine the performance of the cloud model when used sparingly, two cirrus simulations, the 350 mb midlatitude and the 250 mb tropical storm outflow cirrus, were repeated using various applications of the nested model. The development of the cirrus is presented for applications in which the cloud model is called only once and for cases where the model is called once an hour. A precipitation routine is also investigated as a possible solution for limiting the cost of this parameterization when used in conjunction with one call to the cloud model.

## 6.1 Limitied use of the cloud model

The initial design criteria of the upper-level cloud model included the idea to limit the frequency of calling the model to reduce the cost similiar to the use of some radiation schemes. To explore the impact of calling the cloud model less frequently than every host model timestep, three model configurations were tested as possible applications. The first configuration was calling the cloud model only once, after ice has been initiated by the host model. After the cloud model was called, the host model microphysics would be responsible for the remainder of the cloud development. The second application was calling the cloud model once every hour which is equivalent to every fourth host timestep in this case. When the cloud model was not called, the host microphysics computed the cloud variable tendencies. The final configuration examined was calling the cloud model once an hour but to continue to apply the same tendencies computed by the cloud model to the remainder of the hour. In this case, the host microphysics would not be used to compute the tendency of the cloud variables during the host model timesteps in which the cloud model was not called. The results of using the three model configurations on the two cirrus clouds is evaluated below.

### 6.1.1 Calling the cloud model once

As discussed in the previous chapters, the cloud parameterization models a cirrus cloud that deepens with time which may have large ice particles fall out of the main cloud layer and evaporate in the drier layers below the cloud. When the cloud model was not used, the host model would not capture this feature of the cirrus; the cirrus did not deepen significantly and no ice was seen to fall from the cloud. As a compromise between these two configurations, the nested model was called once at the beginning of the lifetime of the cirrus. The premise was to allow the nested cloud model to develop the initial fall out of the larger ice which the host model would continue to model during the cloud development. An application of this nature would be triggered when ice is first nucleated in a given vertical column. To evaluate the success of this application, the results of both cirrus cases are shown in comparison to the simulation in which the cloud model was called every host timestep.

The 350 mb midlatitude cloud which was initialized by a 50% supersaturation with respect to ice, is shown in Fig. 6.1 along with the original cloud model simulation. The difference between the two simulations is quickly apparent. Calling the cloud model once does not adequately create the sedimentation of the larger ice particles. In fact, the final ice mixing ratio in the main cloud layer grows with time. This fact is a result of the host diffusion model creating a large mixing tendency to remove the unstable cloud layer. The larger amount of water vapor from below is mixed upward which results in the nucleation of more ice. Because the time scale of the nested model turbulence is too slow to remove the instability in the 15 minutes during the call to the cloud model, the host diffusion model is presented with the unstable cloud layer. The 350 mb cirrus simulation was repeated with a vertical mixing coefficient one fourth as large to remove the impact of the host model diffusion on this investigation (Fig. 6.2). The increase of ice at 300 mb has been decreased by reducing the vertical mixing coefficient. The results still indicate that by calling the cloud model once, some ice begins to settle out of the cloud deck but then remains at 400 mb until the ice sublimates.

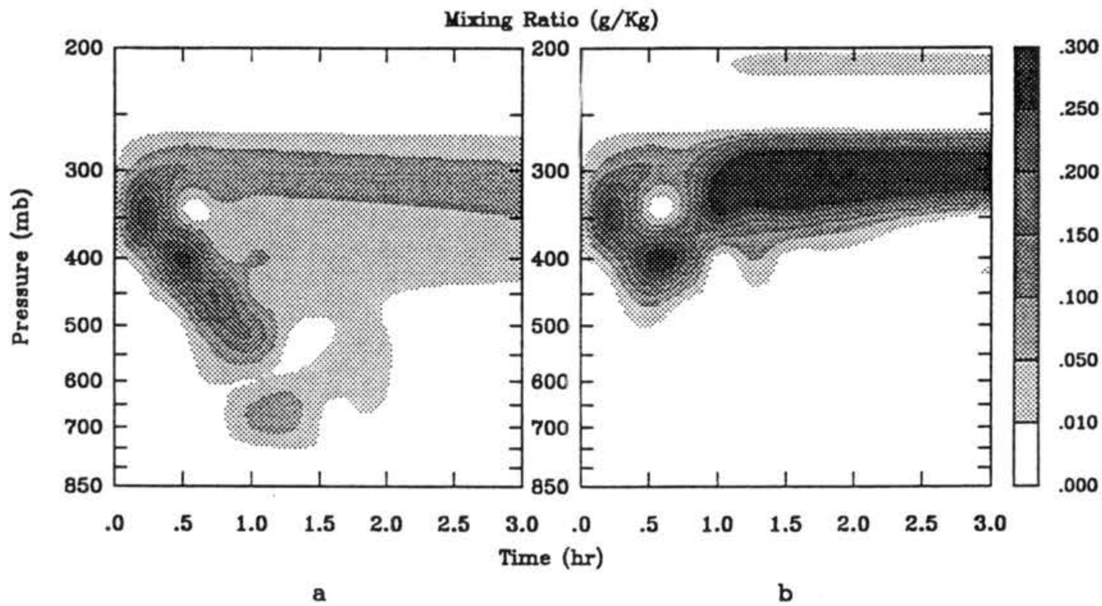


Figure 6.1: Development of the ice species in the 350 mb midlatitude cirrus when (a) the cloud model is called every host timestep and (b) the cloud model is called once.

For the tropical cloud which is initialized by placing 0.5 g/kg of water in a stable layer at 250 mb, the results indicate the same conclusions. Fig. 6.3 shows the original simulation ice water mixing ratios as compared to the modified model configuration simulation. As discussed before, the cloud model begins the process of sedimentation of the large ice but the host model microphysics is not capable of continuing the trend of the cloud development. The ice does not fall further and simply sublimates in place. The ice amount in the main cloud layer is also 0.1 g/kg larger.

As shown by these results, calling the cloud model once will not adequately model the fall out of large ice particles and as a result over-predicts the final amount of ice in the cloud. This application of the cloud model will not provide the GCM with an improved calculation of upper-level clouds.

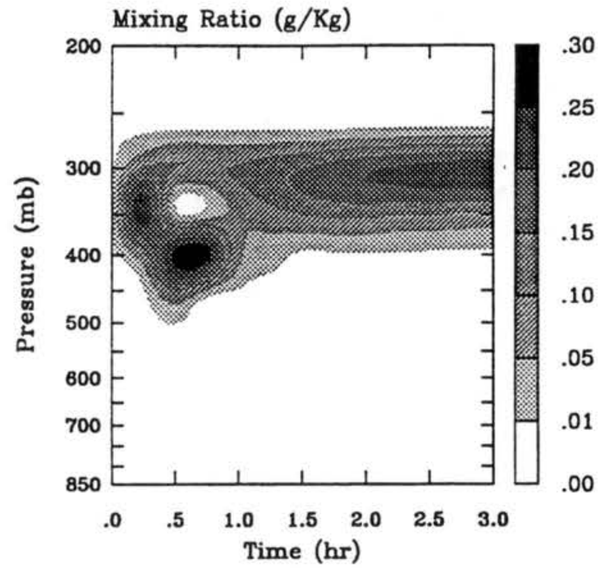


Figure 6.2: Development of the ice species in the 350 mb midlatitude cirrus where the cloud model is called once. Vertical mixing coefficient has been reduced.

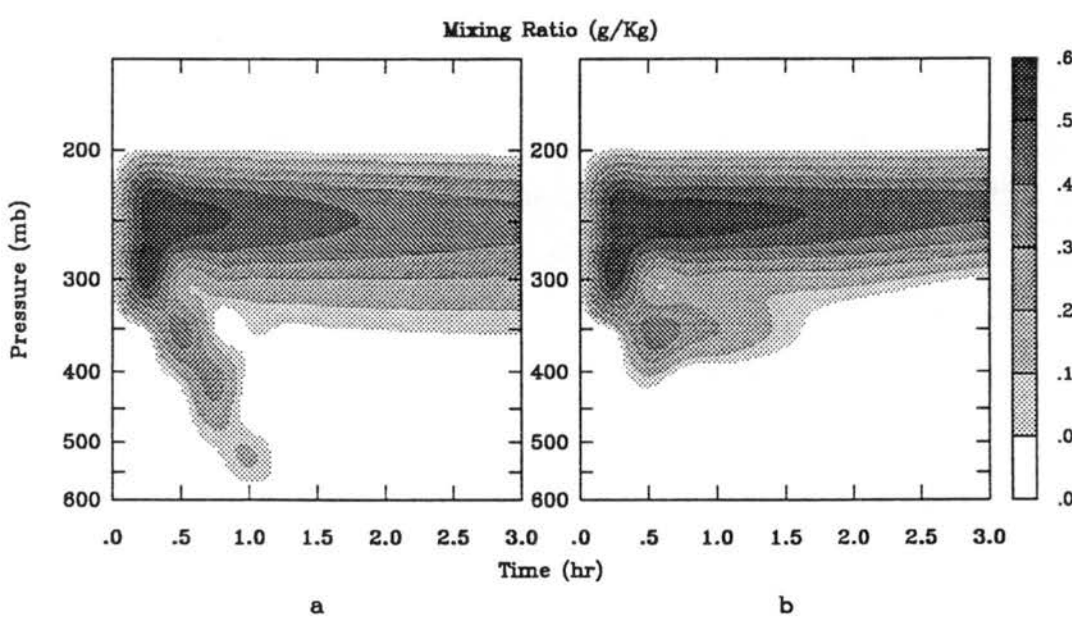


Figure 6.3: Development of the ice species in the 250 mb tropical storm outflow cirrus when (a) the cloud model is called every host timestep and (b) the cloud model is called once.

### 6.1.2 Calling the cloud model once every hour

The simulations were repeated for both the tropical and midlatitude cirrus this time calling the cloud model once every hour. Fig. 6.4 shows the ice mixing ratios for both cirrus cases. Once again, for the 350 mb cirrus, the smaller vertical mixing coefficient has been used. Calling the cloud model once every hour did not significantly change the results compared to only calling the model once. Because most of the ice which had settled out of the cloud layer had sublimated before the second calling of the cloud model, the extra calls to the cloud model does not improve the deepening of the cirrus.

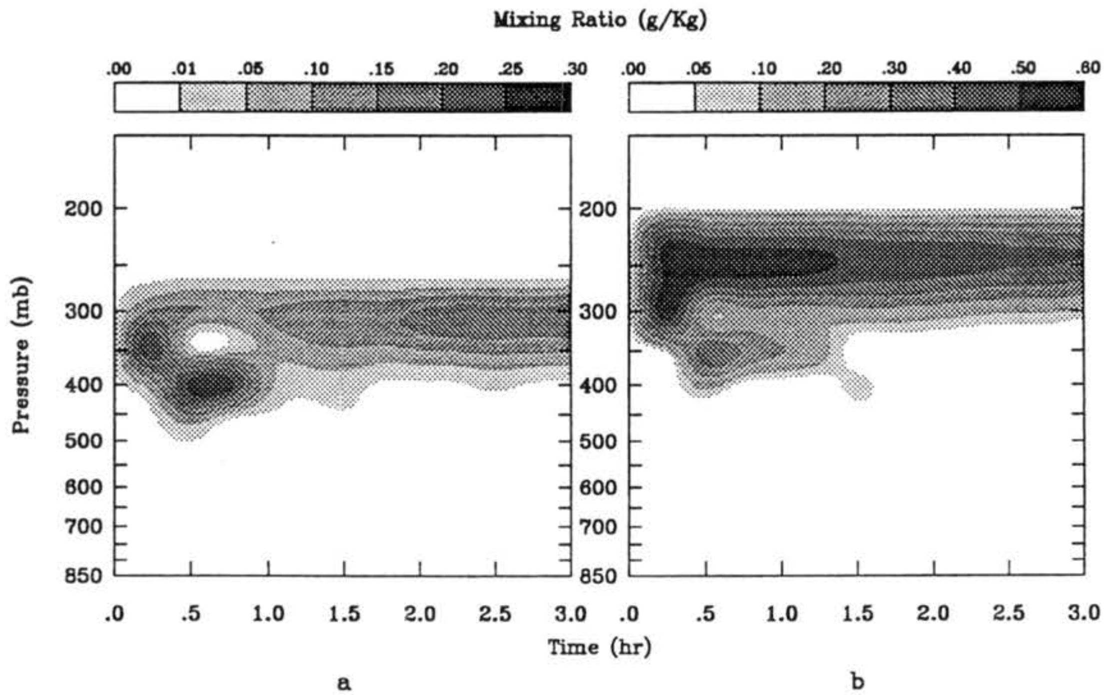


Figure 6.4: Development of the ice species when the cloud model is called once every hour for (a) the 350 mb midlatitude cirrus and (b) the 250 mb tropical storm outflow cirrus.

### 6.1.3 Calling the cloud model once every hour with continued application of the cloud model tendencies

In the section above, during host model timesteps in which the cloud model was not used, the host model computed the microphysical change in water variables as well as temperature. For these simulations the cloud model tendencies were applied during host model timesteps after calling the cloud model until the cloud model was called again. The host microphysics was not used after the initialization of the ice. The results are presented in Fig. 6.5. The sedimentation of the larger ice has reached the same level as originally computed when the cloud model is called each host timestep. But the time needed for the ice to precipitate has been lengthened which will impact the radiative heating. Also, the mixing ratio values in the main cloud layer are greater than the original case. This application of the cloud model does not appear to be a promising solution to limiting the cost of the parameterization.

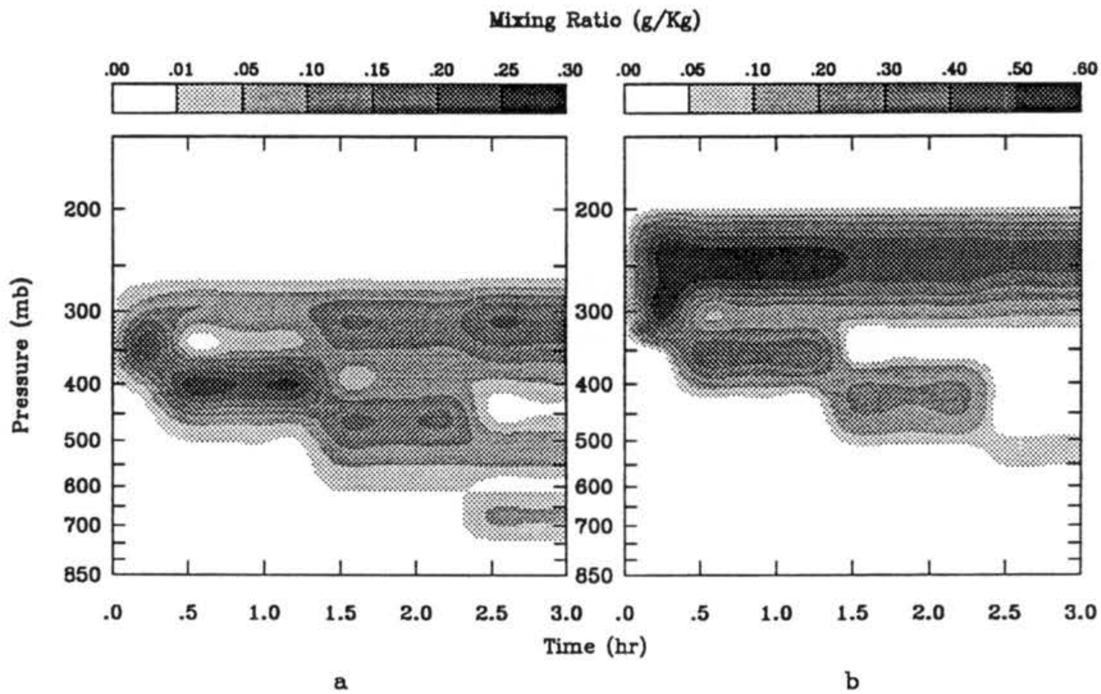


Figure 6.5: Development of the ice species when the cloud model is called once every hour and the cloud model tendencies are used during the other host model timesteps for (a) the 350 mb midlatitude cirrus and (b) the 250 mb tropical storm outflow cirrus.

### 6.1.4 Calling the cloud model during the first hour

The deepening and fall out of large ice appears to occur within the first hour of the simulation for both cirrus. Taking advantage of this characteristic, the simulations were repeated calling the cloud model only during the first hour of the simulation. Fig. 6.6 presents the results for both cirrus cases and appears to be almost identical to the simulations in which the cloud model was called every host timestep. So for this particular cirrus clouds, the cloud model was only necessary during the first hour of the cloud development. This application may not work as successfully when the parameterization interacts with the large-scale circulation in a GCM simulation. Some design decisions pertaining to the cloud model can only be fully answered by actually testing the parameterization in a GCM.

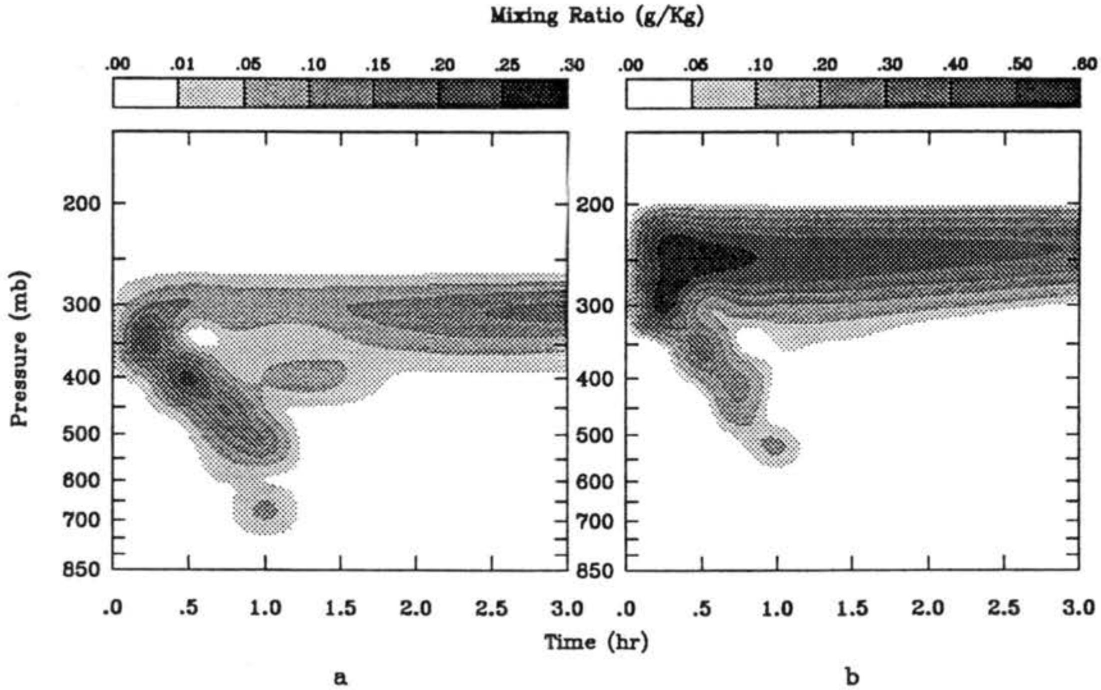


Figure 6.6: Development of the ice species when the cloud model is called for three host timesteps or until one hour for (a) the 350 mb midlatitude cirrus and (b) the 250 mb tropical storm outflow cirrus.

## 6.2 Precipitation parameterization

The limited calling of the cloud model does not appear to be an accurate application of the parameterization. The one feature of the cirrus cloud which the cloud model provided, the sedimentation of larger ice particles, is not captured when the cloud model is called less frequently than every host timestep. A better solution to this problem may be to call the cloud model once and include a parameterization specifically for the fall out of large ice particles. The precipitation tendency could then be applied until either the ice sublimates, melts and evaporates, or reaches the ground. The host model microphysics would be used in conjunction with the precipitation tendencies.

The precipitation parameterization was created using the same microphysical routines as in the cloud model but limiting the calculations to the categories of snow, aggregates, and rain. The physical mechanisms of vapor growth, melting, evaporation, sublimation, collection, and sedimentation were included. Once the cloud model tendencies have been computed for the host model timestep, the precipitation parameterization is called to calculate the future tendencies of the host model variables of total water, ice, temperature. The precipitation routine begins with the snow, aggregate, and, if any, rain amounts at the host grid resolution after the completion of the cloud model calculation. The precipitation routine computes the tendencies at the host vertical spacing for every host timestep but uses a 90 seconds timestep which is internally looped over 10 times. The calculations are continued until the precipitation species have either converted to water vapor or have reached the ground. These precipitation tendencies are then applied in the following host mode timesteps.

The development of the cirrus using this model configuration is shown in Fig. 6.7 for both cirrus cases. Once again, the smaller vertical mixing coefficient has been used for the midlatitude cirrus. The results are disappointing in that the precipitation does not continue to fall but mearly evaporates at its current position. The precipitation routine has altered the final ice amounts creating a more distinct precipitation trail. Even though these results are not promising, different precipitation routine such as proposed by Ghan and Easter (1992) will probably be the most likely solution to the best application of the 1D cloud parameterization.

### 6.3 Conclusions

This preliminary examination has revealed possible solutions to a cost effective implementation of the 1D nested cloud model. The earlier stages of the cirrus cloud development appear to be the most active with a significant amount of large ice particles settling out of the main cloud layer. To capture the feature of deepening and precipitation, the parameterization must be used during the initial cirrus development. The decaying cirrus may not benefit from calling the cloud model; the host microphysics may be sufficient. At this stage, the most successful application of the cloud model for these specific cases appears to

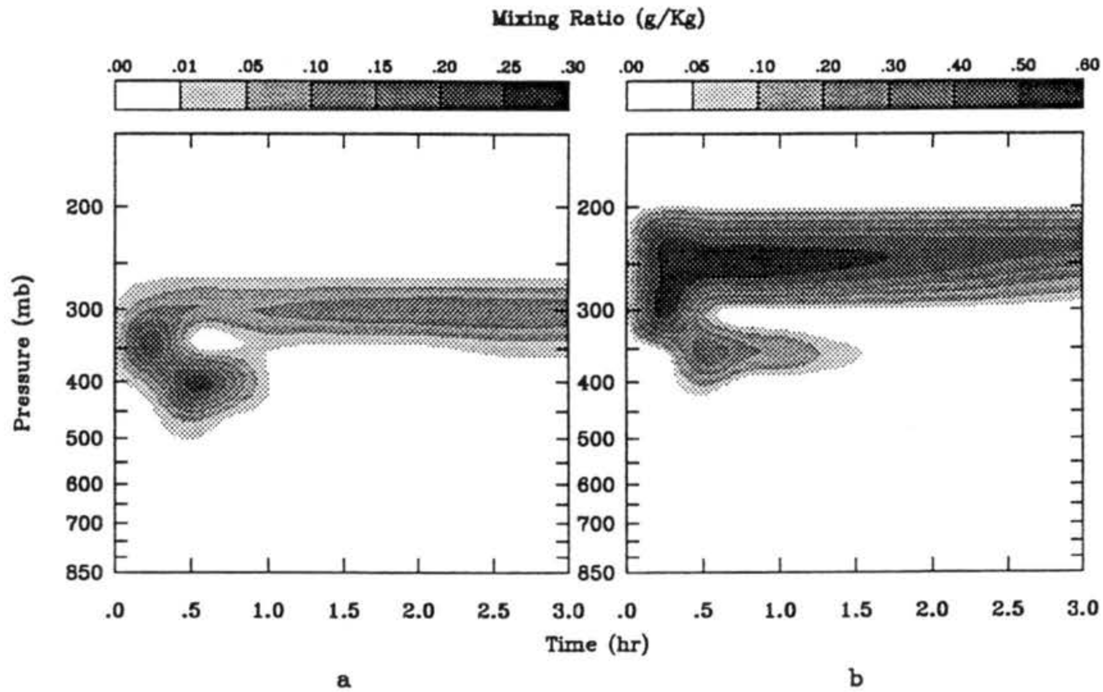


Figure 6.7: Development of the ice species when the cloud model is called once and a precipitation tendency is applied for the remainder of the simulation for (a) the 350 mb midlatitude cirrus and (b) the 250 mb tropical storm outflow cirrus.

be calling the model during the first hour of the simulation. But for real application of this parameterization in which the host model interacts with the cirrus cloud, the nucleation of new ice and creation of large ice particles may not only occur during the first appearance of the cirrus. Sedimentation of large particles may be an important feature during the entire lifetime of the cloud. If this is the case, calling the cloud model during the first hour of the cloud may not be adequate. Therefore, more development of a precipitation routine will most likely be necessary to use in conjunction with the cloud model. But to determine the optimal application of the cloud model, actual testing in a GCM will be necessary.

# Chapter 7

## SUMMARY AND CONCLUSIONS

The purpose of this research was to develop an upper-level cloud model which could be used to improve the processes of clouds and their feedback in large-scale models. Several researchers (Randall, 1989; Cess *et al.* 1990; Ramaswamy and Ramanathan, 1989) have suggested that improving cloud feedback especially upper-level clouds created by convection is of primary importance. Using a cloud parameterization which explicitly models the process of microphysics would have the complexity to handle both upper-level clouds created through large-scale weather disturbances and by convection; a simple parameterization which is only a function of grid volume averaged variables would not have this capacity. The trend in cloud parameterizations for large-scale models is towards developing explicit prediction of cloud species (Sundqvist, 1978; Smith, 1990; Ghan and Easter, 1992). GCM modelers have also explored prognosing cloud variables in a limited application to evalute the impact on the circulations (Smith and Randall, 1992; Fowler and Randall, 1992; Ose, 1993). These facts indicate the development of an upper-level cloud model which predicts cloud water and ice is appropriate at this time.

The cloud model was designed with the following features:

- Model the physical properties essential to simulating an upper-level cloud by including parameterizations for microphysics, turbulence, and radiation.
- Limit the computational cost of the model by using a vertical 1D, nested cloud model to obtain resolution on the order of 500 m and 90 seconds for the cloud-scale processes.
- Provide tendencies for water and potential temperature.
- Require the host GCM to maintain two categories for liquid and ice water as well as total ice number concentration.

The components of the cloud model (microphysics, turbulence and radiation) were taken from RAMS developed at CSU. RAMS was also configured to represent a limited area, large-scale model for testing the parameterization. In order to model the different properties of ice and liquid water, the radiation model originally developed by Chen and Cotton (1983) was modified slightly. The turbulence model (Weissbluth and Cotton, 1993) which was also modified to a 1D format, provided the subgrid parameterization of mixing that would normally be created by cloud-scale circulations. The one dimensional nature of the cloud model is the appropriate level of complexity to model the average features of the upper-level cloud which will be significant to the general circulation. A review of the results from this research are presented below along with suggestions for future research.

## 7.1 Summary of results

The cloud model described above has been designed to encompass all upper-level cloud types. To limit the scope of this research, only clouds cirroform in nature were examined. Several cirrus heights (450 mb to 125 mb) were studied using a psuedo-1D version of RAMS with a high vertical resolution (250 m $\Delta z$). The initialization of the cirrus was done by two methods, either elevating the relative humidity with respect to ice to 150% (large-scale lifting) or by adding 0.5 $g/kg$ of water to the cloud water category (convective outflow). These sensitivity tests provide a broad understanding of the performance of the parameterizations which were used in the cloud model. The conclusions from these simulations are as follows:

- A timestep smaller than 180 seconds is required.
- The vertical spacing of the grid should be on the order of 100-250 m to capture the important features of the radiative heating rate profile.
- Modeling both small and large ice is critical to simulate the gravitational separation by different terminal velocities which deepens the cloud layer.
- For cirrus, the precipitation of large ice from the main cloud layer would alter the radiative heating rates by moistening the layers below the cloud and, therefore, can not be neglected.

- Only clouds with IWC > 10 $mg/m^3$ or optical depths > 0.1 create significant heating rates ($\pm 2°C/day$). Typically the thinner, colder clouds have smaller infrared heating rates.

- Storm outflow cirrus, although at a cold temperature, are optically thick and will impact the atmosphere through radiative heating.

- Upper-level clouds in which water also exists have more complicated heating rate profiles depending on the distribution of ice and liquid water content.

- Day and night simulations demonstrated the solar heating in the cloud acts to reduce the amount of ice nucleated and liquid water present.

- When no radiation feedback was present, the mixing ratios of ice were increased as much as 44% at the end of the 250 mb tropical cirrus simulation. The 450 mb midlatitude cirrus had an increase in cloud droplets of 200% during the middle of the 3 hour simulation which collected more efficiently and resulted in less cloud species at the end of the simulation when compared to the simulation with radiation feedback. The actual impact of radiation on the cloud development was found to be a very complicated interation between the dynamics, microphysics and the heating.

Four of the cirrus simulations used in the sensitivity test were selected for testing the cloud model. Applying the knowledge gained by the sensitivity tests, the cloud parameterization was configured to have a nested timestep of 90 seconds and a vertical spacing of 100 m for most of the simulations. The cirrus were initialized in the first host timestep of 900 seconds by the large-scale RAMS model. By the second host timestep the cloud model was triggered until the end of the 3 hour simulation. Possible applications of the cloud model in the host model were also examined to limit the cost of the routine. Conclusions from these results were as follows:

- The cloud model performance is inherently dependent on initialization. Therefore, the coarser the host model resolution, the less accurate the initialization will be.

- Gravitational settling of large ice particles which cause the cloud to deepen and create precipitation trails is a feature the cloud model was able to simulate well.
- The optimization of the cloud model should include a parameterization for the sedimentation of large ice from the cloud layer and limited frequency of use by the host GCM.

The results presented above suggest that the use of such a upper-level cloud model will be feasible for large-scale models. Some further research is necessary to determine the optimal implementation of the cloud model.

### 7.2 Suggestions for future research

This research has been a preliminary study of a upper-level cloud parameterization. To continue the development of this cloud model, several areas of improvement and further study were found to be necessary. Suggestions are as follows:

- Modify the Ek and Mahrt (1991) fractional cloudiness scheme to work with upper-level clouds and large-scale models.
- Evaluate the performance of cloud fraction in conjunction with the cloud model.
- Extending this research to lower-level clouds.
- Verify the adaptation of the Chen and Cotton (1986) radiation model to include ice by a comparision to a more sophisticated radiation model.
- Use a simplier turbulence model if the 2.5w scheme does not provide large benefits for the GCM.
- Evaluate the cloud model within a GCM framework. The interactions of large-scale dynamics on the development and decay of the upper-level cloud was not possible in the psuedo-1D RAMS format.
- Evaluate the cloud parameterization against a large-eddy or cloud-resolving simulation of tropical and middle latitude, middle and upper tropospheric layer clouds.

**REFERENCES**


Ackerman, T. P., K.-N. Liou, F. P. J. Valero, and L. Pfister, 1988: Heating rates in tropical anvils. *J. Atmos. Sci.*, **45**, 1606-1623.

Arakawa, A., and V. R. Lamb, 1981: A potential enstrophy and energy conserving scheme for the shallow water equations. *Mon. Wea. Rev.*, **109**, 18-36.

Arakawa, A., and W.H. Schubert, 1974: The interactions of a cumulus cloud ensemble with the large-scale environment. Part I. *J. Atmos. Sci.*, **31**, 674-701.

Arnott, W. P., Y. Y. Doug, and J. Hallet, 1993: Cirrus microphysics observations made during FIRE II: Small particles, high concentrations, and probe comparisons. Preprints, *FIRE Cirrus Science Conf.*, June 14-17, 1993, Breckenridge, Colorado, 5-8.

Braham, R. R., Jr., and P. Spyers-Duran, 1967: Survival of cirrus crystals in clear air. *J. Appl. Meteor.*, **6**, 1053-1061.

Cess, R.D., G.L. Potter, J.P. Blanchet, G.J. Boer, A.D. Del Genio, M. Dequie, V. Dynmnikov, V. Galin, W.L. Gates, S.J. Ghan, J.T. Kiehl, A.A. Lacis, H. Le Treut, Z.-X. Li, X.-Z. Liang, B.J. McAvaney, V.P. Meleshko, J.F.B. Mitchell, J.-J. Morcrette, D.A. Randall, L. Rikus, E. Roeckner, J.F. Royer, U. Schlere, D.A. Sheinin, A. Slingo, A.P. Sokolov, K.E. Taylor, W.M. Washington, R.T. Wetherald, I. Yagai, and M.-H. Zhang, 1990: Intercomparison and interpretation of climate feedback processes in 19 atmospheric general circulation models. *J. Geophys. Res.*, **95**, 16,601-16,615.

Chen, C. and W. R. Cotton, 1983: A one-dimensional simulation of the stratocumulus-capped mixed layer. *Boundary-Layer Meteorol.*, **25**, 289-321.

Cotton, W. R. and R. A. Anthes, 1989: Storm and cloud dynamics. *Academic Press, Inc.*, 883 pp.

Cotton, W. R., M. A. Stephens, T. Nehrkorn, and G. J. Tripoli, 1982: The Colorado State University three-dimensional cloud/mesoscale model - 1982. Part II: An ice phase parameterization. *J. de Rech. Atmos.*, **16**, 295-320.

DeMott, P. J., M. P. Meyers, and W. R. Cotton, 1993: Parameterizations and impact of ice initiation processes relevant to numerical model simulations of cirrus clouds. *J. Atmos. Sci.*, **51**, 77-90.

Ek, M. and L. Mahrt, 1991: A formulation for boundary-layer cloud cover. *Annales Geophysicae,* **9**, 716-724.

Emanuel, K.A. 1991: A scheme for representing cumulus convection in large-scale models. *J. Atmos. Sci.,* **48**, 2313-2335.

Feingold, G., 1993: Parameterization of the evaporation of rainfall for use in general circulation models. *J. Atmos. Sci.*, **50**, 3454-3467.

Flatau, P. J., I. Gultepe, G. Nastrom, W. R. Cotton, and A. J. Heymsfield, 1990: Cirrus cloud spectra and layers observed during FIRE and GASP projects. Preprints, *Confererence on cloud physics*, July 23-27, 1990, San Francisco, CA.

Flatau, P. J., G.J. Tripoli, J. Verlinde, W. R. Cotton, 1989: The CSU-RAMS cloud microphysical module: General theory and code documentation. Atmos. Sci. Paper No. 451, Colorado State University, Dept. of Atmospheric Science, Fort Collins, Co 80523. 88 pp.

Fowler, L.D. and D.A. Randall, 1992: Impact of cloud microphysics on the CSU GCM atmospheric moisture budget. Extended Abstracts. Fourth Conference on Global Change Studies. January 17-22, Anaheim, California. pp 90-92.

Geleyn, J.F. 1981: Some diagnostics of the cloud-radiation interaction in the ECMWF forecast model. Workshop on radiation and cloud-radiation interaction in numberical modelling. 15-17 October 1980. ECMWF Reading, 135-162.

Ghan, S.J. and R.C. Easter, 1992: Computationally efficient approximations to stratiform cloud microphysics parameterizations. *Mon. Wea. Rev.,* **120**, 1572-1582.

Harrington, J. L., 1994: Parameterization of ice crystal conversion processes in cirrus clouds using double-moment basis functions. M.S. thesis, Colorado State University, Atmos. Sci. Paper No. 554, Dept. of Atmospheric Science, Fort Collins, Co. 80523, 135 pp.

Hartmann, D. L., H. H. Hendon, and R. A. Houze, Jr., 1983: Some implications of the mesoscale circulations in tropical clouds clusters for large-scale dynamics and climate, *J. Atmos. Sci.*, **41**, 113-121.

Heckman, S. T., 1991: Numerical simulation of cirrus clouds - FIRE case study and sensitivity analysis. M.S. Thesis, Colorado State University, Atmos. Sci. Paper No. 483, Dept. of Atmospheric Science, Fort Collins, Co. 80523, 132 pp.

Hense, A. and E. Heise, 1984: A sensitivity study of cloud parameterizations in general circulation models. *Beitr. Phys. Atmos.*, **57**, 240-258.

Herman, G. and R. Goody, 1976: Formation and persistence of summertime arctic stratus clouds. *J. Atmos. Sci.*, **33**, 1537-1553.

Heymsfield, A. J., 1975a: Cirrus uncinus generating cells and the evolution of cirroform clouds. Part I: Aircraft observations of the growth of the ice phase. *J. Atmos. Sci.*, **32**, 798-808.

—, 1975b: Cirrus uncinus generating cells and the evolution of cirroform clouds. Part II: The structure ans circulations of the cirrus uncinus generating head. *J. Atmos. Sci.*, **32**, 809-819.

—, 1975c: Cirrus uncinus generating cells and the evolution of cirroform clouds. Part III: Numerical computations of the growth of the ice phase. *J. Atmos. Sci.*, **32**, 820-830.

—, 1977: Precipitation development in stratiform ice clouds: A microphysical and dynamical study. *J. Atmos. Sci.*, **34**, 367-381.

Heymsfield, A. J. and R. G. Knollenberg, 1972: Properties of cirrus generating cells. *J. Atmos. Sci.*, **29**, 1358-1366.

Heymsfield, A. J., K. M. Miller, and J. D. Spinhirne, 1990: The 27-28 October 1986 FIRE IFO Cirrus Case Study: Cloud Microstructure. *Mon. Wea. Rev.*, **118**, 2313-2328.

Heymsfield, A. J., and C. M. R. Platt, 1984: A parameterization of the particle size spectrum of ice clouds in terms of the ambient temperature and the ice water content. *J. Atmos. Sci.*, **41**, 846-855.

Hobbs, P. V., L. F. Radke and D. G. Atkinson, 1975: Airborne measurements and observations in cirrus clouds. AFCRL-TR-75-0249, Air Force Geophysics Labratory, Hanscom AFB, 117 pp.

Houze, R. A., Jr., 1982: Cloud clusters and large-scale vertical motions in the tropics. *J. Meteorol. Soc. Jap.*, **60**, 396-410.

Klemp, J. B. and R. B. Wilhelmson, 1978: The simulation of three-dimensional convective storm dynamics. *J. Atmos. Sci.*, **35**, 1070-1096.

Kuo, H.-L. 1965: On formation and intensification of tropical cyclones through latent heat release by cumulus convection. *J. Atmos. Sci.*, **22**, 40-63.

—, 1974: Further studies of the parameterization of the influence of cumulus convection on large-scale flow. *J. Atmos. Sci.*, **31**, 1232-1240.

Leary, C. A. and R. A. Houze, Jr., 1979: Melting and evaporation of hydrometeors in precipitation from anvil clouds of deep tropical convection. *J. Atmos. Sci.*, **36**, 669-679.

Liou, K.-N., 1986: Review: Influence of cirrus clouds on weather and climate processes: a global perspective. *Mon. Wea. Rev.*, **114**, 1167-1199.

Liou, K.-N., 1992: Radiation and cloud processes in the atmosphere. *Oxford University Press*, 487 pp.

Mahrer, Y. and R. A. Pielke, 1977: A numerical study of the airflow over irregular terrain. *Beitrage zur Physik der Atmosphare*, 50, 948-113.

Manabe, S., J. Smagorinsky, and R.F. Strickler, 1965: Simulated climatology of a general circulation model with a hydrologic cycle. *Mon. Wea. Rev.,* **93**, 796-798.

Mellor, G. L. and T. Yamada, 1974: A heirarchy of turbulence closure models for planetary boundary layers. *J. Atmos. Sci.*, **31**, 1791-1806.

Meyers, M. P., 1995: The impact of a two-moment cloud model on the microphysical structure of two precipitation events. Ph.D. dissertation, Atmos. Sci. Paper No. 575, Colorado State University, Dept of Atmospheric Science, Fort Collins, Co. 80523, 165 pp.

Meyers, M. P., P. J. DeMott, and W. R. Cotton 1992: New primary ice nucleation parameterizations in an explicit cloud model. *J. Appl. Meteor.*, **31**, 708-721.

Ose, T., 1993: An examination of the effects of explicit cloud water in the UCLA GCM. *J. Meteor. Soc. Japan,* **71**, 93-109.

Peilke, R. A., W. R. Cotton, R. L. Walko, C. J. Tremback, W. A. Lyons, L. D. Grasso, M. E. Nicholls, M. D. Moran, D. A. Wesley, T. J. Lee, J. H. Copeland, 1992: A comprehensive meteorologocal modeling system-RAMS. *Metero. and Atmos. Phys.*, **49**, 69-91.

Peixoto, J. P., and A. H. Oort, 1992: Physics of climate. *American Institute of Physics*, 520 pp.

Platt, C. M. R., J. C. Scott, and A. C. Dilley, 1986: Remote sounding of high clouds. Part VI: Optical properties of midlatitude and tropical cirrus. *J. Atmos. Sci.*, **44**, 729-747.

Platt, C. M. R., A. C. Dilley, J. C. Scott, I. J. Barton, and G. L. Stephens, 1984: Remote sounding of high clouds. V: Infrared properties and structures of tropical thunderstorm anvils. *J. Climate Appl. Meteor.*, **23**, 1296-1308.

Ramaswamy, V. and V. Ramanathan, 1989: Solar absorption by cirrus clouds and the maintenance of the tropical upper troposphere thermal structure. *J. Atmos. Sci.,* **46**, 2293-2310.

Randall, D.A., 1989: Cloud parameterization for climate modeling: status and prospects. *Atmos. Res.,* **23**, 345-361.

Rhiel, H. and J. S. Malkus, 1958: On the heat balance in the equatorial trough zone. *Geophysica,* **6**, 503-537.

Sasamori, T., 1975: A statistical model for stationary atmospheric cloudiness, liquid water content, and rate of precipitation. *Mon. Wea. Rev.,* **103**, 1037-1049.

Slingo, J.M., 1987: The development of verification of a cloud prediction scheme for the ECMWF model. *Q. J. Roy. Meteor. Soc.,* **113**, 899-927.

Smith, L.D., and D.A. Randall, 1992: Parameterization of cloud microphysics processes in the CSU General Circulation Model. Atmospheric Science Paper No. 491, Colorado State University, Ft Collins, CO.

Smith, L.D., and D.A. Randall, 1992: Inclusion of cloud microphysical processes in the CSU general circulation model. Proceedings Volume II, 11th International Conference in Clouds and Precipitation, Montreal, August 17-21, 1122-1125.

Smith, R.N.B., 1990: A scheme for predicting-layer clouds and their water content on a general circulation model. *Quart. J. Roy. Meteor. Soc.,* **116**, 435-460.

Stackhouse, P. W., Jr., and G. L. Stephens, 1991: A theoretical and observational study of the radiative properties of cirrus: Results from FIRE 1986. *J. Atmos. Sci.,* **48**, 2044-2059.

Starr, D. O., and S. K. Cox, 1985: Cirrus clouds. Part I: A cirrus cloud model. *J. Atmos. Sci.,* **42**, 2663-2681.

Starr, D. O., and S. K. Cox, 1985: Cirrus clouds. Part II: Numerical Experiments on the Formation and Maintenance of Cirrus. *J. Atmos. Sci.,* **42**, 2682-2694.

Stephens, G. L., 1978: Radiative properties of extended water cloud: II Parameterization. *J. Atmos. Sci.*, **35**, 2123-2132.

Stephens, G. L., 1977: The transfer of radiation in cloudy atmosphere, Ph.D. dissertation, Meteorology Dept., University of Melbourne.

Sundqvist, H. 1978: A parameterization scheme for non-convective condensation including prediction of cloud water content. *Q. J. Roy. Meteor. Soc.,* **104**, 677-690.

Tremback, C. J., 1990: Numerical simulation of a mesoscale convective complex: model development and numerical results. Ph.D. dissertation, Atmos. Sci. Paper No. 465, Colorado State University, Dept of Atmospheric Science, Fort Collins, Co. 80523, 246 pp.

Tremback, C. J. and R. Kessler, 1985: A surface temperature and moisture parameterization for use in mesoscale numerical models. Preprints, *7th Conference on Numberical Weather Prediction*, June 17-20, 1985, Montreal, Quebec, AMS.

Tremback, C. J., G. J. Tripoli, and W. R. Cotton, 1985: A regional scale atmospheric numerical model including explicit moist phsics and a hydrostatic time-split scheme. Preprints, *7th Conference on Numberical Weather Prediction*, June 17-20, 1985, Montreal, Quebec, AMS.

Tripoli, G. J., 1986: A numerical investigation of an organic mesoscale convective system. Ph.D. dissertation, Atmos. Sci. Paper No. 401, Colorado State University, Dept. of Atmospheric Science, Fort Collins, Co. 80523, 290 pp.

Tripoli, G. J. and W. R. Cotton, 1982: The use of ice-liquid water potential temperature as a thermodynamic variable in deep atmospheric models. *Mon. Wea. Rev.*, **109**, 1094-1102.

Varley, D. J., I. D. Cohen, and A. A. Barnes, 1980: Cirrus particle distribution study, Part VII: AFGL-TR-80-0324, Air Force Geophysics Laboratory, Hanscom AFB, 82 pp.

Verlinde, J., P. J. Flatau, and W. R. Cotton, 1990: Analytical solutions to the collection growth equation: Comparison with approximate methods and application to cloud microphysics parameterization schemes. *J. Atmos. Sci.*, **47**, 2871-2880.

Walko, R. L., W. R. Cotton, J. L. Harrington, and M. P. Meyers, 1993: New RAMS cloud microphysics parameterization. Part I: The single-moment scheme. *Atmos Res.*, **34**. In Press.

Webster, P. J. and G. L. Stephens, 1980: Tropical upper-tropospheric extended clouds: inferences from winter MONEX. *J. Atmos. Sci.*, **37**, 1521-1541.

Weickmann, H. K., 1945: Formem und Bildung atmosphärisher Eiskristalle. *Beitr. Phys. Atmos*, **28**, 12-52.

—, 1947: Die Eisphase in der Atmosphäres. Library Trans. 273, Royal Aircraft Establishment, 96 pp.

Weissbluth, M. J. and W. R. Cotton, 1993: The representation of convection in mesoscale models. Part I: Scheme fabrication and calibration. *J. Atmos. Sci.*, **50**, 3852-3872.

Xu, K.-M. and S.K. Krueger, 1991: Evaluation of cloudiness parameterizations using a cumulus ensemble model. *Mon. Wea. Rev.*, **119**, 342-367.